



Universität Hamburg  
DER FORSCHUNG | DER LEHRE | DER BILDUNG

# Variational approaches to non-local Coulomb interactions in Mott-Hubbard systems

Dissertation  
zur Erlangung des Doktorgrades  
an der Fakultät für Mathematik, Informatik und  
Naturwissenschaften  
Fachbereich Physik  
der Universität Hamburg

vorgelegt von

Edin Kapetanović

Hamburg

2024



Gutachter/innen der Dissertation:	Prof. Dr. Tim O. Wehling Prof. Dr. Alexander Lichtenstein
Zusammensetzung der Prüfungskommission:	Prof. Dr. Tim O. Wehling Prof. Dr. Alexander Lichtenstein Prof. Dr. Martin Eckstein Prof. Dr. Michael Potthoff PD Dr. Jens Wiebe
Vorsitzende/r der Prüfungskommission:	Prof. Dr. Michael Potthoff
Datum der Disputation:	10.12.2024
Vorsitzender des Fach-Promotionsausschusses PHYSIK:	Prof. Dr. Markus Drescher
Leiter des Fachbereichs PHYSIK:	Prof. Dr. Wolfgang J. Parak
Dekan der Fakultät MIN:	Prof. Dr.-Ing. Norbert Ritter



## Abstract

Von Hochtemperatur-supraleitenden Kupraten bis zu neuartigen Materialien wie das verdrehte Zweilagengraphen gibt es eine große Notwendigkeit, zweidimensionale, wechselwirkende Systeme akkurat zu modellieren. Der Grundstein zum Verständnis wechselwirkender Elektronen auf einem periodischen Gitter ist das Hubbard-Modell, welches trotz seiner simplen Idee für viele, wichtige Fälle weiterhin ungelöst ist. Die drei Projekte, die in dieser Arbeit präsentiert werden, haben das Ziel, numerische Simulationsmöglichkeiten zu erweitern und zum Verständnis von ansonsten unzugänglichen Parameterbereichen beizutragen. In den ersten zwei Projekten wurde ein Variationsansatz entwickelt, um erweiterte Hubbard-Modelle mit sowohl nichtlokaler, abstoßender sowie der Austausch-Wechselwirkung durch Systeme mit effektiver, ausschließlich lokaler Interaktion zu beschreiben. Als Letztes wird die Implementierung einer Dual-Fermion Störungstheorie vorgestellt, welche die Zielsetzung hat, das berühmte Vorzeichenproblem in Quanten-Monte-Carlo Methoden zu umgehen. Alle Ansätze werden hier für das periodische Quadratgitter angewendet, aber lassen sich mit weiteren Entwicklungen zukünftig auch auf wesentlich komplexere Probleme übertragen.



## **Abstract**

From the high-temperature superconducting cuprates to novel materials such as twisted bilayer graphene, adequate modelling of two-dimensional, interacting systems is of tremendous interest. At the center of interacting electrons on a lattice stands the Hubbard model which, despite its simplicity, remains unsolved for many important cases. The three works and ideas presented in this thesis share the goal of improving computational possibilities and broaden the understanding of otherwise inaccessible parameter regimes. To that end, within the first two projects, a variational scheme has been developed which describes extended Hubbard models with both nonlocal repulsive and exchange interactions through an effective, purely local Hubbard system. Lastly, an implementation of a strong-coupling perturbation theory is presented, which has the aim of circumventing the famous, fermionic Monte Carlo sign problem. While we treat the important square lattice in all cases, the hope is that with further developments, these novel approaches may be applied to much more complex problems.





## Contents

<b>1. Introduction</b>	<b>3</b>
<b>2. Theoretical Basics</b>	<b>6</b>
2.1. Second Quantization . . . . .	6
2.2. Thermodynamics and Statistics . . . . .	8
2.2.1. Canonical and Grand-Canonical Ensemble for Fermions . . . . .	8
2.2.2. Wick-Theorem . . . . .	10
2.2.3. Example: Four-Particle Correlators . . . . .	12
2.3. Matsubara Formalism . . . . .	14
2.4. The Tight-Binding Model . . . . .	16
2.5. The Hubbard Model . . . . .	19
2.6. Extended Hubbard Models . . . . .	20
<b>3. Peierls-Feynman-Bogoliubov Variational Principle</b>	<b>22</b>
3.1. Formalism . . . . .	22
3.2. Example: Mean-Field Theory of the Heisenberg-Model . . . . .	24
3.3. Applications . . . . .	28
3.3.1. $U$ - $J$ -Model to $U$ - $B$ -Model . . . . .	28
3.3.2. $U$ - $V$ -Model to $U$ -Model . . . . .	30
3.3.3. General Interactions . . . . .	32
<b>4. Numerical Methods and Approximations</b>	<b>35</b>
4.1. Determinantal QMC . . . . .	35
4.1.1. Classical Monte Carlo . . . . .	35
4.1.2. DQMC Algorithm . . . . .	37
4.1.3. Measurements . . . . .	40
4.2. Dual Fermion Perturbation Theory . . . . .	42
4.3. DMFT and DCA . . . . .	47
4.4. CT-AUX . . . . .	50
<b>5. Nonlocal Exchange Interactions in Strongly Correlated Electron Systems</b>	<b>52</b>
5.1. Scope of the work and Statement of Contributions . . . . .	52
5.2. Actual Paper . . . . .	52
<b>6. Charge correlation, doublon-holon binding and screening in the doped Hubbard model</b>	<b>61</b>
6.1. Scope of the work and Statement of Contributions . . . . .	61
6.2. Actual Paper . . . . .	61
6.3. Implementations in the QUEST code . . . . .	70
<b>7. Overcoming the fermionic QMC sign problem through Dual Fermion Perturbation Theory</b>	<b>77</b>
7.1. Time-Dependent measurements in QUEST . . . . .	79

---

7.2. Implementations for the Dual-Fermion Approach . . . . .	85
7.2.1. Compilation . . . . .	85
7.2.2. Building the Reference System . . . . .	86
7.2.3. Second Run - Perturbation Theory . . . . .	87
7.2.4. Parallelization . . . . .	96
7.2.5. Examples . . . . .	98
7.3. Open Problems . . . . .	104
<b>8. Conclusions and Future Outlook</b>	<b>105</b>
<b>A. Acknowledgements/Danksagung</b>	<b>106</b>
<b>B. Declaration</b>	<b>107</b>
<b>C. Publications</b>	<b>108</b>
<b>D. Conference Contributions</b>	<b>109</b>
<b>E. Bibliography</b>	<b>110</b>
<b>F. List of changes/Liste der Änderungen</b>	<b>118</b>

## 1. Introduction

Introduced already in the 1960s by Hubbard, Gutzwiller and Kanamori, [1, 2, 3, 4, 5], the Hubbard model is the simplest model of interacting electrons on a lattice. In its simplest form, the main idea consists of electrons hopping between neighbouring, localized orbitals with an amplitude  $t$  and interacting with a coupling strength  $U$  only if they happen to be at the same atom. In the case of the bare Coulomb interaction, which scales with the distance as  $\sim 1/r$ , this constitutes the biggest cutoff imaginable. Despite the simplicity of the model, it exhibits surprisingly diverse (and still debated) phase diagrams on many geometries, and has since become the foundation of understanding strongly correlated materials.

The original papers discuss the model in the context of itinerant ferromagnetism in narrow bands and other correlation phenomena in materials where  $d$ - and  $f$ -orbitals determine the electronic properties. A hugely important finding is the metal-insulator transition [3, 6], which describes how a sufficiently strong local interaction can open an energy gap and turn the material into a so-called Mott-insulator.

While the model can be solved in one dimension [7] through a Bethe-Ansatz, the cases  $d = 2, 3$  which resemble problems in real materials are much more interesting. At strong coupling  $U \gg t$ , the Hamiltonian can be mapped to an antiferromagnetic Heisenberg [8] problem with an effective, kinetic exchange coupling of  $J \sim 4t^2/U$ . This competes with other mechanisms which may be very close in energy: The ground state ( $T = 0$ ) of a half-filled (i.e. one electron per orbital/site) square lattice is an antiferromagnetic insulator for all  $U > 0$ , but, in the limit  $U \rightarrow \infty$ , removing a single electron leads to ferromagnetism [9, 10]. Other, interesting phenomena in the doped square lattice include the formation of domain walls [11], nematic fluctuations [12] and fluctuating stripes [13] in the 3-band case. Over a wide range of fillings, the Hubbard model exhibits the behaviour of a strange metal, whose resistivity scales linearly with the temperature  $T$  [14]. The almost empty case in two dimensions is known to be a weakly-coupled Fermi-liquid [15].

An important aspect to discuss is the connection between the square lattice Hubbard model and high-temperature superconducting cuprates such as  $\text{La}_2\text{CuO}_4$ : While they are still not fully understood after many decades, their state under normal conditions is effectively a two-dimensional, antiferromagnetic insulator [16, 17]. More precisely, experiments with angular resolved photoemission spectroscopy (ARPES) [18] and calculations [19] show that, near the Fermi surface, copper  $d$ -type and oxygen  $p$ -type bands are at the center of the electronic properties. Considering the crystal structure, this forms an effective 3-band model on a square lattice such as in [20], although arguments have been made that this can be further condensed into a one-band model [21]. The antiferromagnetic correlations are known to be related to the  $d$ -wave symmetry [22] of the superconductivity.

Throughout this work, extensive use is made of a powerful method known as Determinantal Quantum Monte Carlo (DQMC) [23]. While quantum Monte Carlo methods provide an unbiased way of studying the Hubbard model, they are heavily restricted

---

in a broad parameter regime by the famous fermionic sign problem which is related to quantum critical points [24] and is known to be NP-hard [25]. Special cases like the square lattice at half filling with only nearest neighbour hopping (i.e.  $t' = 0$ ), which are particle-hole symmetric, are free of the sign problem. However, even though other cases are apparently very close in parameter space, depending on the temperature and the interaction strength, even the smallest deviations from an unproblematic case may render a simulation impossible. In fact, it is the sign problem that, despite a massive increase in computational power over the last decades, prevents us from studying the parameter regime where superconductivity is expected. Thus, in order to obtain any information beyond Hartree-Fock mean-field theory, sophisticated methods and ideas are necessary.

One way to make the model more realistic (and even more difficult) is to choose a less radical cutoff for the Coulomb interaction, i.e. include nonlocal interaction terms, leading to so-called extended Hubbard models. In two-dimensional materials such as graphene, the respective interaction strengths become quite large [26] as the screening is generally greatly reduced compared to a bulk material. Nonlocal repulsive interactions favor a charge-density wave (CDW) [27, 28, 29] which, at half filling on a bipartite lattice, competes with the antiferromagnetic spin-density wave (SDW) ground state. A recent DQMC study has set the phase boundaries more precisely at half filling [30].

Another possibility is to include the nonlocal exchange interaction which favors a ferromagnetic ordering in its simplest form. Usually, it is ignored due to its weakness (for  $3d$ -electrons in a bulk:  $J \approx 1/40\text{eV}$  compared to the local interaction  $U \approx 10\text{eV}$ . [1]) but, considering the reduced screening in two dimensions and the fact that many magnetic orderings may be very close to each other energetically (e.g. the Nagaoka case [9]), even a little nudge towards ferromagnetism may have a large effect on the otherwise antiferromagnetic ground state. Especially in the large- $U$  limit,  $J$  would compete against a rather small  $4t^2/U$ -coupling.

Of course, both extensions make the sign problem even worse if a direct lattice QMC simulation is attempted, which is the motivation for a set of new approaches presented in this work.

This thesis is structured as follows: We briefly go through the relevant basics of statistical quantum and many-particle physics for electrons on a lattice, and introduce the Hubbard Hamiltonian together with its extensions. Afterwards, the Peierls-Feynman-Bogoliubov variational principle is introduced [31] which allows us to map an arbitrarily complicated Hamiltonian onto a simpler, effective system. It is the basis of the first two works presented. The derivations which are used in the papers to incorporate nonlocal interactions into purely local Hubbard models are discussed in more detail, and a possible generalization is proposed. We then go over to the numerical and computational aspects, starting with a detailed introduction of the heavily used Determinantal Quantum Monte Carlo [23, 32] algorithm. The dual-fermion perturbation theory [33, 34] which is at the center of the last chapter follows. The Dynamical Mean-Field Theory (DMFT) and the Dynamical Cluster Approximation (DCA) [35]

are also explained, together with a continuous-time Monte Carlo solver.

The presentation of the three projects which constitute the research of this thesis is done in a semi-cumulative fashion: Two works are attached as papers, while the third documents implementations done by me and Alexander Lichtenstein in a pedagogical way.

The first work, which has been published in Physical Review B [36], extends the Hubbard model by a nonlocal exchange interaction, modeled by a ferromagnetic Heisenberg term. Through the variational principle mentioned before, self-consistency equations are derived which map the problem onto an auxiliary model with a broken spin-symmetry and an effective, purely local interaction. Pros and Cons of this method are discussed, and it is shown how it correctly predicts continuous transitions of anti-ferromagnetic to ferromagnetic correlations where Hartree-Fock mean-field theory [37] displays first-order phase transitions.

The second paper (available on arXiv: [38]) treats the extended Hubbard model on a doped square lattice, where a next-neighbour repulsive term with the strength  $V$  is included. As mentioned above, the Monte Carlo methods one could apply to the doped problem break down quickly due to the sign problem. In order to gain some insight on how the  $V$ -term affects the system, we thus make use of the variational principle, and derive a self-consistency equation for an effective local interaction  $\tilde{U}$ . Such a mapping was already used to discuss how the local interaction is screened [39] and how the order of the metal-insulator transition is affected [40]. However, here, we extend it to a broad range of parameters and fillings. Surprisingly, our data which is obtained both from direct lattice DQMC and within the DCA hints that the screening is more effective when hole-doping the system away from half filling. Furthermore, we implemented the measurement of static four-particle correlators into a DQMC code, and use it to study how doubly-occupied and empty sites are spatially distributed. Contrary to an intuitive picture where two holes are expected to move together in an antiferromagnetic background, we found that it is doubly-occupied and empty sites that are bound to each other.

In the last chapter, implementations done by me and Alexander Lichtenstein are presented. Specifically, we implemented a first version of the strong-coupling dual fermion perturbation theory discussed in Ch.(4) as a module which makes use of the QUEST-toolbox [41]. The relevant code snippets, basic usage and optimizations are explained together with open tasks for the future. A few first results for the Green's functions on a square lattice are presented.

In summary, we present three novel approaches towards the understanding of strongly correlated materials. In the future, with the emergence of new and better solvers, and the further improvement of computational resources, we hope that the ideas discussed in this work lead to further advances.

---

## 2. Theoretical Basics

Given a system which is governed by the Hamiltonian operator  $\hat{H}$  and a set of states  $\{|\Psi\rangle\}$  on a Hilbert space, the Schrödinger-equation [42] stands at the center of quantum mechanical descriptions:

$$i\hbar\frac{\partial}{\partial t}|\Psi\rangle = \hat{H}|\Psi\rangle$$

Assuming that  $\hat{H}$  is  $t$ -independent, the time-dependence can be separated, and one obtains a stationary eigenvalue problem:

$$\hat{H}|\Psi\rangle = E|\Psi\rangle$$

While solving this equation for one particle with different setups is a standard problem treated in all basic books, the many-particle problem poses a significant challenge. Assuming that the particles interact with each other (e.g. the standard Coulomb interaction between electrons/protons), for a macroscopic system, one arrives at a hugely complex problem with  $\sim 10^{23}$  coupled differential equations. For this reason, many methods and reasonable approximations have been developed. As such, in this chapter, we will briefly go through the necessary basics of many-particle physics and statistics.

### 2.1. Second Quantization

Given its relevance, and to make some notations clear, we quickly review some basics of the so-called *second quantization* [43]. The mathematical formalism was introduced by Fock [44] in order to treat many-particle systems in a more convenient fashion. Contrary to a classical system, identical quantum particles cannot be distinguished, which leads to only very specific possible many-body states.

Let us assume a set of single-particle states  $\{|\phi_{\alpha_i}\rangle\}$  (which stem from the solution of the Schrödinger equation), and let  $|\dots\phi_{\alpha_i}^{(i)}\dots\rangle$  denote an  $N$ -particle state where the  $i$ 'th particle is in the single-particle state  $|\phi_{\alpha_i}\rangle$ . Since the particles cannot be distinguished, applying the transposition operator  $\hat{P}_{ij}$  may only change the many-particle state by a phase factor  $\lambda$ :

$$\hat{P}_{ij}|\dots\phi_{\alpha_i}^{(i)}\dots\phi_{\alpha_j}^{(j)}\dots\rangle = |\dots\phi_{\alpha_i}^{(j)}\dots\phi_{\alpha_j}^{(i)}\dots\rangle \stackrel{!}{=} \lambda|\dots\phi_{\alpha_i}^{(i)}\dots\phi_{\alpha_j}^{(j)}\dots\rangle \quad (2.1.1)$$

Since  $\hat{P}_{ij}^2 = 1$ , the phase factor follows as  $\lambda = \pm 1$ . This leads to two separate subsets of the full Hilbert space,  $\mathcal{H}_N^{(+)}$  and  $\mathcal{H}_N^{(-)}$ , which contain the possible states of the many-body system.

The  $N$ -particle states  $|\psi_N^{(\varepsilon)}\rangle$  (with  $(\varepsilon = \pm)$ ) can be constructed from a simple product of one-particle states by applying the symmetrization and antisymmetrization

operators  $\hat{S}_\varepsilon$  on them:

$$|\psi_N^{(\varepsilon)}\rangle = \frac{1}{N!} \hat{S}_\varepsilon \left( |\phi_{\alpha_1}^{(1)}\rangle |\phi_{\alpha_2}^{(2)}\rangle \dots |\phi_{\alpha_N}^{(N)}\rangle \right) \quad (2.1.2)$$

$$\hat{S}_\varepsilon = \sum_{\mathcal{P}} \varepsilon^p \mathcal{P} \quad (2.1.3)$$

$\mathcal{P}$  performs  $p$  applications of the transposition operator  $\hat{P}_{ij}$ ; The sum in Eq.(2.1.3) runs over all possible permutations.  $1/N!$  is a normalization factor. For the case of  $\varepsilon = -$ , Eq.(2.1.2) can be conveniently rewritten as a so-called *Slater determinant*:

$$|\psi_N^{(-)}\rangle = \frac{1}{\sqrt{N!}} \det \begin{pmatrix} |\phi_{\alpha_1}^{(1)}\rangle & |\phi_{\alpha_2}^{(1)}\rangle & \dots & |\phi_{\alpha_N}^{(1)}\rangle \\ |\phi_{\alpha_1}^{(2)}\rangle & |\phi_{\alpha_2}^{(2)}\rangle & \dots & |\phi_{\alpha_N}^{(2)}\rangle \\ \vdots & \vdots & \ddots & \vdots \\ |\phi_{\alpha_1}^{(N)}\rangle & |\phi_{\alpha_2}^{(N)}\rangle & \dots & |\phi_{\alpha_N}^{(N)}\rangle \end{pmatrix} \quad (2.1.4)$$

On the other hand, in the  $\varepsilon = +$  case,  $|\psi_N^{(\varepsilon)}\rangle$  can be written as a permanent. The spin-statistics theorem [45] links  $\mathcal{H}_N^{(-)}$  to fermions (electrons, positrons, protons etc.) with half-integer spin (in units of  $\hbar$ ) and  $\mathcal{H}_N^{(+)}$  to bosons (e.g. photons, phonons, magnons etc.) with integer spin. In this work, only the first one is relevant as we will deal with fermionic systems only.

Instead of solving Eq.(2.1.4), many-body states  $|\psi_N^{(\varepsilon)}\rangle$  can be constructed out of the *vacuum state*  $|0\rangle$  (with  $\langle 0|0\rangle = 1$ ). To that end, the so-called *creation* and *annihilation operators*  $c_\beta^\dagger, c_\beta$  are introduced. The occupation numbers  $n_i$  of the one-particle states then characterize an  $N$ -particle state fully:

$$|\psi_N^{(\varepsilon)}\rangle = |n_1 n_2 \dots n_i \dots\rangle^{(\varepsilon)} \quad (2.1.5)$$

These states are known as *Fock states* and are elements of the *Fock space*  $\mathcal{H}^{(\varepsilon)} = \bigoplus_{N=0}^{\infty} \mathcal{H}_N^{(\varepsilon)}$ . The creation operator  $c_\beta^\dagger$  is defined as:

$$c_\beta^\dagger |\dots n_\beta \dots\rangle^{(\varepsilon)} = \varepsilon^{N_\beta} \sqrt{n_\beta + 1} |\dots (n_\beta + 1) \dots\rangle^{(\varepsilon)} \quad , \quad N_\beta = \sum_{i=1}^{\beta-1} n_i \quad (2.1.6)$$

The  $N$ -particle states can then be constructed by:

$$|n_1 \dots n_i \dots\rangle^{(\varepsilon)} = \prod_{\beta=1}^{\sum n_\beta = N} \frac{\varepsilon^{N_\beta}}{\sqrt{n_\beta!}} (c_\beta^\dagger)^{n_\beta} |0\rangle \quad (2.1.7)$$

The adjoint of  $c_\beta^\dagger$  defines the corresponding annihilation operator, i.e.  $c_\beta = (c_\beta^\dagger)^\dagger$ . In

the fermionic case, the operators act on the states in the following way:

$$c_\beta^\dagger \underbrace{|\dots n_\beta \dots\rangle^{(-)}}_{\in \mathcal{H}_N^{(-)}} = (-1)^{N_\beta} \delta_{n_\beta,0} \underbrace{|\dots (n_\beta + 1) \dots\rangle^{(-)}}_{\in \mathcal{H}_{N+1}^{(-)}} \quad (2.1.8)$$

$$c_\beta \underbrace{|\dots n_\beta \dots\rangle^{(-)}}_{\in \mathcal{H}_N^{(-)}} = (-1)^{N_\beta} \delta_{n_\beta,1} \underbrace{|\dots (n_\beta - 1) \dots\rangle^{(-)}}_{\in \mathcal{H}_{N-1}^{(-)}} \quad (2.1.9)$$

Furthermore, the following anticommutation relations are valid for fermions and contain the respective statistical properties (Pauli-principle and Fermi-Dirac-Distribution):

$$\{c_\alpha, c_\beta\} = 0 \quad , \quad \{c_\alpha^\dagger, c_\beta^\dagger\} = 0 \quad , \quad \{c_\alpha, c_\beta^\dagger\} = \delta_{\alpha\beta} \quad (2.1.10)$$

Lastly, we express arbitrary operators  $\hat{O}$ , consisting of one- and two-particles terms  $\hat{O}_{(1)}$ ,  $\hat{O}_{(2)}$ , in second quantization:

$$\hat{O} \equiv \sum_{ij} \underbrace{\langle \phi_{\alpha_i} | \hat{O}_{(1)} | \phi_{\alpha_j} \rangle}_{O_{ij}^{(1)}} c_i^\dagger c_j + \sum_{ijkl} \underbrace{\langle \phi_{\alpha_i}^{(1)} | \langle \phi_{\alpha_j}^{(2)} | \hat{O}_{(2)} | \phi_{\alpha_k}^{(1)} \rangle | \phi_{\alpha_l}^{(2)} \rangle}_{O_{ijkl}^{(2)}} c_i^\dagger c_j^\dagger c_k c_l \quad (2.1.11)$$

If a set of one-particle states  $\{|\phi_{\alpha_i}\rangle\}$  is known, the *matrix elements*  $O_{ij}^{(1)}$  and  $O_{ijkl}^{(2)}$  can be evaluated explicitly. An example will be discussed later in the context of the Hubbard model.

## 2.2. Thermodynamics and Statistics

In the following, a short overview of the necessary statistical basics for quantum systems is provided. After discussing the ideas of the canonical and grand-canonical ensemble for quantum systems and how to obtain thermodynamic properties, the Wick-Theorem for non-interacting systems is explained and applied to four-particle correlators which are evaluated numerically in the second paper (Ch. (6)).

### 2.2.1. Canonical and Grand-Canonical Ensemble for Fermions

The idea of statistical ensembles for describing physical systems with huge particle numbers has been established as early as 1902 by Gibbs [46]. Since it is the most relevant one for our work, we specifically focus on the quantum case of the grand-canonical ensemble for fermions, while explaining differences to the canonical case on the way. For broader introductions, we refer to [47, 48].

The grand-canonical ensemble describes a (quantum-)mechanical system which is in thermal equilibrium with a reservoir (i.e. a macroscopic surrounding). The system can exchange energy and particles with the reservoir, controlled by the chemical potential  $\mu$  and the temperature  $T$  (we will mostly write the inverse temperature  $\beta = 1/k_B T$  for simplicity), which are the thermodynamic variables. Mechanical variables such as



the volume  $V$  also play an important role, but are not considered explicitly here, as we mostly compare systems at equal size.

At the center stands the grand-canonical *partition function*  $\mathcal{Z}$ , which, for a given Hamiltonian  $H$  of a system, is defined as:

$$\mathcal{Z} = \text{Tr} \left( e^{-\beta H} \right) \quad (2.2.1)$$

The trace is a sum over all possible configurations of the system. With  $\mathcal{Z}$  as a normalization factor, the thermodynamic average  $\langle A \rangle$  of an operator  $A$  is defined as:

$$\langle A \rangle = \frac{1}{\mathcal{Z}} \text{Tr} \left( A e^{-\beta H} \right) \quad (2.2.2)$$

Compared to a (non-degenerate) ground state  $|\text{GS}\rangle$  at  $T = 0$ , where the expectation value would simply be  $\langle A \rangle = \langle \text{GS} | A | \text{GS} \rangle$ , one has to sum over all possible states weighted by the factor  $e^{-\beta H}$  in order to take thermal fluctuations into account.

As an example on how to evaluate such average quantities, we derive the average occupation  $\langle n_k \rangle$  (i.e. the Fermi function) for a non-interacting fermion system. The starting point is the fermionic, non-interacting grand-canonical Hamiltonian in its eigenbasis  $\{k\}$ :

$$H = \sum_k \varepsilon_k c_k^\dagger c_k - \mu \sum_k c_k^\dagger c_k = \sum_k (\varepsilon_k - \mu) n_k \quad (2.2.3)$$

First, the partition function is expressed as:

$$\begin{aligned} \mathcal{Z} &= \text{Tr} \left( e^{-\beta \sum_k (\varepsilon_k - \mu) n_k} \right) = \text{Tr} \left( \prod_k e^{-\beta (\varepsilon_k - \mu) n_k} \right) \\ &= \prod_k \sum_{n_k=0,1} e^{-\beta (\varepsilon_k - \mu) n_k} = \prod_k \left( 1 + e^{-\beta (\varepsilon_k - \mu)} \right) \end{aligned} \quad (2.2.4)$$

Next, the expectation value can be evaluated by expressing the operator  $n_k$  under trace as a derivative:

$$\begin{aligned} \langle n_k \rangle &= \frac{1}{\mathcal{Z}} \text{Tr} \left( n_k e^{-\beta H} \right) = \left( -\frac{1}{\beta} \right) \frac{1}{\mathcal{Z}} \frac{\partial}{\partial \varepsilon_k} \text{Tr} \left( e^{-\beta H} \right) \\ &= \frac{\partial}{\partial \varepsilon_k} \underbrace{\left( -\frac{1}{\beta} \ln \mathcal{Z} \right)}_{=: \Phi} \\ &= \frac{\partial}{\partial \varepsilon_k} \left( -\frac{1}{\beta} \sum_k \ln \left( 1 + e^{-\beta (\varepsilon_k - \mu)} \right) \right) \\ &= -\frac{1}{\beta} \frac{e^{-\beta (\varepsilon_k - \mu)}}{1 + e^{-\beta (\varepsilon_k - \mu)}} (-\beta) = \frac{1}{1 + e^{\beta (\varepsilon_k - \mu)}} \end{aligned} \quad (2.2.5)$$

The last expression is the well-known Fermi-function. As can be seen in this derivation, some average values can be obtained through partial derivatives (with respect to parameters in  $H$ ) of the grand canonical potential  $\Phi$ . In the canonical case, where the particle number  $N$  is fixed and consequently no  $\mu$ -term appears in  $H$ ,  $\Phi$  is the free energy of the system. Quantities such as the average total particle number  $N$  and the entropy  $S$  also follow from the grand canonical potential:

$$N = -\left.\frac{\partial\Phi}{\partial\mu}\right|_{T=\text{const.}}, \quad S = -\left.\frac{\partial\Phi}{\partial T}\right|_{\mu=\text{const.}} \quad (2.2.6)$$

In the following, we will show an example of Wick's theorem which, for non-interacting systems, allows us to obtain higher-order thermodynamic averages.

### 2.2.2. Wick-Theorem

*Wick's theorem* [49] provides a useful recipe for evaluating higher-order correlators of a non-interacting system. Since non-interacting systems are the basis of most perturbation theories, the theorem is of huge importance. To gain some intuition, and inspired by an exercise in [50], we go through the proof for static two-particle correlators, but it should be kept in mind that the same idea holds for both higher-order correlators and for time-dependent operators in the Heisenberg-picture as well. More extensive discussions and a general proof are found in [51, 52].

The starting point is a non-interacting, fermionic Hamiltonian  $H$  in its diagonal basis  $\{k\}$ :

$$H = \sum_k (\varepsilon_k - \mu) c_k^\dagger c_k \quad (2.2.7)$$

For the diagonal basis, where  $H$  does not allow hoppings between different states  $k_i$ , the expression  $\langle c_{k_1}^\dagger c_{k_2}^\dagger c_{k_3} c_{k_4} \rangle$  can only be nonzero if the indices fulfill the condition  $k_1 = k_4$ ,  $k_2 = k_3$  or  $k_1 = k_3$ ,  $k_2 = k_4$ . Thus, we have:

$$\langle c_{k_1}^\dagger c_{k_2}^\dagger c_{k_3} c_{k_4} \rangle = \langle n_{k_1} n_{k_2} \rangle \delta_{k_1, k_4} \delta_{k_2, k_3} - \langle n_{k_1} n_{k_2} \rangle \delta_{k_1, k_3} \delta_{k_2, k_4} \quad (2.2.8)$$

The minus-sign in the second term simply comes from the swapping of the fermionic operators.

Average occupations ( $\langle n_k \rangle = \langle c_k^\dagger c_k \rangle$ ) are given by the Fermi-function (Eq.(2.2.5)), and it is easy to see that for two different states  $k_1 \neq k_2$ :

$$\frac{\partial}{\partial \varepsilon_{k_1}} \langle n_{k_2} \rangle = 0 \quad (2.2.9)$$

We now evaluate the same expression (with a prefactor  $-1/\beta$  for convenience) from

the definition of thermodynamic averages (Eq.(2.2.2)):

$$\begin{aligned}
 -\frac{1}{\beta} \frac{\partial}{\partial \varepsilon_{k_1}} \langle n_{k_2} \rangle &= -\frac{1}{\beta} \frac{\partial}{\partial \varepsilon_{k_1}} \left[ \frac{\text{Tr} \left( n_{k_2} e^{-\beta \sum_k (\varepsilon_k - \mu) n_k} \right)}{\text{Tr} \left( e^{-\beta \sum_k (\varepsilon_k - \mu) n_k} \right)} \right] \\
 &= \frac{\text{Tr} \left( n_{k_1} n_{k_2} e^{-\beta \sum_k (\varepsilon_k - \mu) n_k} \right)}{\text{Tr} \left( e^{-\beta \sum_k (\varepsilon_k - \mu) n_k} \right)} \\
 &\quad - \frac{\text{Tr} \left( n_{k_2} e^{-\beta \sum_k (\varepsilon_k - \mu) n_k} \right) \text{Tr} \left( n_{k_1} e^{-\beta \sum_k (\varepsilon_k - \mu) n_k} \right)}{\left( \text{Tr} \left( e^{-\beta \sum_k (\varepsilon_k - \mu) n_k} \right) \right)^2} \\
 &= \frac{\text{Tr} \left( n_{k_1} n_{k_2} e^{-\beta H} \right)}{\mathcal{Z}} - \frac{\text{Tr} \left( n_{k_1} e^{-\beta H} \right) \text{Tr} \left( n_{k_2} e^{-\beta H} \right)}{\mathcal{Z}^2} \\
 &= \langle n_{k_1} n_{k_2} \rangle - \langle n_{k_1} \rangle \langle n_{k_2} \rangle
 \end{aligned} \tag{2.2.10}$$

Since this expression vanishes, we obtain:

$$\langle n_{k_1} n_{k_2} \rangle = \langle n_{k_1} \rangle \langle n_{k_2} \rangle \tag{2.2.11}$$

Thus, in the eigenbasis of  $H$ , we arrive at the following statement:

$$\langle c_{k_1}^\dagger c_{k_2}^\dagger c_{k_3} c_{k_4} \rangle = \langle c_{k_1}^\dagger c_{k_4} \rangle \langle c_{k_2}^\dagger c_{k_3} \rangle \delta_{k_1, k_4} \delta_{k_2, k_3} - \langle c_{k_1}^\dagger c_{k_3} \rangle \langle c_{k_2}^\dagger c_{k_4} \rangle \delta_{k_1, k_3} \delta_{k_2, k_4} \tag{2.2.12}$$

From this result, it is possible to go to an arbitrary, non-diagonal basis  $\{a\}$  through a unitary transformation, defined by coefficients  $q_{a_i, k_j}^{(*)}$ :

$$\langle c_{a_1}^\dagger c_{a_2}^\dagger c_{a_3} c_{a_4} \rangle = \sum_{a_1, a_2, a_3, a_4} q_{a_1, k_1}^* q_{a_2, k_2}^* q_{a_3, k_3} q_{a_4, k_4} \langle c_{k_1}^\dagger c_{k_2}^\dagger c_{k_3} c_{k_4} \rangle \tag{2.2.13}$$

Inserting Eq.(2.2.12) and evaluating the transformation leads to the final result:

$$\begin{aligned}
 \langle c_{a_1}^\dagger c_{a_2}^\dagger c_{a_3} c_{a_4} \rangle &= \sum_{a_1, a_2, a_3, a_4} q_{a_1, k_1}^* q_{a_2, k_2}^* q_{a_3, k_3} q_{a_4, k_4} \times \\
 &\quad \left( \langle c_{k_1}^\dagger c_{k_4} \rangle \langle c_{k_2}^\dagger c_{k_3} \rangle \delta_{k_1, k_4} \delta_{k_2, k_3} - \langle c_{k_1}^\dagger c_{k_3} \rangle \langle c_{k_2}^\dagger c_{k_4} \rangle \delta_{k_1, k_3} \delta_{k_2, k_4} \right) \\
 &= \langle c_{a_1}^\dagger c_{a_4} \rangle \langle c_{a_2}^\dagger c_{a_3} \rangle - \langle c_{a_1}^\dagger c_{a_3} \rangle \langle c_{a_2}^\dagger c_{a_4} \rangle
 \end{aligned} \tag{2.2.14}$$

In summary, higher-order correlators can be decomposed into a sum of all products of possible one-particle correlators. For the correct sign of the terms, one needs to keep track of the necessary number of permutations of the fermionic operators. More extensive derivations of a few specific four-particle correlators are shown next.

### 2.2.3. Example: Four-Particle Correlators

Here, a set of four-particle correlators which are measured during Monte-Carlo simulations in the second paper (Ch.(6)) are derived. Again, consider a non-interacting Hamiltonian, but this time, with a spin-index  $\sigma$ :

$$H = \sum_{\substack{ij \\ \sigma}} t_{ij} c_{i\sigma}^\dagger c_{j\sigma} - \mu \sum_{i\sigma} n_{i\sigma} \quad (2.2.15)$$

We define a *doublon*- and a *holon*-operator which measure whether a state (lattice site in the paper)  $i$  is doubly occupied or empty:

$$d_i = n_{i\uparrow} n_{i\downarrow} \quad (2.2.16)$$

$$h_i = (1 - n_{i\uparrow})(1 - n_{i\downarrow}) \quad (2.2.17)$$

In the paper, we examine how doublon-pairs, holon-pairs and doublon-holon-pairs are distributed on a lattice. In order to do so, one must measure the correlators  $\langle d_i d_j \rangle$ ,  $\langle h_i h_j \rangle$  and  $\langle d_i h_j \rangle$ . We start with the Wick-factorization of the holon-holon correlator:

$$\langle h_i h_j \rangle = \langle (1 - n_{i\uparrow})(1 - n_{i\downarrow})(1 - n_{j\uparrow})(1 - n_{j\downarrow}) \rangle \quad (2.2.18)$$

Multiplying out all the brackets and sorting the terms according to their order leads to:

$$\begin{aligned} \langle h_i h_j \rangle &= 1 - \langle n_{j\uparrow} \rangle - \langle n_{j\downarrow} \rangle - \langle n_{i\uparrow} \rangle - \langle n_{i\downarrow} \rangle \\ &\quad + \langle n_{j\uparrow} n_{j\downarrow} \rangle + \langle n_{i\uparrow} n_{i\downarrow} \rangle + \langle n_{i\uparrow} n_{j\uparrow} \rangle + \langle n_{i\uparrow} n_{j\downarrow} \rangle + \langle n_{i\downarrow} n_{j\uparrow} \rangle + \langle n_{i\downarrow} n_{j\downarrow} \rangle \\ &\quad - \langle n_{i\uparrow} n_{j\uparrow} n_{j\downarrow} \rangle - \langle n_{i\downarrow} n_{j\uparrow} n_{j\downarrow} \rangle - \langle n_{i\uparrow} n_{i\downarrow} n_{j\uparrow} \rangle - \langle n_{i\uparrow} n_{i\downarrow} n_{j\downarrow} \rangle \\ &\quad + \langle n_{i\uparrow} n_{i\downarrow} n_{j\uparrow} n_{j\downarrow} \rangle \end{aligned} \quad (2.2.19)$$

We now start Wick-factorizing the terms of order two and higher. It should be kept in mind that  $H$  does not flip any spins, i.e. terms such as  $\langle c_{i\uparrow}^\dagger c_{j\downarrow} \rangle$  are zero, which reduces the number of pairings that need to be considered. For the two-particle terms, the decompositions are:

$$\langle n_{i\uparrow} n_{i\downarrow} \rangle = \langle c_{i\uparrow}^\dagger c_{i\uparrow} c_{i\downarrow}^\dagger c_{i\downarrow} \rangle = \langle c_{i\uparrow}^\dagger c_{i\uparrow} \rangle \langle c_{i\downarrow}^\dagger c_{i\downarrow} \rangle \quad (2.2.20)$$

$$\langle n_{i\uparrow} n_{j\downarrow} \rangle = \langle c_{i\uparrow}^\dagger c_{i\uparrow} c_{j\downarrow}^\dagger c_{j\downarrow} \rangle = \langle c_{i\uparrow}^\dagger c_{i\uparrow} \rangle \langle c_{j\downarrow}^\dagger c_{j\downarrow} \rangle \quad (2.2.21)$$

$$\langle n_{i\uparrow} n_{j\uparrow} \rangle = \langle c_{i\uparrow}^\dagger c_{i\uparrow} c_{j\uparrow}^\dagger c_{j\uparrow} \rangle = \langle c_{i\uparrow}^\dagger c_{i\uparrow} \rangle \langle c_{j\uparrow}^\dagger c_{j\uparrow} \rangle + \langle c_{i\uparrow}^\dagger c_{j\uparrow} \rangle \langle c_{i\uparrow} c_{j\uparrow}^\dagger \rangle \quad (2.2.22)$$

Due to the absence of spin-flips, decomposing the three-particle terms becomes simple as only pairings with the same spin contribute:

$$\langle n_{i\uparrow} n_{j\uparrow} n_{j\downarrow} \rangle = \langle c_{i\uparrow}^\dagger c_{i\uparrow} c_{j\uparrow}^\dagger c_{j\uparrow} c_{j\downarrow}^\dagger c_{j\downarrow} \rangle = \langle c_{j\downarrow}^\dagger c_{j\downarrow} \rangle \left( \langle c_{i\uparrow}^\dagger c_{i\uparrow} \rangle \langle c_{j\uparrow}^\dagger c_{j\uparrow} \rangle + \langle c_{i\uparrow}^\dagger c_{j\uparrow} \rangle \langle c_{i\uparrow} c_{j\uparrow}^\dagger \rangle \right) \quad (2.2.23)$$

$$\langle n_{i\downarrow} n_{j\uparrow} n_{j\downarrow} \rangle = \langle c_{i\downarrow}^\dagger c_{i\downarrow} c_{j\uparrow}^\dagger c_{j\uparrow} c_{j\downarrow}^\dagger c_{j\downarrow} \rangle = \langle c_{j\uparrow}^\dagger c_{j\uparrow} \rangle \left( \langle c_{i\downarrow}^\dagger c_{i\downarrow} \rangle \langle c_{j\downarrow}^\dagger c_{j\downarrow} \rangle + \langle c_{i\downarrow}^\dagger c_{j\downarrow} \rangle \langle c_{i\downarrow} c_{j\downarrow}^\dagger \rangle \right) \quad (2.2.24)$$

$$\langle n_{j\uparrow} n_{i\uparrow} n_{i\downarrow} \rangle = \langle c_{j\uparrow}^\dagger c_{j\uparrow} c_{i\uparrow}^\dagger c_{i\uparrow} c_{i\downarrow}^\dagger c_{i\downarrow} \rangle = \langle c_{i\downarrow}^\dagger c_{i\downarrow} \rangle \left( \langle c_{j\uparrow}^\dagger c_{j\uparrow} \rangle \langle c_{i\uparrow}^\dagger c_{i\uparrow} \rangle + \langle c_{j\uparrow}^\dagger c_{i\uparrow} \rangle \langle c_{j\uparrow} c_{i\uparrow}^\dagger \rangle \right) \quad (2.2.25)$$

$$\langle n_{j\downarrow} n_{i\uparrow} n_{i\downarrow} \rangle = \langle c_{j\downarrow}^\dagger c_{j\downarrow} c_{i\uparrow}^\dagger c_{i\uparrow} c_{i\downarrow}^\dagger c_{i\downarrow} \rangle = \langle c_{i\uparrow}^\dagger c_{i\uparrow} \rangle \left( \langle c_{j\downarrow}^\dagger c_{j\downarrow} \rangle \langle c_{i\downarrow}^\dagger c_{i\downarrow} \rangle + \langle c_{j\downarrow}^\dagger c_{i\downarrow} \rangle \langle c_{j\downarrow} c_{i\downarrow}^\dagger \rangle \right) \quad (2.2.26)$$

Lastly, the four-particle correlator yields:

$$\begin{aligned} \langle n_{i\uparrow} n_{i\downarrow} n_{j\uparrow} n_{j\downarrow} \rangle &= \langle n_{i\uparrow} n_{j\uparrow} n_{i\downarrow} n_{j\downarrow} \rangle = \langle c_{i\uparrow}^\dagger c_{i\uparrow} c_{j\uparrow}^\dagger c_{j\uparrow} c_{i\downarrow}^\dagger c_{i\downarrow} c_{j\downarrow}^\dagger c_{j\downarrow} \rangle \\ &= \left( \langle c_{i\uparrow}^\dagger c_{i\uparrow} \rangle \langle c_{j\uparrow}^\dagger c_{j\uparrow} \rangle + \langle c_{i\uparrow}^\dagger c_{j\uparrow} \rangle \langle c_{i\uparrow} c_{j\uparrow}^\dagger \rangle \right) \\ &\quad \times \left( \langle c_{i\downarrow}^\dagger c_{i\downarrow} \rangle \langle c_{j\downarrow}^\dagger c_{j\downarrow} \rangle + \langle c_{i\downarrow}^\dagger c_{j\downarrow} \rangle \langle c_{i\downarrow} c_{j\downarrow}^\dagger \rangle \right) \end{aligned} \quad (2.2.27)$$

It is easy to see that this four-particle expectation value already corresponds to the doublon-doublon correlator, i.e.  $\langle d_i d_j \rangle$ . What is left is the doublon-holon correlator  $\langle d_i h_j \rangle$ , which we will multiply out in a similar fashion:

$$\begin{aligned} \langle d_i h_j \rangle &= \langle n_{i\uparrow} n_{i\downarrow} (1 - n_{j\uparrow}) (1 - n_{j\downarrow}) \rangle \\ &= \langle n_{i\uparrow} n_{i\downarrow} \rangle - \langle n_{i\uparrow} n_{i\downarrow} n_{j\uparrow} \rangle - \langle n_{i\uparrow} n_{i\downarrow} n_{j\downarrow} \rangle + \langle n_{i\uparrow} n_{i\downarrow} n_{j\uparrow} n_{j\downarrow} \rangle \end{aligned} \quad (2.2.28)$$

The individual terms can also be read off from the decompositions already done above.

### 2.3. Matsubara Formalism

Instead of solving a complex problem (i.e. an interacting many-particle system) in its entirety, it is a common approach to focus only on obtaining certain correlation functions (*Green's functions*) which already yield results such as the spectrum, electrical and thermal conductivity, magnetic susceptibilities etc. that can be verified in a laboratory. The Matsubara method [53] is a formalism which treats such a problem at thermal equilibrium. An extensive introduction (which we follow here) with proofs and derivations is given in [52], and a more compact introduction can be found in [51]. Here, we only go through the basic definitions of Green's functions and their properties. An introduction to diagrammatic techniques is also skipped, since the Monte Carlo methods used in later chapters often provide a direct access to Green's functions of interest.

Assuming a grand canonical Hamiltonian  $H$  (at an inverse temperature  $\beta = 1/k_B T$ ) with its diagonal basis  $\{k\}$ , and having time-dependent, fermionic operators such as  $c_{k\sigma}(t)$  ( $\sigma$  being the spin) in the Heisenberg picture, one can define a fermion Green's function as:

$$G_k(t, t') = \frac{1}{\mathcal{Z}} \text{Tr} \left( e^{-\beta H} c_{k\sigma}(t) c_{k\sigma}^\dagger(t') \right) \quad (2.3.1)$$

with  $c_{k\sigma}(t) = e^{itH} c_{k\sigma} e^{-itH}$  and  $\mathcal{Z} = \text{Tr} \left( e^{-\beta H} \right)$

A problem arises when one splits up the Hamiltonian into  $H = H_0 + V$ , with  $V$  containing the interaction terms, in order to do perturbation expansions. The  $V$ -term which is commonly treated as a perturbation appears both in the exponentials defining the time-dependency and the thermal factor  $e^{-\beta H}$ . The idea within the Matsubara formalism is to put these terms on equal footing by defining an *imaginary time*  $\tau = it$ , i.e. treating  $t$  and  $\beta$  as the real and imaginary parts of a complex variable. Arbitrary time-dependent Green's functions are then defined for  $-\beta \leq \tau \leq \beta$ :

$$G_k(\tau, \tau') = -\langle T_\tau c_{k\sigma}(\tau) c_{k\sigma}^\dagger(\tau') \rangle \quad (2.3.2)$$

with  $c_{k\sigma}(\tau) = e^{\tau H} c_{k\sigma} e^{-\tau H}$

$T_\tau$  is the time-ordering operator, which sorts the order of the operators that follow it so that the *earliest* times (i.e. closest to  $-\beta$ ) appear to the right. With the anticommutation relations of fermions, it can be shown that the Green's function only depends on time differences  $\tau - \tau'$ , leading to an equivalent definition of  $G$ :

$$G_k(\tau) = -\langle T_\tau c_{k\sigma}(\tau) c_{k\sigma}^\dagger(0) \rangle \quad (2.3.3)$$

The following symmetry holds for fermions:

$$G(\tau) = -G(\tau + \beta) \quad \text{for} \quad -\beta < \tau < 0 \quad (2.3.4)$$

With these properties, the Fourier expansion of  $G$  can be defined:

$$G(\tau) = \frac{1}{\beta} \sum_n e^{-i\omega_n \tau} G(i\omega_n) \quad (2.3.5)$$

$$G(i\omega_n) = \int_0^\beta d\tau e^{i\omega_n \tau} G(\tau) \quad (2.3.6)$$

$$\text{with } \omega_n = \frac{(2n+1)\pi}{\beta} \quad (2.3.7)$$

$\omega_n$  are known as the fermionic *Matsubara frequencies*. For the non-interacting Hamiltonian in its diagonal basis, i.e.

$$H = H_0 = \sum_k (\varepsilon_k - \mu) c_k^\dagger c_k$$

the single-particle Green's function can be evaluated exactly in both representations:

$$G_k^0(\tau) = -e^{-(\varepsilon_k - \mu)\tau} [\Theta(\tau) - n_F(\varepsilon_k - \mu)] \quad (2.3.8)$$

$$G_k^0(i\omega_n) = \frac{1}{i\omega_n - (\varepsilon_k - \mu)} \quad (2.3.9)$$

$\Theta(\tau)$  denotes the Heaviside step function, while  $n_F(E)$  is the Fermi function (see Eq.(2.2.5)).

For the interacting case, where a term  $V \neq 0$  appears in the Hamiltonian, it can be shown that the interacting Green's function fulfills the *Dyson equation*:

$$G_k(i\omega_n) = G_k^0(i\omega_n) + G_k^0(i\omega_n) \Sigma_k(i\omega_n) G_k(i\omega_n) \quad (2.3.10)$$

This can be rewritten as:

$$G_k(i\omega_n) = \frac{1}{i\omega_n - (\varepsilon_k - \mu) - \Sigma_k(i\omega_n)} \quad (2.3.11)$$

The *self-energy*  $\Sigma_k(i\omega_n)$  contains all many-particle effects, and describes how the  $k$ - and frequency-dependency changes compared to the non-interacting case. Perturbative, diagrammatic methods have the goal of obtaining an accurate self-energy within certain approximations.

Lastly, it should be mentioned that, if a Matsubara Green's function  $G(i\omega_n)$  is known, one can obtain the *retarded* Green's function  $G_k^R(\omega)$  by performing the analytical continuation  $i\omega_n \rightarrow \omega + i\delta$ , where  $\omega$  is a real frequency (in contrast to the discrete, imaginary  $i\omega_n$ ) and a small  $\delta$  is introduced to guarantee convergence at large times:

$$G(i\omega_n) \xrightarrow{i\omega_n \rightarrow \omega + i\delta} G_k^R(\omega) \quad (2.3.12)$$

The retarded Green's function is important because its imaginary part leads to the *spectral function*  $A_k(\omega)$ :

$$A_k(\omega) = -2 \text{Im}(G_k^R(\omega)) \quad (2.3.13)$$

As the name suggests,  $A_k(\omega)$  can be measured through spectroscopy, validating or invalidating theories and approximations used to obtain  $\Sigma_k(i\omega_n)$ .

## 2.4. The Tight-Binding Model

Within the Born-Oppenheimer approximation [50], due to the big difference in mass between electrons and protons/neutrons, electron and core dynamics are seen as decoupled. If, additionally, the electron-electron interaction is neglected, one arrives at an electronic one-particle problem known as the *tight-binding model*. Assuming a periodic lattice with one orbital per lattice site, the Hamiltonian  $H$  reads as:

$$H = \sum_{ij,\sigma} t_{ij} c_{i\sigma}^\dagger c_{j\sigma} \quad (2.4.1)$$

The atomic orbitals are assumed to be strongly bound to their cores (hence, the name of the model). For  $i \neq j$ , the matrix elements  $t_{ij}$  describe the *hopping* of electrons from the site  $j$  to  $i$ . The diagonal elements  $t_{ii} = \varepsilon_0 - \mu$  contain the orbital energy  $\varepsilon_0$  (often set to zero) and the chemical potential  $\mu$ .

An important system which is the focus within this thesis is the square lattice. For hoppings between nearest neighbours  $\langle i, j \rangle$  and next nearest neighbours  $\langle\langle i, j \rangle\rangle$  with amplitudes  $t$  and  $t'$ , respectively, we show that by introducing the spatial Fourier transform of the fermionic operators,  $H$  can be diagonalized. The Hamiltonian  $H$  for this specific case reads as:

$$H = -t \underbrace{\sum_{\langle i,j \rangle, \sigma} (c_{i\sigma}^\dagger c_{j\sigma} + \text{h.c.})}_{H_t} - t' \underbrace{\sum_{\langle\langle i,j \rangle\rangle, \sigma} (c_{i\sigma}^\dagger c_{j\sigma} + \text{h.c.})}_{H_{t'}} - \mu \sum_{i\sigma} n_{i\sigma} \quad (2.4.2)$$

The Fourier transform of the creation and annihilation operators is defined as:

$$c_{i\sigma} = \frac{1}{\sqrt{N}} \sum_{\mathbf{k}} e^{-i\mathbf{k}\mathbf{R}_i} c_{\mathbf{k}\sigma} \quad , \quad c_{i\sigma}^\dagger = \frac{1}{\sqrt{N}} \sum_{\mathbf{k}} e^{+i\mathbf{k}\mathbf{R}_i} c_{\mathbf{k}\sigma}^\dagger \quad (2.4.3)$$

$N$  is the total number of lattice sites.  $\mathbf{R}_i$  contains the coordinates of the lattice site  $i$ , while, for periodic systems, sum over  $\mathbf{k}$ -vectors go over the so-called Brillouin-zone.

The last term with the occupation number operators transforms directly as:

$$\sum_{i\sigma} c_{i\sigma}^\dagger c_{i\sigma} = \frac{1}{N} \sum_{\mathbf{k}\mathbf{k}'\sigma} \sum_i e^{i(\mathbf{k}-\mathbf{k}')\mathbf{R}_i} c_{\mathbf{k}\sigma}^\dagger c_{\mathbf{k}'\sigma} = \sum_{\mathbf{k}\mathbf{k}'\sigma} \delta_{\mathbf{k}\mathbf{k}'} c_{\mathbf{k}\sigma}^\dagger c_{\mathbf{k}'\sigma} = \sum_{\mathbf{k}\sigma} c_{\mathbf{k}\sigma}^\dagger c_{\mathbf{k}\sigma} \quad (2.4.4)$$

Here, we made use of the fact that, due to orthogonality of the plane waves on a periodic lattice, the  $i$ -sum reduces to  $\sum_i e^{i(\mathbf{k}-\mathbf{k}')\mathbf{R}_i} = N \delta_{\mathbf{k}\mathbf{k}'}$ . For the transformation of the hopping terms, it is helpful to rewrite sums over e.g.  $\langle i, j \rangle$  as  $\sum_{\langle i, j \rangle} \dots \rightarrow \sum_{i\delta}$ , where  $\delta$  are the displacements from the lattice site  $i$ , i.e.  $j \rightarrow i + \delta$  (with the vector  $\mathbf{R}_i + \delta$ ). The Fourier transform of  $H_t$  can then be evaluated:

$$\begin{aligned} H_t &= \sum_{i\delta\sigma} c_{i\sigma}^\dagger c_{i+\delta,\sigma} = \frac{1}{N} \sum_{\mathbf{k}\mathbf{k}'\sigma} \sum_{i\delta} \underbrace{e^{+i\mathbf{k}\mathbf{R}_i} e^{-i\mathbf{k}'\mathbf{R}_i}}_{e^{i(\mathbf{k}-\mathbf{k}')\mathbf{R}_i}} e^{-i\mathbf{k}'\delta} c_{\mathbf{k}\sigma}^\dagger c_{\mathbf{k}'\sigma} \\ &= \sum_{\mathbf{k}\mathbf{k}'\sigma} \sum_{\delta} \delta_{\mathbf{k}\mathbf{k}'} e^{-i\mathbf{k}'\delta} c_{\mathbf{k}\sigma}^\dagger c_{\mathbf{k}'\sigma} = \sum_{\mathbf{k}\sigma} \left( \sum_{\delta} e^{-i\mathbf{k}\delta} \right) c_{\mathbf{k}\sigma}^\dagger c_{\mathbf{k}\sigma} \end{aligned} \quad (2.4.5)$$



On the square lattice, assuming a lattice constant of  $a = 1$ , the vectors connecting adjacent sites are:

$$\boldsymbol{\delta} = \left\{ \begin{pmatrix} 1 \\ 0 \end{pmatrix}, \begin{pmatrix} -1 \\ 0 \end{pmatrix}, \begin{pmatrix} 0 \\ 1 \end{pmatrix}, \begin{pmatrix} 0 \\ -1 \end{pmatrix} \right\} \quad (2.4.6)$$

With the identity  $2 \cos(x) = e^{ix} + e^{-ix}$ , the  $\delta$ -sum in Eq.(2.4.5) yields:

$$\sum_{\boldsymbol{\delta}} e^{-i\mathbf{k}\boldsymbol{\delta}} = e^{-ik_x} + e^{+ik_x} + e^{-ik_y} + e^{+ik_y} = -2(\cos(k_x) + \cos(k_y)) \quad (2.4.7)$$

At this point, it should be noted that the Fourier transform of  $H_t'$  can be done in a similar fashion. The only difference is a different set of displacement vectors. For next nearest neighbors, the vectors are:

$$\boldsymbol{\delta} = \left\{ \begin{pmatrix} 1 \\ 1 \end{pmatrix}, \begin{pmatrix} 1 \\ -1 \end{pmatrix}, \begin{pmatrix} -1 \\ -1 \end{pmatrix}, \begin{pmatrix} -1 \\ 1 \end{pmatrix} \right\} \quad (2.4.8)$$

The  $\delta$ -sum for this case then reads as:

$$\begin{aligned} \sum_{\boldsymbol{\delta}} e^{-i\mathbf{k}\boldsymbol{\delta}} &= e^{-ik_x} e^{-ik_y} + e^{-ik_x} e^{+ik_y} + e^{+ik_x} e^{+ik_y} + e^{+ik_x} e^{-ik_y} \\ &= \left( e^{-ik_x} + e^{+ik_x} \right) \left( e^{-ik_y} + e^{+ik_y} \right) = 4 \cos(k_x) \cos(k_y) \end{aligned} \quad (2.4.9)$$

In summary, the square lattice model with hoppings between nearest and next nearest neighbours is diagonalized through the spatial Fourier transform, and one obtains:

$$\begin{aligned} H &= \sum_{\mathbf{k}\sigma} \varepsilon_{\mathbf{k}} c_{\mathbf{k}\sigma}^{\dagger} c_{\mathbf{k}\sigma} \quad \text{with} \\ \varepsilon_{\mathbf{k}} &= -2t(\cos(k_x) + \cos(k_y)) - 4t' \cos(k_x) \cos(k_y) - \mu \end{aligned} \quad (2.4.10)$$

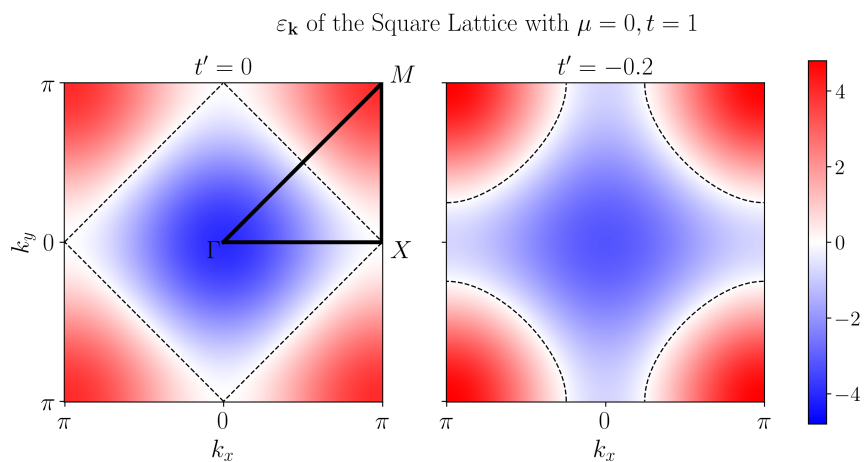


Figure 2.4.1: Color-plots of the dispersion for a square lattice on the first Brillouin zone, with hopping between nearest ( $t$ ) and next-nearest neighbours ( $t'$ ). The dashed lines represent the Fermi-surface and arcs.

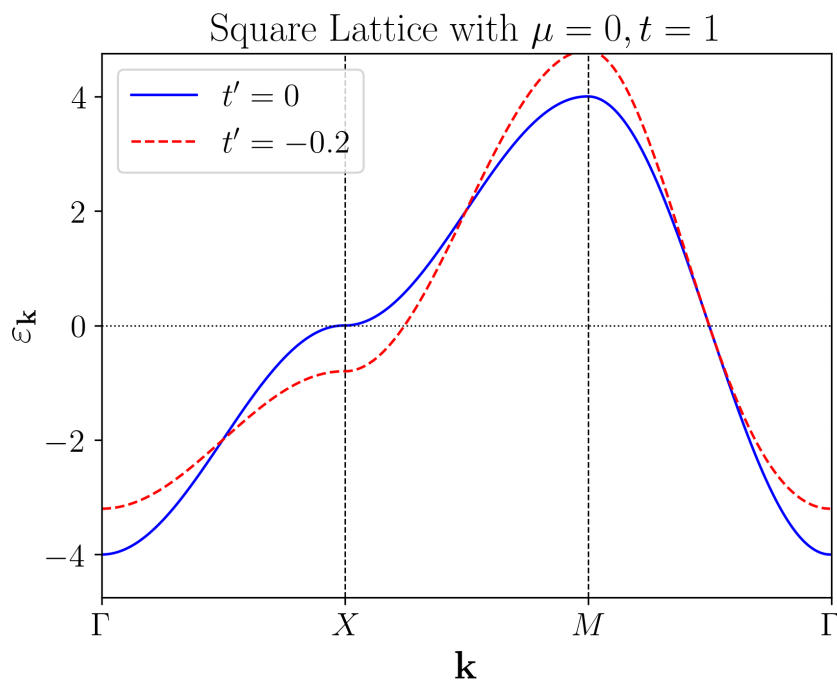


Figure 2.4.2: Line-plots of the dispersion along the high-symmetry lines for a square lattice on the first Brillouin zone, with hopping between nearest ( $t$ ) and next-nearest neighbours ( $t'$ ).

## 2.5. The Hubbard Model

In strongly correlated systems, the interaction between electrons can not be neglected as in the previous chapter. Assuming again the simple case of a (static) lattice with one electronic orbital per site, the interacting Hamiltonian generally reads as:

$$H = \sum_{\substack{ij \\ \sigma\sigma'}} t_{ij} c_{i\sigma}^\dagger c_{j\sigma} + \sum_{ijkl} U_{ijkl} c_{i\sigma}^\dagger c_{j\sigma'}^\dagger c_{k\sigma'} c_{l\sigma} \quad (2.5.1)$$

Following Eq.(2.1.11), and assuming a set of localized real-space orbitals  $\{\phi_i(\mathbf{r})\}$  with a distance-dependent interaction  $V(|\mathbf{r} - \mathbf{r}'|)$ , the matrix elements scale as:

$$U_{ijkl} \propto \int d^3r \int d^3r' \phi_i^*(\mathbf{r}) \phi_j^*(\mathbf{r}') V(|\mathbf{r} - \mathbf{r}'|) \phi_k(\mathbf{r}) \phi_l(\mathbf{r}') \quad (2.5.2)$$

From the structure of this integral, it is intuitive to see that the *local* interaction, i.e. the matrix element  $U_{iiii}$ , is generally the dominant one. Thus, the simplest approximation of the interaction one can make is to neglect all elements except  $U = U_{iiii}$ , which is known as the *Hubbard model* [1, 2, 3]:

$$H = \sum_{\substack{ij \\ \sigma}} t_{ij} c_{i\sigma}^\dagger c_{j\sigma} + U \sum_i n_{i\uparrow} n_{i\downarrow} \quad (2.5.3)$$

One should note that, on a periodic lattice, the one-particle part of  $H$  is diagonal in  $\mathbf{k}$ -space, while the purely local interaction is already diagonal in real space. Thus, if either the  $t_{ij}$  or  $U$  are small, one may treat it perturbatively. For example, assuming hopping between adjacent sites with an amplitude  $t$  only, and  $U \gg t$ , one obtains, for half filling, an effective Heisenberg model  $H \approx (-4t^2/U) \sum_{\langle i,j \rangle} \mathbf{S}_i \cdot \mathbf{S}_j$  [8] or a so-called  $t-J$ -model [54] for the doped case. However, although the model seems simple, many interesting phenomena such as a metal-insulator transition [3, 6] occur in the parameter space which is not trivially accessible. Furthermore, ground states with vastly different properties may be very close to each other, which makes accurate predictions difficult. For example, on a half-filled bipartite lattice, the ground state is an antiferromagnetic *spin density wave* (SDW), while removing a single electron from the lattice can lead to a ferromagnetic state in the Nagaoka limit [9]. In dimensions  $d < 3$ , however, such orderings are destroyed for  $T > 0$  due to Mermin-Wagner fluctuations [55].

While the one-dimensional Hubbard model can be solved [7], the two-dimensional case, which is of interest in this thesis, has been an ongoing research topic for decades. Tremendous progress has been made (more detailed reviews can be found in [56, 57, 58]), although the doped 2D case at finite temperature remains a difficult problem. To that end, we discuss and implement a novel dual fermion method in the later chapters.

## 2.6. Extended Hubbard Models

So-called *extended* Hubbard models include certain nonlocal interactions in addition to the Hubbard- $U$ -term. In three-dimensional systems, they are often neglected due to generally stronger screening of the Coulomb interaction between electrons. However, this screening is strongly reduced in the two-dimensional case, which applies to many novel quantum materials. One example is to include matrix elements which represent a density-density interaction between electrons ( $i = k$  and  $j = l$  in Eq.(2.5.1)). The one-orbital Hamiltonian then reads as

$$H = \sum_{\substack{ij \\ \sigma}} t_{ij} c_{i\sigma}^\dagger c_{j\sigma} + U \sum_i n_{i\uparrow} n_{i\downarrow} + \underbrace{\frac{1}{2} \sum_{\substack{i \neq j \\ \sigma \sigma'}} V_{ij} n_{i\sigma} n_{j\sigma'}}_{H_V} \quad (2.6.1)$$

with the matrix elements:

$$V_{ij} \propto \int d^3 r \int d^3 r' |\phi_i(\mathbf{r})|^2 V(|\mathbf{r} - \mathbf{r}'|) |\phi_j(\mathbf{r}')|^2 \quad (2.6.2)$$

The factor  $1/2$  in  $H_V$  prevents double counting of terms. The biggest contribution, which is generally the density-density interaction between electrons on adjacent sites, favors a so-called *charge density wave* (CDW) [27, 28, 29] at half filling on a bipartite lattice. This competes against the spin density wave ground state of the purely local Hubbard model and influences many other properties, which makes the phase diagram more complex. For cuprates such as  $\text{La}_2\text{CuO}_4$  and  $\text{HgBa}_2\text{CuO}_4$ , downfoldings to a one-band model [59] estimate  $V_{ij}$  for nearest neighbours to be on a scale of  $U/V \approx 4 \dots 5$ , which is large enough to potentially affect the properties of the material.

Another possible extension is to include the *exchange* interaction between two electrons, which corresponds to the matrix elements  $J_{ij}$  with  $i = l$  and  $j = k$  in Eq.(2.5.1):

$$H = \sum_{\substack{ij \\ \sigma}} t_{ij} c_{i\sigma}^\dagger c_{j\sigma} + U \sum_i n_{i\uparrow} n_{i\downarrow} + \underbrace{\frac{1}{2} \sum_{\substack{i \neq j \\ \sigma \sigma'}} J_{ij} c_{i\sigma}^\dagger c_{j\sigma'}^\dagger c_{i\sigma'} c_{j\sigma}}_{H_J} \quad (2.6.3)$$

$$J_{ij} \propto \int d^3 r \int d^3 r' \phi_i^*(\mathbf{r}) \phi_j^*(\mathbf{r}') V(|\mathbf{r} - \mathbf{r}'|) \phi_j(\mathbf{r}) \phi_i(\mathbf{r}') \quad (2.6.4)$$

Compared to the direct density-density interaction, it is not intuitively clear from the structure of  $H_J$  and  $J_{ij}$  which ground state is favored. In order to gain an understanding of its behaviour,  $H_J$  can be rewritten in terms of the following, dimensionless spin-1/2-operators:

$$S_i^+ = c_{i\uparrow}^\dagger c_{i\downarrow}, \quad S_i^- = c_{i\downarrow}^\dagger c_{i\uparrow}, \quad S_i^z = \frac{1}{2} (n_{i\uparrow} - n_{i\downarrow}) \quad (2.6.5)$$

$$S_i^x S_j^x + S_i^y S_j^y = \frac{1}{2} (S_i^+ S_j^- + S_i^- S_j^+) \quad (2.6.6)$$

The operators in  $H_J$  are then expressed as:

$$\begin{aligned}
 \sum_{\sigma\sigma'} c_{i\sigma}^\dagger c_{j\sigma'}^\dagger c_{i\sigma'} c_{j\sigma} &= \sum_{\sigma} \left( \underbrace{-n_{i\sigma} n_{j\sigma}}_{\sigma=\sigma'} + \underbrace{c_{i\sigma}^\dagger c_{j\bar{\sigma}}^\dagger c_{i\bar{\sigma}} c_{j\sigma}}_{\sigma \neq \sigma'} \right) \\
 &= -(n_{i\uparrow} n_{j\uparrow} + n_{i\downarrow} n_{j\downarrow}) - \sum_{\sigma} \underbrace{c_{i\sigma}^\dagger c_{i\bar{\sigma}} c_{j\bar{\sigma}}^\dagger c_{j\sigma}}_{S_i^+ S_j^- + S_i^- S_j^+} \\
 &= - \left( 2(S_i^x S_j^x + S_i^y S_j^y) + n_{i\uparrow} n_{j\uparrow} + n_{i\downarrow} n_{j\downarrow} \right) \quad (2.6.7)
 \end{aligned}$$

The density-density terms can be written as:

$$\begin{aligned}
 n_{i\uparrow} n_{j\uparrow} + n_{i\downarrow} n_{j\downarrow} &= \frac{1}{2}(n_{i\uparrow} - n_{i\downarrow})(n_{j\uparrow} - n_{j\downarrow}) + \frac{1}{2}(n_{i\uparrow} + n_{i\downarrow})(n_{j\uparrow} + n_{j\downarrow}) \\
 &= 2S_i^z S_j^z + \frac{1}{2} \sum_{\sigma\sigma'} n_{i\sigma} n_{j\sigma'} \quad (2.6.8)
 \end{aligned}$$

With these reformulations, we arrive at the final expression for the nonlocal exchange interaction:

$$\sum_{\sigma\sigma'} c_{i\sigma}^\dagger c_{j\sigma'}^\dagger c_{i\sigma'} c_{j\sigma} = -2 \mathbf{S}_i \cdot \mathbf{S}_j - \frac{1}{2} \sum_{\sigma\sigma'} n_{i\sigma} n_{j\sigma'} \quad (2.6.9)$$

For  $J > 0$ , the spin-spin interaction prefers a ferromagnetic configuration, and the smaller density-density term is attractive. The interplay between  $H_J$  and the kinetic, antiferromagnetic exchange effects of the Hubbard model is extensively discussed in the first publication, while the effects of  $H_V$  are the topic of the second paper (Ch.(5) and (6), respectively).

---

### 3. Peierls-Feynman-Bogoliubov Variational Principle

Here, we review and apply the method known as Peierls-Feynman-Bogoliubov variational principle (in literature, often only referred to as the Bogoliubov variational principle). It allows us to map an arbitrary system, usually too difficult to solve numerically, onto a simpler one. For the basics and proofs, we will closely follow the comparably compact and intuitive derivation in [50]. For a more extensive discussion, we also refer to [60] and the review in [31].

#### 3.1. Formalism

Let us consider a grand canonical system defined by its Hamiltonian  $H$  and the chemical potential  $\mu$ . We investigate the following functional for an arbitrary density operator  $\rho$ :

$$\tilde{\Phi}[\rho] = \text{Tr} \left[ \rho \left( H - \mu N + \frac{1}{\beta} \ln(\rho) \right) \right] \quad (3.1.1)$$

$\beta = 1/k_B T$  is the inverse temperature, while  $N$  denotes the particle number. Inserting the grand canonical density operator  $\rho_G$  into Eq.(3.1.1) explicitly leads to:

$$\rho_G = \frac{1}{\mathcal{Z}_G} e^{-\beta(H-\mu N)} \quad , \quad \mathcal{Z}_G = \text{Tr} \left( e^{-\beta(H-\mu N)} \right) \quad (3.1.2)$$

$$\begin{aligned} \tilde{\Phi}[\rho_G] &= \text{Tr} \left[ \rho_G \left( H - \mu N + \frac{1}{\beta} \ln(e^{-\beta(H-\mu N)}) - \frac{1}{\beta} \ln \mathcal{Z}_G \right) \right] \\ &= -\frac{1}{\beta} \ln \mathcal{Z}_G \underbrace{\text{Tr}(\rho_G)}_{=1} \equiv \Phi_H \end{aligned} \quad (3.1.3)$$

The functional  $\tilde{\Phi}[\rho]$  yields the system's grand potential (or free energy in the canonical case)  $\Phi_H$  if we set  $\rho = \rho_G$ . The next step is to prove that, for an arbitrary density operator  $\rho$ , the *Bogoliubov inequality* [61] holds:

$$\tilde{\Phi}[\rho_G] \leq \tilde{\Phi}[\rho] \quad (3.1.4)$$

Its rather intuitive meaning is that a system's grand potential is minimized by its actual density operator  $\rho_G$ . Thus, even if we cannot evaluate  $\rho_G$  due to the complexity of a system, we can find upper bounds for  $\Phi_H$  by defining trial density operators  $\rho$ . This is the basis for development of many variational approaches.

As a starting point for the proof of Eq.(3.1.4), we first show that, for two density operators  $\rho, \rho'$ , the *Gibbs inequality* [62] holds:

$$\text{Tr}(\rho \ln(\rho)) \geq \text{Tr}(\rho \ln(\rho')) \quad (3.1.5)$$

Let  $\{|i\rangle\}$  and  $\{|j\rangle\}$  be the eigenbases of  $\rho$  and  $\rho'$ , respectively. Then, by using the inequality  $\ln x \leq x - 1$ , we get:

$$\begin{aligned}
 \text{Tr} [\rho \ln(\rho')] - \text{Tr} [\rho \ln(\rho)] &= \sum_i \{ \rho_i (\langle i | [\ln(\rho')] | i \rangle - \langle i | i \rangle \ln(\rho_i)) \} \\
 &= \sum_{ij} \{ \rho_i (\langle i | j \rangle \ln(\rho'_j) \langle j | i \rangle - \langle i | j \rangle \langle j | i \rangle \ln(\rho_i)) \} \\
 &= \sum_{ij} \{ \rho_i |\langle i | j \rangle|^2 (\ln(\rho'_j) - \ln(\rho_i)) \} \\
 &= \sum_{ij} \left\{ \rho_i |\langle i | j \rangle|^2 \ln \left( \frac{\rho'_j}{\rho_i} \right) \right\} \\
 &\leq \sum_{ij} \left\{ \rho_i |\langle i | j \rangle|^2 \left( \frac{\rho'_j}{\rho_i} - 1 \right) \right\} \\
 &= \sum_{ij} (|\langle i | j \rangle|^2 \rho'_j - |\langle i | j \rangle|^2 \rho_i) \\
 &= \text{Tr}(\rho') - \text{Tr}(\rho) = 0
 \end{aligned} \tag{3.1.6}$$

Now, we consider  $\tilde{\Phi}[\rho]$  for an arbitrary density operator  $\rho$  and, by using Eq.(3.1.5), show that Eq.(3.1.4) holds:

$$\begin{aligned}
 \tilde{\Phi}[\rho] &= \text{Tr} (\rho(H - \mu N)) + \frac{1}{\beta} \text{Tr} (\rho \ln \rho) \\
 &\geq \text{Tr} (\rho(H - \mu N)) + \frac{1}{\beta} \text{Tr} (\rho \ln \rho_G) \\
 &= \text{Tr} (\rho(H - \mu N)) + \frac{1}{\beta} \text{Tr} [\rho(-\beta(H - \mu N) - \ln \mathcal{Z}_G)] \\
 &= -\frac{1}{\beta} \ln \mathcal{Z}_G = \tilde{\Phi}[\rho_G]
 \end{aligned} \tag{3.1.7}$$

Let  $\tilde{H}(x_1, x_2, \dots)$  be an effective Hamiltonian which depends on a set of (variational) parameters  $(x_1, x_2, \dots)$ . We insert its density operator  $\rho_{\tilde{H}}$  into the functional  $\tilde{\Phi}$ :

$$\begin{aligned}
 \tilde{\Phi}[\rho_{\tilde{H}}] &= \text{Tr} \left[ \rho_{\tilde{H}} \left( H - \mu N + \frac{1}{\beta} \ln \rho_{\tilde{H}} \right) \right] \\
 &= \text{Tr} \left[ \rho_{\tilde{H}} \left( H - \mu N - \tilde{H} + \mu N - \frac{1}{\beta} \ln \mathcal{Z}_{\tilde{H}} \right) \right] \\
 &= \text{Tr} \left[ \rho_{\tilde{H}} (H - \tilde{H}) \right] - \frac{1}{\beta} \ln \mathcal{Z}_{\tilde{H}} \\
 &= \langle H - \tilde{H} \rangle_{\tilde{H}} - \frac{1}{\beta} \ln \mathcal{Z}_{\tilde{H}}
 \end{aligned} \tag{3.1.8}$$

Applying the Bogoliubov inequality Eq.(3.1.4) then leads to:

$$\Phi_H \leq \langle H - \tilde{H} \rangle_{\tilde{H}} + \Phi_{\tilde{H}} \tag{3.1.9}$$

$\Phi_H$  denotes the original system's grand potential while  $\Phi_{\tilde{H}}$  is the grand potential of the effective (or auxiliary) model  $\tilde{H}$ . Adjusting the auxiliary model's parameters  $(x_1, x_2, \dots)$  in a variational fashion which minimizes the right hand side of the expression in Eq.(3.1.9) provides the effective  $\tilde{H}$  which approximates the original model's grand potential as good as possible.

Assuming an interacting problem  $H$ , the simplest choice of  $\tilde{H}$  would be a non-interacting system, which leads to a variety of so-called *mean-field* theories. We shall discuss a common textbook example in the next subsection. However, this approach is often only a first step and fails to capture behaviour and properties related to strong correlations. As such, we will choose  $\tilde{H}$ 's which still contain (less complex) interactions, but are easier to solve than the original problem, in order to get a more accurate description of  $H$ .

### 3.2. Example: Mean-Field Theory of the Heisenberg-Model

As a simple example on how mean-field theories can be derived from the variational principle generally, we formulate a mean-field theory for the Heisenberg model within the formalism and show that the results are indeed the same as common textbook solutions which are based on decoupling interaction terms into specific channels.

Let us start with a Heisenberg Hamiltonian which couples spins on adjacent lattice sites  $\langle i, j \rangle$  with a coupling constant  $J$ :

$$H = -J \sum_{\langle i, j \rangle} \hat{S}_i \cdot \hat{S}_j \quad (3.2.1)$$

For simplicity, we stay within a canonical framework by assuming that there is one spin on each lattice site. In textbook examples, one approximates this Hamiltonian by assuming that the spins do not interact directly, but rather only feel an average magnetic field (hence, the naming *mean-field*) which stems from all the other spins:

$$H \approx -J \sum_{\langle i, j \rangle} \left( \langle \hat{S}_i \rangle \hat{S}_j + \langle \hat{S}_j \rangle \hat{S}_i - \langle \hat{S}_i \rangle \langle \hat{S}_i \rangle \right)$$

Since this approximate Hamiltonian is now non-interacting (as  $\langle \hat{S}_i \rangle$  are only expectation values), one can evaluate thermodynamic properties like the magnetization, which however will depend on itself, leading to a self-consistency equation.

Here, we derive the same solution by defining an auxiliary system  $\tilde{H}$  as a simple paramagnet within an effective, magnetic field  $\tilde{B}$  in  $z$ -direction:

$$\tilde{H} = -\tilde{B} \sum_i S_i^z \quad (3.2.2)$$

For the spins, we set  $\hbar = 1$ , i.e.  $S_i^z = \pm 1/2$  for electrons. We now wish to evaluate



and minimize the functional  $\tilde{\Phi}$  from Eq.(3.1.9):

$$\begin{aligned}\tilde{\Phi} &= \langle H - \tilde{H} \rangle_{\tilde{H}} + \Phi_{\tilde{H}} \\ &= -J \sum_{\langle i,j \rangle} \langle \hat{S}_i \cdot \hat{S}_j \rangle_{\tilde{H}} + \tilde{B} \sum_i \langle S_i^z \rangle_{\tilde{H}} + \Phi_{\tilde{H}}\end{aligned}\quad (3.2.3)$$

As  $\tilde{H}$  is non-interacting, we can evaluate all components analytically. To that end, we start with the partition function and the free energy  $\Phi_{\tilde{H}}$ :

$$\begin{aligned}\mathcal{Z} &= \text{Tr} \left( e^{-\beta \tilde{H}} \right) = \text{Tr} \left( \prod_i e^{\beta \tilde{B} S_i^z} \right) = \prod_i \sum_{S_i^z = \pm 1/2} e^{\beta \tilde{B} S_i^z} \\ \mathcal{Z} &= \left( e^{-\frac{\beta \tilde{B}}{2}} + e^{+\frac{\beta \tilde{B}}{2}} \right)^N = \left[ 2 \cosh \left( \frac{\beta \tilde{B}}{2} \right) \right]^N\end{aligned}\quad (3.2.4)$$

$$\Phi_{\tilde{H}} = -\frac{1}{\beta} \ln \mathcal{Z} = -\frac{N}{\beta} \ln \left[ 2 \cosh \left( \frac{\beta \tilde{B}}{2} \right) \right]\quad (3.2.5)$$

From the free energy  $\Phi_{\tilde{H}}$ , we derive the total magnetization via the derivative:

$$\sum_i \langle S_i^z \rangle_{\tilde{H}} = -\frac{\partial \Phi_{\tilde{H}}}{\partial \tilde{B}} = \frac{N}{2} \tanh \left( \frac{\beta \tilde{B}}{2} \right)\quad (3.2.6)$$

The product  $\langle \hat{S}_i \cdot \hat{S}_j \rangle_{\tilde{H}}$  can be Wick-factorized and, considering that  $\tilde{H}$  does not flip any spins (i.e.  $\langle S_i^{x,y} \rangle = 0$ ), only products of Spin- $z$ -components remain:

$$\sum_{\langle i,j \rangle} \langle \hat{S}_i \cdot \hat{S}_j \rangle_{\tilde{H}} = \sum_{\langle i,j \rangle} \langle S_i^z \rangle_{\tilde{H}} \langle S_j^z \rangle_{\tilde{H}} = \frac{NZ}{2} \langle S_i^z \rangle_{\tilde{H}}^2 = \frac{NZ}{8} \tanh^2 \left( \frac{\beta \tilde{B}}{2} \right)\quad (3.2.7)$$

Here, assuming translational invariance of the system,  $Z$  is the coordination number (i.e. number of next neighbors). Inserting everything (Eq.(3.2.5),(3.2.6) and (3.2.7)) into Eq.(3.2.3), we end up with the following expression for  $\tilde{\Phi}$ :

$$\tilde{\Phi} = -\frac{NZJ}{8} \tanh^2 \left( \frac{\beta \tilde{B}}{2} \right) + \frac{N\tilde{B}}{2} \tanh \left( \frac{\beta \tilde{B}}{2} \right) - \frac{N}{\beta} \ln \left[ 2 \cosh \left( \frac{\beta \tilde{B}}{2} \right) \right]\quad (3.2.8)$$

We will now look for minima of  $\tilde{\Phi}$  and under which condition they appear for  $\tilde{B} \neq 0$  by looking at the derivative with respect to  $\tilde{B}$ :

$$\begin{aligned}\frac{\partial \tilde{\Phi}}{\partial \tilde{B}} &= -\frac{NZJ}{8} \frac{\tanh \left( \frac{\beta \tilde{B}}{2} \right)}{\cosh^2 \left( \frac{\beta \tilde{B}}{2} \right)} \beta + \frac{N}{2} \tanh \left( \frac{\beta \tilde{B}}{2} \right) + \frac{N\tilde{B}}{4} \frac{\beta}{\cosh^2 \left( \frac{\beta \tilde{B}}{2} \right)} - \frac{N}{2} \tanh \left( \frac{\beta \tilde{B}}{2} \right) \\ &= \frac{N}{4} \frac{\beta}{\cosh^2 \left( \frac{\beta \tilde{B}}{2} \right)} \left[ -\frac{ZJ}{2} \tanh \left( \frac{\beta \tilde{B}}{2} \right) + \tilde{B} \right] \stackrel{!}{=} 0\end{aligned}$$

$$\Rightarrow \tilde{B} = \frac{ZJ}{2} \tanh\left(\frac{\beta\tilde{B}}{2}\right) := f(\tilde{B}) \quad (3.2.9)$$

For a linear chain ( $Z = 2$ ), the function  $f(\tilde{B})$  is plotted in Fig.(3.2.1). Nontrivial solutions  $\tilde{B} \neq 0$  exist if  $\partial_{\tilde{B}}f(\tilde{B})|_{\tilde{B}=0} \geq 1$ , which allows us to find the critical temperature  $T_C$  for the phase transition:

$$\left.\frac{\partial f(\tilde{B})}{\partial \tilde{B}}\right|_{\tilde{B}=0} = \frac{ZJ}{2} \frac{\beta}{2} \frac{1}{\cosh^2\left(\frac{\beta\tilde{B}}{2}\right)} \Big|_{\tilde{B}=0} = \frac{ZJ\beta_C}{4} \stackrel{!}{=} 1$$

$$\Rightarrow k_B T_C = \frac{ZJ}{4} \quad (3.2.10)$$

Eq.(3.2.10) is indeed what one would find in literature [43, 47], showing that the variational treatment is completely analogous.

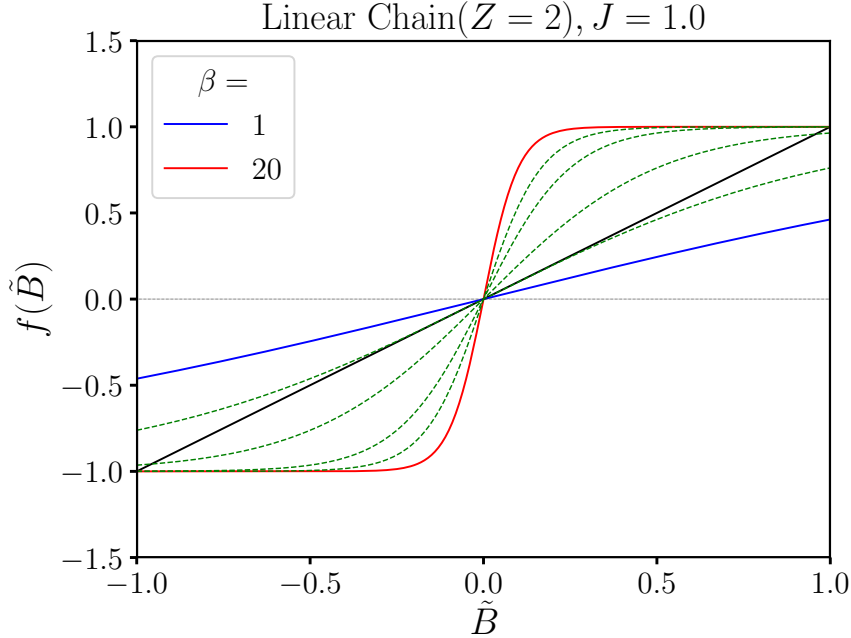


Figure 3.2.1: Function  $f(\tilde{B})$  vs.  $\tilde{B}$  from Eq.(3.2.9) for a linear chain. Intersection points of the colored curves with the black one define self-consistent solutions for  $\tilde{B}$ .

Mean-field theories, however, all have some common flaws: Phase transitions are predicted (as here for a linear chain) where they can not exist according to the Mermin-Wagner theorem [63], and in the cases where they can occur (for  $H$  here, the system's dimension  $d$  would need to be  $d > 2$ ), the critical temperature  $T_C$  is overestimated. Furthermore, correlations are not captured accurately; In the case presented here, for

instance, the average spin-spin correlator would generally be  $\langle \hat{S}_i \cdot \hat{S}_j \rangle_{\tilde{H}} = 0$  for  $\tilde{B} = 0$ . The actual Heisenberg model  $H$ , however, exhibits nonzero correlations even if there is no actual magnetic ordering.

For these reasons, we make use of the fact that the variational equation, Eq.(3.1.9) allows us to choose *any*  $\tilde{H}$  that we deem more appropriate. In the following subsection, we will consider extended Hubbard models and map them to simpler models which are still interacting, albeit with renormalized coupling strengths.

### 3.3. Applications

The two distinct problems and mappings which are at the center of both attached papers are discussed in more detail here. Furthermore, for future work, a general recipe is provided on how to map any nonlocal, direct Coulomb interaction  $V(q)$  onto a pure Hubbard model.

#### 3.3.1. $U$ - $J$ -Model to $U$ - $B$ -Model

In the first attached publication (Ch.(5)), we develop an approximation for the Hubbard-Heisenberg model on a square lattice, with next-neighbor interactions and hoppings at half filling:

$$H = -t \sum_{\langle i,j \rangle, \sigma} (c_{i\sigma}^\dagger c_{j\sigma} + \text{h.c.}) + U \sum_i n_{i\uparrow} n_{i\downarrow} - J \sum_{\langle i,j \rangle} \hat{S}_i \cdot \hat{S}_j \quad (3.3.1)$$

Assuming  $J > 0$  (i.e., the Heisenberg coupling is ferromagnetic), we wish to map  $H$  onto a Hubbard model with renormalized on-site interaction  $\tilde{H}$  and an effective field  $\tilde{B}$  in  $z$ -direction which is meant to describe ferromagnetic correlations:

$$\tilde{H} = -t \sum_{\langle i,j \rangle, \sigma} (c_{i\sigma}^\dagger c_{j\sigma} + \text{h.c.}) + U \sum_i n_{i\uparrow} n_{i\downarrow} - \tilde{B} \sum_i S_i^z \quad (3.3.2)$$

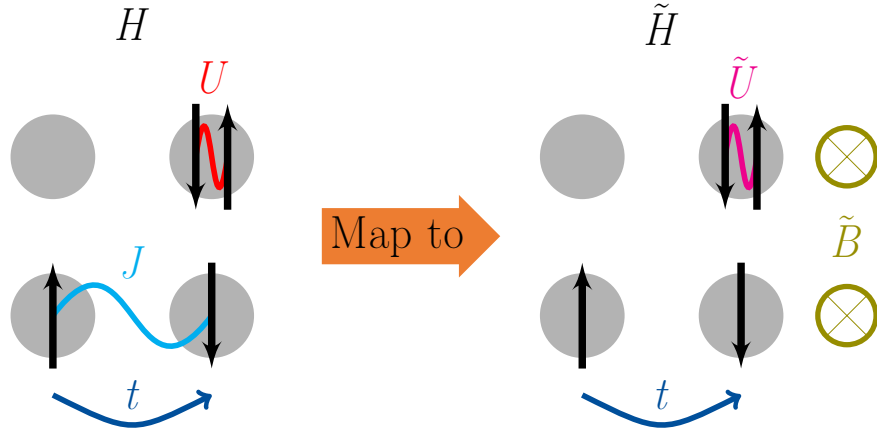


Figure 3.3.1: Illustration of the original problem and the auxiliary system.  $\tilde{H}$  has a renormalized on-site interaction  $\tilde{U}$  and an auxiliary field  $\tilde{B}$  which couples to the spins in  $z$ -direction.

Evaluating the functional  $\tilde{\Phi}$  (Eq.(3.1.9)) for  $H$  and  $\tilde{H}$  yields:

$$\tilde{\Phi} = (U - \tilde{U}) \sum_i \langle n_{i\uparrow} n_{i\downarrow} \rangle_{\tilde{H}} - J \sum_{\langle i,j \rangle} \langle \hat{S}_i \cdot \hat{S}_j \rangle_{\tilde{H}} + \tilde{B} \sum_i \langle S_i^z \rangle_{\tilde{H}} + \Phi_{\tilde{H}} \quad (3.3.3)$$

In contrast to non-interacting mean-field theories where we can obtain correlators (e.g.  $\langle n_{i\uparrow} n_{i\downarrow} \rangle_{\tilde{H}}$ ,  $\langle \hat{S}_i \cdot \hat{S}_j \rangle_{\tilde{H}}$ ) analytically, here we must generally obtain them from numerical simulations of  $\tilde{H}$ . Finding the free energy  $\Phi_{\tilde{H}}$  however, needs a few more considerations.

Since we are only looking for  $(\tilde{U}, \tilde{B})$  which *minimize*  $\tilde{\Phi}$ , one can circumvent the explicit evaluation of  $\Phi_{\tilde{H}}$  by looking at the known partial derivatives:

$$\frac{\partial \Phi_{\tilde{H}}}{\partial \tilde{U}} = \sum_i \langle n_{i\uparrow} n_{i\downarrow} \rangle_{\tilde{H}} \quad , \quad -\frac{\partial \Phi_{\tilde{H}}}{\partial \tilde{B}} = \sum_i \langle S_i^z \rangle_{\tilde{H}} \quad (3.3.4)$$

With this, we can write down the partial derivatives of  $\tilde{\Phi}$ . We abbreviate the notation of the derivatives with  $(\partial_{\tilde{U}}, \partial_{\tilde{B}})$ :

$$\begin{aligned} \partial_{\tilde{U}} \tilde{\Phi} &= (U - \tilde{U}) \sum_i \partial_{\tilde{U}} \langle n_{i\uparrow} n_{i\downarrow} \rangle_{\tilde{H}} - J \sum_{\langle i,j \rangle} \partial_{\tilde{U}} \langle \hat{S}_i \cdot \hat{S}_j \rangle_{\tilde{H}} + \tilde{B} \sum_i \partial_{\tilde{U}} \langle S_i^z \rangle_{\tilde{H}} \\ &\quad - \sum_i \langle n_{i\uparrow} n_{i\downarrow} \rangle_{\tilde{H}} + \partial_{\tilde{U}} \Phi_{\tilde{H}} \end{aligned} \quad (3.3.5)$$

$$\begin{aligned} \partial_{\tilde{B}} \tilde{\Phi} &= (U - \tilde{U}) \sum_i \partial_{\tilde{B}} \langle n_{i\uparrow} n_{i\downarrow} \rangle_{\tilde{H}} - J \sum_{\langle i,j \rangle} \partial_{\tilde{B}} \langle \hat{S}_i \cdot \hat{S}_j \rangle_{\tilde{H}} + \tilde{B} \sum_i \partial_{\tilde{B}} \langle S_i^z \rangle_{\tilde{H}} \\ &\quad + \sum_i \langle S_i^z \rangle_{\tilde{H}} + \partial_{\tilde{B}} \Phi_{\tilde{H}} \end{aligned} \quad (3.3.6)$$

In both equations, the last two terms cancel each other. We further simplify the notation by defining  $\nabla_{\tilde{U}, \tilde{B}} = (\partial_{\tilde{U}}, \partial_{\tilde{B}})$ , and with the condition for extremal points, i.e.  $\nabla_{\tilde{U}, \tilde{B}} = 0$ , we can write:

$$\vec{0} = (U - \tilde{U}) \sum_i \nabla_{\tilde{U}, \tilde{B}} \langle n_{i\uparrow} n_{i\downarrow} \rangle_{\tilde{H}} - J \sum_{\langle i,j \rangle} \nabla_{\tilde{U}, \tilde{B}} \langle \hat{S}_i \cdot \hat{S}_j \rangle_{\tilde{H}} + \tilde{B} \sum_i \nabla_{\tilde{U}, \tilde{B}} \langle S_i^z \rangle_{\tilde{H}} \quad (3.3.7)$$

Another approach (which is used in the publication) is to solve  $\tilde{H}$  on a dense grid of parameters  $(\tilde{U}, \tilde{B})$ , evaluate the free energy  $\Phi_{\tilde{H}}$  up to a constant by integration, and then solve Eq.(3.3.3). To that end, we make use of the known partial derivatives (Eqs.(3.3.4)) and integrate from the point where  $\tilde{U}, \tilde{B} = 0$ :

$$\Phi_{\tilde{H}} = \sum_i \int_0^{\tilde{U}} dU' \langle n_{i\uparrow} n_{i\downarrow} \rangle_{\tilde{H}}(U', 0) - \sum_i \int_0^{\tilde{B}} dB' \langle S_i^z \rangle_{\tilde{H}}(\tilde{U}, B') + \Phi_{\tilde{H}}(0, 0) \quad (3.3.8)$$

The constant  $\Phi_{\tilde{H}}(\tilde{U} = 0, \tilde{B} = 0)$  may be evaluated analytically since it is just the free energy of a tight-binding model, but is not required for the search of minima in  $\tilde{\Phi}$ .

Although both formulas are technically equivalent, one should favor one over the other depending on how  $\tilde{H}$  is solved numerically. Since we rely on noisy Monte Carlo data in the publication, the integral formulation can be preferable as noise tends to cancel itself out while integrating, while numerical evaluation of derivatives is very sensitive to it.

### 3.3.2. $U$ - $V$ -Model to $U$ -Model

Here, we wish to map an extended Hubbard model with next-neighbor density-density interactions to a Hubbard model with local, renormalized interactions only. This approach was already proposed in [39] and later used for more extensive studies of thermodynamic properties [40] of extended Hubbard models. The main difference is that, here, we extend the method to the doped case, i.e. different fillings of the system. To that end, we consider  $H$  and  $\tilde{H}$  in the grand canonical ensemble:

$$H = -t \sum_{\langle i,j \rangle, \sigma} (c_{i\sigma}^\dagger c_{j\sigma} + \text{h.c.}) + U \sum_i n_{i\uparrow} n_{i\downarrow} + V \sum_{\langle i,j \rangle} n_i n_j - \mu \sum_i n_i \quad (3.3.9)$$

$$\tilde{H} = -t \sum_{\langle i,j \rangle, \sigma} (c_{i\sigma}^\dagger c_{j\sigma} + \text{h.c.}) + \tilde{U} \sum_i n_{i\uparrow} n_{i\downarrow} - \tilde{\mu} \sum_i n_i \quad (3.3.10)$$

$n_i = n_{i\uparrow} + n_{i\downarrow}$  denotes the total occupation on a site, while  $(\mu, \tilde{\mu})$  are the chemical potentials.  $\langle i, j \rangle$  runs over next-neighboring pairs of sites.

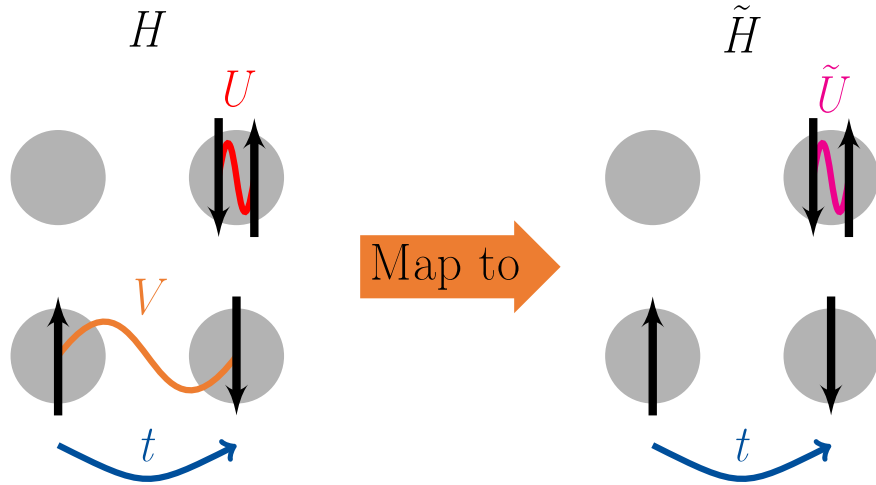


Figure 3.3.2: Illustration of the original problem and the auxiliary system. The effect of the  $V$ -term is incorporated in a renormalized on-site interaction  $\tilde{U}$ .

Evaluating Eq.(3.1.9) for  $\tilde{\Phi}$  leads to:

$$\tilde{\Phi} = (U - \tilde{U}) \sum_i \langle n_{i\uparrow} n_{i\downarrow} \rangle_{\tilde{H}} + V \sum_{\langle i,j \rangle} \langle n_i n_j \rangle_{\tilde{H}} - (\mu - \tilde{\mu}) \sum_i \langle n_i \rangle_{\tilde{H}} + \Phi_{\tilde{H}} \quad (3.3.11)$$

In contrast to the canonical case,  $\Phi_{\tilde{H}}$  here is the grand potential instead of the free energy. Generally, in order to obtain specific, desired fillings  $\langle n_i \rangle$  within  $H$  and  $\tilde{H}$ , the dependencies on  $\mu, \tilde{\mu}$  differ due to the interactions. Ideally, we would like to look for minima of  $\tilde{\Phi}$  along curves of constant filling, i.e.  $\langle n_i \rangle_{\tilde{H}} = \text{const.}$ , which we achieve by choosing  $\tilde{\mu} = \tilde{\mu}(\tilde{U})$  to fulfill this condition. With this,  $\tilde{U}$  remains as the sole variational parameter, and we can evaluate the derivative of  $\tilde{\Phi}$ :

$$\begin{aligned} \partial_{\tilde{U}} \tilde{\Phi} = & - \sum_i \langle n_{i\uparrow} n_{i\downarrow} \rangle_{\tilde{H}} + (U - \tilde{U}) \sum_i \partial_{\tilde{U}} \langle n_{i\uparrow} n_{i\downarrow} \rangle_{\tilde{H}} + V \sum_{\langle i,j \rangle} \partial_{\tilde{U}} \langle n_i n_j \rangle_{\tilde{H}} \\ & + (\partial_{\tilde{U}} \tilde{\mu}) \sum_i \langle n_i \rangle_{\tilde{H}} - (\mu - \tilde{\mu}) \sum_i \underbrace{\partial_{\tilde{U}} \langle n_i \rangle_{\tilde{H}}}_{=0, \langle n_i \rangle_{\tilde{H}} = \text{const.}} + \partial_{\tilde{U}} \Phi_{\tilde{H}} \end{aligned} \quad (3.3.12)$$

Due to the choice of  $\tilde{\mu} = \tilde{\mu}(\tilde{U})$ , the derivative of the grand potential  $\Phi_{\tilde{H}}$  with respect to  $\tilde{U}$  has an extra term:

$$\partial_{\tilde{U}} \Phi_{\tilde{H}} = + \sum_i \langle n_{i\uparrow} n_{i\downarrow} \rangle_{\tilde{H}} - (\partial_{\tilde{U}} \tilde{\mu}) \sum_i \langle n_i \rangle_{\tilde{H}} \quad (3.3.13)$$

Inserting this into Eq.(3.3.12), we see that some terms cancel each other, leaving:

$$\partial_{\tilde{U}} \tilde{\Phi} = (U - \tilde{U}) \sum_i \partial_{\tilde{U}} \langle n_{i\uparrow} n_{i\downarrow} \rangle_{\tilde{H}} + V \sum_{\langle i,j \rangle} \partial_{\tilde{U}} \langle n_i n_j \rangle_{\tilde{H}} \stackrel{!}{=} 0 \quad (3.3.14)$$

Arranging this equation to  $\tilde{U}$  on the left hand side leads to a self-consistency equation:

$$\tilde{U} = U + V \frac{\sum_{\langle i,j \rangle} \partial_{\tilde{U}} \langle n_i n_j \rangle_{\tilde{H}}}{\sum_i \partial_{\tilde{U}} \langle n_{i\uparrow} n_{i\downarrow} \rangle_{\tilde{H}}} \quad (3.3.15)$$

Defining the prefactor in front of  $V$  as a *screening factor*  $\alpha$  leads to the result:

$$\alpha(\tilde{U}) = - \frac{\sum_{\langle i,j \rangle} \partial_{\tilde{U}} \langle n_i n_j \rangle_{\tilde{H}}}{\sum_i \partial_{\tilde{U}} \langle n_{i\uparrow} n_{i\downarrow} \rangle_{\tilde{H}}} \quad (3.3.16)$$

$$\tilde{U} = U - \alpha(\tilde{U})V \quad (3.3.17)$$

Eq.(3.3.17) is one of the central equations in the second paper (Ch.(6)) for the investigation of local screening effects which stem from the  $V$ -term in the extended Hubbard model.

As a last note,  $\alpha$  can be expressed in a simpler fashion if we assume translational invariance of expectation values  $\langle \dots \rangle_{\tilde{H}}$  on the lattice: Sums over all lattice sites  $i$  yield  $N$  terms, while the sum over pairs of next neighbors gives  $NZ/2$  terms, with  $Z$  being the coordination number.

$$\alpha(\tilde{U}) = - \frac{Z}{2} \frac{\partial_{\tilde{U}} \langle n_i n_j \rangle_{\tilde{H}}}{\partial_{\tilde{U}} \langle n_{i\uparrow} n_{i\downarrow} \rangle_{\tilde{H}}} \quad (3.3.18)$$

### 3.3.3. General Interactions

Although not used in the publications, but perhaps relevant for future reference, it is possible to derive a mapping to a local Hubbard model for any general density-density interaction. Let us assume again that  $H$  is an extended Hubbard model, while  $\tilde{H}$  is the same as in the previous subchapter:

$$H = \underbrace{H_t}_{\text{One-Particle Terms}} + U \sum_i n_{i\uparrow} n_{i\downarrow} + \underbrace{H_V}_{\text{Nonlocal Terms}} \quad (3.3.19)$$

$$\tilde{H} = H_t + \tilde{U} \sum_i n_{i\uparrow} n_{i\downarrow} \quad (3.3.20)$$

Assuming a distance-dependent density-density interaction, i.e.

$$H_V = \frac{1}{2} \sum_{\substack{i \neq j \\ \sigma \sigma'}} V_{|\mathbf{R}_i - \mathbf{R}_j|} n_{i\sigma} n_{j\sigma'} \quad (3.3.21)$$

and going through the same steps as above, one arrives at a more general version of Eq.(3.3.15):

$$\tilde{U} = U + \frac{\partial_{\tilde{U}} \left( \sum_{i \neq j, \sigma \sigma'} \frac{V_{|\mathbf{R}_i - \mathbf{R}_j|}}{2} \langle n_{i\sigma} n_{j\sigma'} \rangle_{\tilde{H}} \right)}{\partial_{\tilde{U}} \left( \sum_i \langle n_{i\uparrow} n_{i\downarrow} \rangle_{\tilde{H}} \right)} \quad (3.3.22)$$

As it can be quite tedious to obtain all real-space matrix elements  $V_{ij} = V_{|\mathbf{R}_i - \mathbf{R}_j|}$ , it is useful to transform the whole equation to Fourier space. To that end, we transform  $H_V$  explicitly:

$$\begin{aligned} H_V &= \frac{1}{2} \sum_{i \neq j, \sigma \sigma'} V_{|\mathbf{R}_i - \mathbf{R}_j|} c_{i\sigma}^\dagger c_{i\sigma} c_{j\sigma'}^\dagger c_{j\sigma'} \\ &= \frac{1}{N^2} \sum_{\substack{\mathbf{k}_1 \mathbf{k}_2 \\ \mathbf{k}_3 \mathbf{k}_4}} \frac{1}{2} \sum_{\substack{i \neq j \\ \sigma \sigma'}} V_{|\mathbf{R}_i - \mathbf{R}_j|} \underbrace{e^{i\mathbf{k}_1 \mathbf{R}_i} e^{-i\mathbf{k}_2 \mathbf{R}_i} e^{i\mathbf{k}_3 \mathbf{R}_j} e^{-i\mathbf{k}_4 \mathbf{R}_j}}_{\substack{e^{i(\mathbf{k}_1 - \mathbf{k}_2) \mathbf{R}_i + i(\mathbf{k}_3 - \mathbf{k}_4) \mathbf{R}_j} \\ = e^{i(\mathbf{k}_1 - \mathbf{k}_2 + \mathbf{k}_3 - \mathbf{k}_4) \mathbf{R}_i} e^{i(\mathbf{k}_3 - \mathbf{k}_4) (\mathbf{R}_j - \mathbf{R}_i)}}} c_{\mathbf{k}_1 \sigma}^\dagger c_{\mathbf{k}_2 \sigma} c_{\mathbf{k}_3 \sigma'}^\dagger c_{\mathbf{k}_4 \sigma'} \end{aligned}$$

We define  $\boldsymbol{\delta} = \mathbf{R}_j - \mathbf{R}_i$  as the possible vectors connecting two non-equal sites. The double sum over sites can then be rewritten as  $\sum_{i \neq j} \dots \rightarrow \sum_{i, \boldsymbol{\delta}} \dots$ , and we obtain:

$$\begin{aligned} H_V &= \frac{1}{N^2} \sum_{\substack{\mathbf{k}_1 \mathbf{k}_2 \\ \mathbf{k}_3 \mathbf{k}_4}} \frac{1}{2} \sum_{\sigma \sigma'} \sum_{i \boldsymbol{\delta}} V_{|\boldsymbol{\delta}|} \underbrace{e^{i(\mathbf{k}_1 - \mathbf{k}_2 + \mathbf{k}_3 - \mathbf{k}_4) \mathbf{R}_i}}_{i\text{-sum: } N \cdot \delta_{\mathbf{k}_2, \mathbf{k}_1 + \mathbf{k}_3 - \mathbf{k}_4}} e^{i(\mathbf{k}_3 - \mathbf{k}_4) \boldsymbol{\delta}} c_{\mathbf{k}_1 \sigma}^\dagger c_{\mathbf{k}_2 \sigma} c_{\mathbf{k}_3 \sigma'}^\dagger c_{\mathbf{k}_4 \sigma'} \\ &= \frac{1}{N} \sum_{\mathbf{k}_1 \mathbf{k}_3 \mathbf{k}_4} \frac{1}{2} \sum_{\sigma \sigma'} \sum_{\boldsymbol{\delta}} V_{|\boldsymbol{\delta}|} e^{i(\mathbf{k}_3 - \mathbf{k}_4) \boldsymbol{\delta}} c_{\mathbf{k}_1 \sigma}^\dagger c_{\mathbf{k}_1 + \mathbf{k}_3 - \mathbf{k}_4 \sigma} c_{\mathbf{k}_3 \sigma'}^\dagger c_{\mathbf{k}_4 \sigma'} \end{aligned}$$



Defining  $\mathbf{q} = \mathbf{k}_3 - \mathbf{k}_4$  and renaming  $(\mathbf{k}_1, \mathbf{k}_3)$  to  $(\mathbf{k}, \mathbf{k}')$  leads to:

$$H_V = \frac{1}{N} \sum_{\mathbf{q}} \underbrace{\left( \sum_{\delta} \frac{V_{|\delta|}}{2} e^{i\mathbf{q}\delta} \right)}_{F(\mathbf{q})} \sum_{\sigma\sigma'} \sum_{\mathbf{k}\mathbf{k}'} c_{\mathbf{k}\sigma}^\dagger c_{\mathbf{k}+\mathbf{q}\sigma} c_{\mathbf{k}'\sigma'}^\dagger c_{\mathbf{k}'-\mathbf{q}\sigma'} \quad (3.3.23)$$

With this, we can express the necessary expectation values in Eq.(3.3.22) in Fourier space:

$$\sum_{\substack{i \neq j \\ \sigma\sigma'}} \frac{V_{|\mathbf{R}_i - \mathbf{R}_j|}}{2} \langle n_{i\sigma} n_{j\sigma'} \rangle_{\tilde{H}} = \frac{1}{N} \sum_{\mathbf{q}} F(\mathbf{q}) \sum_{\sigma\sigma'} \sum_{\mathbf{k}\mathbf{k}'} \langle c_{\mathbf{k}\sigma}^\dagger c_{\mathbf{k}+\mathbf{q}\sigma} c_{\mathbf{k}'\sigma'}^\dagger c_{\mathbf{k}'-\mathbf{q}\sigma'} \rangle_{\tilde{H}} \quad (3.3.24)$$

The same steps are valid for the local Hubbard-interaction, although the prefactor  $F(\mathbf{q})$  is simply one and only electrons with opposite spins interact:

$$\sum_i \langle n_{i\uparrow} n_{i\downarrow} \rangle_{\tilde{H}} = \frac{1}{N} \sum_{\mathbf{q}} \sum_{\mathbf{k}\mathbf{k}'} \langle c_{\mathbf{k}\uparrow}^\dagger c_{\mathbf{k}+\mathbf{q}\uparrow} c_{\mathbf{k}'\downarrow}^\dagger c_{\mathbf{k}'-\mathbf{q}\downarrow} \rangle_{\tilde{H}} \quad (3.3.25)$$

At this point, one should note the definition of the susceptibility for  $\tau \rightarrow 0$ , i.e. the static structure factor:

$$\chi_{\sigma\sigma'}(\mathbf{q}, \tau \rightarrow 0) = \chi_{\sigma\sigma'}(\mathbf{q}) = -\frac{1}{N} \sum_{\mathbf{k}\mathbf{k}'} \langle c_{\mathbf{k}\sigma}^\dagger c_{\mathbf{k}+\mathbf{q}\sigma} c_{\mathbf{k}'\sigma'}^\dagger c_{\mathbf{k}'-\mathbf{q}\sigma'} \rangle \quad (3.3.26)$$

The expectation values above are then expressed as:

$$\sum_{\substack{i \neq j \\ \sigma\sigma'}} \frac{V_{|\mathbf{R}_i - \mathbf{R}_j|}}{2} \langle n_{i\sigma} n_{j\sigma'} \rangle_{\tilde{H}} = - \sum_{\mathbf{q}} F(\mathbf{q}) \sum_{\sigma\sigma'} \chi_{\sigma\sigma'}(\mathbf{q}) \quad (3.3.27)$$

$$\sum_i \langle n_{i\uparrow} n_{i\downarrow} \rangle_{\tilde{H}} = - \sum_{\mathbf{q}} \chi_{\uparrow\downarrow}(\mathbf{q}) \quad (3.3.28)$$

Inserting these expressions back into Eq.(3.3.22) yields:

$$\tilde{U} = U + \frac{\sum_{\mathbf{q}} F(\mathbf{q}) \sum_{\sigma\sigma'} \partial_{\tilde{U}}(\chi_{\sigma\sigma'}(\mathbf{q}))}{\sum_{\mathbf{q}} \partial_{\tilde{U}}(\chi_{\uparrow\downarrow}(\mathbf{q}))} \quad (3.3.29)$$

If we want to write this equation depending on the *full*  $\mathbf{q}$ -dependent interaction  $V(\mathbf{q})$  instead of only the nonlocal  $F(\mathbf{q})$ , we can add and subtract the missing, local part in the numerator:

$$\tilde{U} = U + \frac{\sum_{\mathbf{q}} \sum_{\sigma\sigma'} V^{\sigma\sigma'}(\mathbf{q}) \partial_{\tilde{U}}(\chi_{\sigma\sigma'}(\mathbf{q})) - U \sum_{\mathbf{q}} \partial_{\tilde{U}}(\chi_{\uparrow\downarrow}(\mathbf{q}))}{\sum_{\mathbf{q}} \partial_{\tilde{U}}(\chi_{\uparrow\downarrow}(\mathbf{q}))} \quad (3.3.30)$$

The spin-indices in  $V^{\sigma\sigma'}(\mathbf{q})$  are due to the constraint that local interactions occur only with opposing spins. The second term in the numerator cancels with the denominator and the first  $U$  in the equation, and the final result is:

$$\tilde{U} = \frac{\sum_{\mathbf{q}} \sum_{\sigma\sigma'} V^{\sigma\sigma'}(\mathbf{q}) \partial_{\tilde{U}}(\chi_{\sigma\sigma'}(\mathbf{q}))}{\sum_{\mathbf{q}} \partial_{\tilde{U}}(\chi_{\uparrow\downarrow}(\mathbf{q}))} \quad (3.3.31)$$

In summary, if the static structure factor (i.e. static charge-charge correlator)  $\chi_{\sigma\sigma'}(\mathbf{q})$  of the Hubbard model is known, this result provides a recipe for downfolding an arbitrary density-density interaction  $V^{\sigma\sigma'}(\mathbf{q})$  onto a renormalized, purely local interaction  $\tilde{U}$ .

## 4. Numerical Methods and Approximations

Here, the necessary numerical and computational methods are discussed. The Determinantal Quantum Monte Carlo (DQMC) algorithm will be the biggest focus, as it was used extensively and subtle implementations have been done. The Dynamical Cluster Approximation (DCA) and the algorithm of the CT-AUX solver will be summarized in a shorter fashion due to them having been used without further, new implementations. We also introduce the dual fermion perturbation theory which is at the center of the last project.

### 4.1. Determinantal QMC

The Determinantal Quantum Monte Carlo algorithm was initially proposed by Hirsch [23]. Shortly after, it has been applied to the Hubbard model on a two-dimensional lattice [64] and to gain insights on its pairing interaction vertices [65], and has since been developed and applied extensively. We mainly follow the first Hirsch paper [23] and the introduction in [32].

#### 4.1.1. Classical Monte Carlo

First, we introduce the general idea of Monte Carlo system by considering an important classical system known as the Ising-Model [66]:

$$H = -J \sum_{\langle i,j \rangle} S_i^z S_j^z \quad (4.1.1)$$

The spins  $S_i^z = \pm 1$  are classical variables, and we restrict ourselves to the next-neighbor interaction case denoted by the sum over  $\langle i, j \rangle$ . A positive coupling strength,  $J > 0$ , favors a ferromagnetic alignment of spin, while  $J < 0$  favors (if the lattice is not frustrated) an antiferromagnetic Néel state where neighboring spins are antiparallel. In contrast to the Heisenberg model, which is no longer a classical problem, the Ising Hamiltonian does not flip any spins, which makes it diagonal in real space. Theoretically, in such a case, one could evaluate the partition function  $\mathcal{Z} = \text{Tr}(e^{-\beta H})$  directly. However, the number of possible configurations that need to be summed over scales exponentially, i.e.  $2^N$  for  $N$  spins. For example, a 20x20 square lattice (i.e.  $N = 400$ ) already has more than  $2.58 \cdot 10^{120}$  possible configurations.

It is for this reason that it makes sense to consider the fact that some configurations are *more important* than others, which leads to the idea of *importance sampling* [67] for the partition function. A widely used method for implementing said importance sampling is the *Metropolis algorithm* [68], which ideally generates a set of the most likely configurations.

In our case of the classical Ising model, the probability of finding a given configuration  $C$  of the spins (e.g.  $C \equiv |\uparrow, \uparrow, \dots, \downarrow, \uparrow\rangle$ ) with the energy  $E(C)$  is given by the Boltzmann factor  $p(C) \propto \exp(-\beta E(C))$ , with  $\beta = 1/k_B T$  being the inverse temperature. One starts with a random initial configuration  $C$ , then go through a loop over

all spins, while attempting to flip them. After each individual flip (which generates a new configuration  $C'$  with the energy  $E(C')$ ), an acceptance ratio  $r'$  is calculated from the energy difference  $\Delta E = E(C') - E(C)$ :

$$r' = \frac{p(C')}{p(C)} = \exp(-\beta\Delta E) \quad (4.1.2)$$

In the case  $\Delta E < 0$ ,  $C'$  is accepted as the new configuration as it is energetically favored. If  $\Delta E > 0$ ,  $C'$  is accepted only with a probability  $r'$ , which mimicks thermal fluctuations that allow a system to temporarily go to energetically unfavorable states. Indeed, for  $T \rightarrow 0$ , i.e.  $\beta \rightarrow \infty$ ,  $r'$  goes to zero, suppressing any fluctuations.

It should be noted that the choice of the acceptance ratio is not unique; Instead of  $r'$ , there are also choices such as the *heat bath algorithm*, where the ratio  $r$  is defined as:

$$r = \frac{r'}{1 + r'} \quad (4.1.3)$$

However, for efficiency reasons, it is rarely used, as the choice  $r'$  above generally allows more fluctuations, which leads to a broader sampling with the same computational resources.

When starting the algorithm with an initial configuration, one usually defines a number of sweeps where no measurements are taken, in order to let the system move to the relevant area within the configuration space first. This process is known as *warming up* or *thermalizing* the system. Furthermore, in order to avoid autocorrelation effects between two distinct measurements, it is helpful to perform a few sweeps without measurements between the two. With this, assuming that the sample configurations are independent, thermodynamic averages  $\langle A \rangle$  of an observable  $A$  are obtained simply by averaging the  $N_{\text{meas}}$  measurements  $A_i$ :

$$\langle A \rangle \approx \bar{A} = \frac{1}{N_{\text{meas}}} \sum_{i=1}^{N_{\text{meas}}} A_i \quad (4.1.4)$$

For independent  $A_i$ , the central limit theorem [47] becomes valid, and statistical errors can be estimated as:

$$\delta A = \sqrt{\frac{\langle A^2 \rangle - \langle A \rangle^2}{N_{\text{meas}}}} \quad (4.1.5)$$

In practice, for the error estimation, as measuring  $\langle A^2 \rangle$  for Eq.(4.1.5) can be quite tedious in a quantum system, one can instead also group the individual measurements into a number of distinct averages (often called *bins*), and apply resampling methods such as the Jackknife method [69].

### 4.1.2. DQMC Algorithm

We start with a general Hubbard Hamiltonian  $H$  in the grand canonical ensemble that we wish to solve via a Monte Carlo approach:

$$H = \sum_{\substack{ij \\ \sigma}} t_{ij} c_{i\sigma}^\dagger c_{j\sigma} + U \sum_i n_{i\uparrow} n_{i\downarrow} - \mu \sum_i n_i \quad (4.1.6)$$

As in previous chapters,  $n_i = n_{i\uparrow} + n_{i\downarrow}$  denotes the total occupation of a site.  $t_{ij}$  are the hopping matrix elements and on-site energies,  $U$  the strength of the local Hubbard interaction and  $\mu$  denotes the chemical potential. Compared to the classical Ising model above, in quantum systems, the individual terms in  $H$  (e.g. the hopping and the  $U$ -terms) do not commute with each other, leading to fundamental correlations and indistinguishability of the particles. As such, one must first rewrite the partition function,  $\mathcal{Z} = \text{Tr}(e^{-\beta H})$ , in a way where approaches such as the Metropolis algorithm can be used.

To that end, we start with the *Suzuki-Trotter decomposition* [70] for exponentials of non-commuting operators  $A, B$ :

$$e^{x(A+B)} = e^{xA} e^{xB} + \mathcal{O}[x^2[A, B]] \quad (4.1.7)$$

Its meaning is that, if the prefactor  $x$  is small, exponentials of non-commuting operators can be separated up to a reasonable accuracy. Since  $\beta$  in the exponential appearing in  $\mathcal{Z}$  need not be small, we write it as  $\beta = \Delta\tau L$ , and invoke the decomposition afterwards:

$$e^{-\beta H} = e^{-\beta(K+V)} = \left( e^{\Delta\tau(K+V)} \right)^L = \left( e^{\Delta\tau K} e^{\Delta\tau V} \right)^L + \mathcal{O}[(\Delta\tau)^2 U] \quad (4.1.8)$$

Here, we split up  $H = K + V$ , with  $K$  containing all terms which are bilinear in the operators, while  $V$  contains the quartic part (i.e. the Hubbard interaction). The commutator in the error term then becomes  $[K, V] = U$ . With the naming of  $\Delta\tau$ , the analogy to the path integral formalism is visible, although we do not take the limit of  $\Delta\tau \rightarrow 0$  explicitly. Rather, we work with discrete imaginary *time slices* from 0 to  $\beta$  and choose  $L$  large enough (i.e.  $\Delta\tau$  small enough) to provide a good accuracy. Typically [32], one should choose at least  $\Delta\tau = \sqrt{0.125/U}$ .

The next step is to rewrite the interaction term. For  $U = 0$ , where only terms which are bilinear in creation/annihilation operators appear, evaluating the partition function  $\mathcal{Z} = \text{Tr}(e^{-\beta H})$  would be reduced to a rather simple diagonalization problem. For quartic terms, it becomes much more tedious, which is why they will be cast into a bilinear form, at the cost of adding additional degrees of freedom. With the definitions  $n = n_\uparrow + n_\downarrow$  and  $m = n_\uparrow - n_\downarrow$  for the total occupation and magnetization, and the fact that  $n_\sigma^2 = n_\sigma = 0, 1$  for fermions, the individual interaction terms for each site (the

index is omitted here) can be written as squares of operators:

$$n_{\uparrow}n_{\downarrow} = -\frac{m^2}{2} + \frac{n}{2} \quad (4.1.9)$$

$$n_{\uparrow}n_{\downarrow} = \frac{n^2}{2} - \frac{n}{2} \quad (4.1.10)$$

With this, consider the following Gaussian integral:

$$e^{\frac{A^2}{2}} = \sqrt{2\pi} \int_{-\infty}^{\infty} dx e^{-\frac{x^2}{2} - xA} \quad (4.1.11)$$

As  $A$  only appears linearly on the right hand side, this integral gives a general idea on how to express squares of operators in a linear way, at the cost of evaluating the additional  $x$ -integral. Instead of an integral over a continuous variable  $x$ , it is also possible to do a sum over discrete Ising variables  $s = \pm 1$ , and use Eq.(4.1.9) to rewrite the exponential of the interaction term in the following way:

$$\begin{aligned} e^{-\Delta\tau U n_{\uparrow}n_{\downarrow}} &= \frac{1}{2} e^{-\Delta\tau \frac{U}{2} n} \sum_{s=\pm 1} e^{-s\lambda m} \\ &= \frac{1}{2} \sum_{s=\pm 1} \prod_{\sigma=\uparrow,\downarrow} e^{-(\sigma s\lambda + \Delta\tau \frac{U}{2} n_{\sigma})} \end{aligned} \quad (4.1.12)$$

It should be noted that this equation is used for the repulsive model (i.e.  $U > 0$ ). Although not used throughout our work, for the attractive model ( $U < 0$ ), one makes use of Eq.(4.1.10) to obtain:

$$e^{-\Delta\tau |U| n_{\uparrow}n_{\downarrow}} = \frac{1}{2} \sum_{s=\pm 1} \prod_{\sigma=\uparrow,\downarrow} e^{(s\lambda + \Delta\tau \frac{|U|}{2}) (n_{\sigma} - \frac{1}{2})} \quad (4.1.13)$$

In both cases, the constant  $\lambda$  is given by:

$$\cosh \lambda = e^{\Delta\tau \frac{|U|}{2}} \quad (4.1.14)$$

Instead of the on-site interaction, depending on whether  $U > 0$  or  $U < 0$ , we now have either the magnetization or the charge coupled to fluctuating Ising fields. Applying this transformation to the interaction term of the  $N$  lattice sites and  $L$  time-slices leads to a new expression for the partition function:

$$\mathcal{Z} = \left(\frac{1}{2}\right)^{NL} \text{Tr}_{\{s\}} \text{Tr} \prod_{l=L}^1 \prod_{\sigma=\uparrow,\downarrow} e^{-\Delta\tau \sum_{ij} c_{i\sigma}^{\dagger} K_{ij} c_{j\sigma}} e^{-\Delta\tau \sum_i c_{i\sigma}^{\dagger} V_i^{\sigma}(l) c_{i\sigma}} \quad (4.1.15)$$

The additional trace, denoted by  $\text{Tr}_{\{s\}}$ , is a sum over all possible configurations of the  $N \times L$  auxiliary Ising-spins  $s_i(l) = \pm 1$ . It should also be noted that the product over time slices runs from the last to the first, i.e. from  $L$  to 1. Depending on the

implementation used (e.g. QUEST [41]), the time discretization can also be chosen to go from 0 to  $(L - 1)\Delta\tau$ .  $K_{ij}$  contain the elements of the hopping matrix  $\mathbf{K}$ , e.g. for hopping between nearest neighbours, they read as:

$$[\mathbf{K}]_{ij} = K_{ij} = \begin{cases} -t & (i, j) \text{ are nearest neighbours,} \\ 0 & \text{otherwise} \end{cases} \quad (4.1.16)$$

$V_i^\sigma(l)$  are elements of a  $N \times N$  diagonal matrix  $\mathbf{V}^\sigma(l)$  containing the dependency on the Ising-spins for each time slice:

$$[\mathbf{V}^\sigma(l)]_i = V_i^\sigma(l) = \frac{1}{\Delta\tau} \lambda \sigma s_i(l) + \left( \mu - \frac{U}{2} \right) \quad (4.1.17)$$

While we skip the details here and refer back to [32], the important part is that the exponentials of a bilinear form of fermionic operators can be traced out explicitly. With the definition

$$\mathbf{B}_l^\sigma \equiv e^{-\Delta\tau K} e^{-\Delta\tau V^\sigma(l)} \quad (4.1.18)$$

we can write:

$$\mathcal{Z} = \left( \frac{1}{2} \right)^{NL} \text{Tr}_{\{s\}} \prod_{\sigma} \det [\mathbf{1} + \mathbf{B}_L^\sigma \mathbf{B}_{L-1}^\sigma \dots \mathbf{B}_1^\sigma] \quad (4.1.19)$$

We further define

$$\mathbf{O}^\sigma(\{s\}) \equiv \mathbf{1} + \mathbf{B}_L^\sigma \mathbf{B}_{L-1}^\sigma \dots \mathbf{B}_1^\sigma \quad (4.1.20)$$

and arrive at the final expression for the partition function:

$$\mathcal{Z} = \text{Tr}_{\{s\}} \underbrace{\left[ \left( \frac{1}{2} \right)^{NL} \det \mathbf{O}^\uparrow(\{s\}) \det \mathbf{O}^\downarrow(\{s\}) \right]}_{\equiv \rho(\{s\})} \quad (4.1.21)$$

In summary, we expressed  $\mathcal{Z}$  as a trace over Ising-spins of a product of determinants.  $\rho(\{s\})$  defines an *effective* density operator which could be used as a weight for the Monte Carlo importance sampling. However, aside from special cases, the product of (fermionic) determinants is not positive definite, leading to the known *sign problem* which limits the applicability of many Quantum Monte Carlo methods for fermions.

For a fixed configuration of the Ising-spins,  $C \equiv \{s\}$ , the statistical weight  $p(C) = \det \mathbf{O}^\uparrow(C) \det \mathbf{O}^\downarrow(C)$  and with the definition of  $S(C) = \text{sgn}(p(C))$ , the sign problem is treated by rewriting average quantities of an observable  $A$  as follows:

$$\begin{aligned} \langle A \rangle_p &= \frac{\sum_C p(C) A(C)}{\sum_C p(C)} = \frac{\sum_C |p(C)| S(C) A(C)}{\sum_C |p(C)| S(C)} \\ &= \frac{[\sum_C |p(C)| S(C) A(C)] / [\sum_C |p(C)|]}{[\sum_C |p(C)| S(C)] / [\sum_C |p(C)|]} = \frac{\langle SA \rangle_{|p|}}{\langle S \rangle_{|p|}} \end{aligned} \quad (4.1.22)$$

In short, the absolute value of the statistical weight can still be used for the sampling, but one pays the price of dividing measured values by the *average sign*, which, if it is not  $\langle S \rangle \simeq 1$ , significantly deteriorates the accuracy. It is thus necessary to stretch simulation time on a scale of  $\langle S \rangle^{-2}$  to obtain a similar quality. The sign is known to deteriorate exponentially, i.e.  $\langle S \rangle \sim e^{-\beta N \gamma}$  with  $\gamma$  depending on the filling and the Hubbard- $U$ .

With the basics understood, actual measurements during the simulation will be discussed next.

### 4.1.3. Measurements

We start out with *equal-time* correlators for two operators  $A$  and  $B$ , which, following the derivation of the final expression for the partition function, can be expressed as:

$$\langle AB \rangle = \frac{1}{\mathcal{Z}} \text{Tr}_{\{s\}} \text{Tr} \left[ AB \prod_{l\sigma} e^{-\Delta\tau K} e^{-\Delta\tau V^\sigma(l)} \right] \quad (4.1.23)$$

For one specific configuration of the Ising-fields  $\{s\}$ , the correlator is:

$$\langle AB \rangle_{\{s\}} = \frac{1}{\rho(\{s\})} \text{Tr} \left[ AB \prod_{l\sigma} e^{-\Delta\tau K} e^{-\Delta\tau V^\sigma(l)} \right] \quad (4.1.24)$$

With these expressions, it is straightforward to see that:

$$\langle AB \rangle = \frac{1}{\mathcal{Z}} \text{Tr}_{\{s\}} \langle AB \rangle_{\{s\}} \rho(\{s\}) \quad (4.1.25)$$

In short, average values  $\langle AB \rangle$  are obtained by sampling over the specific field configurations  $\{s\}$  and weighting them by  $\rho(\{s\})$ . The single-particle, equal-time Green's function plays a special role, as it is crucial [32] for the simulation itself:

$$\langle c_{i\sigma} c_{j\sigma}^\dagger \rangle_{\{s\}} = [(\mathbf{1} + \mathbf{B}_L^\sigma \mathbf{B}_{L-1}^\sigma \dots \mathbf{B}_1^\sigma)^{-1}]_{ij} = [(\mathbf{O}^\sigma(\{s\}))^{-1}]_{ij} \quad (4.1.26)$$

One should note that, in many QMC methods, the Green's function is defined with a positive sign, compared to e.g. the standard Matsubara definition.

The time dependency of an operator  $a$  is given in the Heisenberg-picture for the imaginary time:

$$a(l) = a(\tau) = e^{\tau H} a e^{-\tau H} \quad \text{with} \quad \tau \equiv l\Delta\tau \quad (4.1.27)$$

The equal-time Green's function such as in Eq.(4.1.26) has a time-slice dependence, i.e.  $\langle c_{i\sigma}(l) c_{j\sigma}^\dagger(l) \rangle_{\{s\}}$  has a dependency on  $l$ , and they become approximately equal only after a longer runtime. For generic  $l$ , the equal-time correlator is:

$$\mathbf{g}^\sigma(l) = \langle c_{i\sigma}(l) c_{j\sigma}^\dagger(l) \rangle_{\{s\}} = [\mathbf{1} + \mathbf{A}^\sigma(l)]^{-1} \quad (4.1.28)$$

with  $\mathbf{A}^\sigma(l) = \mathbf{B}_{l-1}^\sigma \mathbf{B}_{l-2}^\sigma \dots \mathbf{B}_1^\sigma \mathbf{B}_L^\sigma \dots \mathbf{B}_l^\sigma$



The time-indices of the equal-time Green's function can be *shifted* to adjacent time-slices by multiplying with the B-matrices and their inverse from the left or right, respectively. For example,  $\mathbf{g}^\sigma(l+1)$  can be obtained from  $\mathbf{g}^\sigma(l)$  by:

$$\mathbf{g}^\sigma(l+1) = \mathbf{B}_l^\sigma \mathbf{g}^\sigma(l) [\mathbf{B}_l^\sigma]^{-1} \quad (4.1.29)$$

Using Eq.(4.1.29) is much faster than calculating all  $\mathbf{g}^\sigma(l)$  from scratch for each configuration, but can usually only be done a limited number of times before rounding errors accumulate. Shifting only one of the  $l$ -indices yields the *unequal*-time Green's functions, which are not essential to the simulation itself, but lead to many important observables. For two time-indices with  $l_1 > l_2$ , the unequal time Green's function is obtained via:

$$G_{ij}^\sigma(l_1, l_2) = \langle c_{i\sigma}(l_1) c_{j\sigma}^\dagger(l_2) \rangle_{\{s\}} = [\mathbf{B}_{l_1}^\sigma \mathbf{B}_{l_1-1}^\sigma \dots \mathbf{B}_{l_2+1}^\sigma \mathbf{g}^\sigma(l_2+1)]_{ij} \quad (4.1.30)$$

It is important to note that, due to the Hubbard-Stratonovich transformation, Wick's theorem holds for a fixed configuration of Ising-fields. From this, all higher-order correlators (with or without time-dependencies) of interest can be obtained, e.g.:

$$\langle c_{i_1}^\dagger c_{i_2} c_{i_3}^\dagger c_{i_4} \rangle_{\{s\}} = \langle c_{i_1}^\dagger c_{i_2} \rangle_{\{s\}} \langle c_{i_3}^\dagger c_{i_4} \rangle_{\{s\}} + \langle c_{i_1}^\dagger c_{i_4} \rangle_{\{s\}} \langle c_{i_2} c_{i_3}^\dagger \rangle_{\{s\}} \quad (4.1.31)$$

Specific examples and more details relevant for our work are discussed in the chapter where numerical developments have been done within the QUEST-code.

Lastly, we note that the determinants in Eq.(4.1.21) need not be evaluated explicitly to obtain an *acceptance ratio* such as in Eq.(4.1.2)). Let us assume a configuration  $\{s\}$  where we flip one of the Ising-spins for one specific site and time slice  $(i, l)$ , yielding a new configuration  $\{s'\}$ . With the Metropolis algorithm, the acceptance ratio is the ratio between the two statistical weights:

$$r' = \frac{\rho(\{s'\})}{\rho(\{s\})} = \frac{\det \mathbf{O}^\uparrow(\{s'\}) \det \mathbf{O}^\downarrow(\{s'\})}{\det \mathbf{O}^\uparrow(\{s\}) \det \mathbf{O}^\downarrow(\{s\})} = R_\uparrow R_\downarrow \quad (4.1.32)$$

$$\text{with } R_\sigma = \frac{\det \mathbf{O}^\sigma(\{s'\})}{\det \mathbf{O}^\sigma(\{s\})} \quad (4.1.33)$$

Omitting the details here, the important part is that  $R_\sigma$ , for an Ising spin-flip at  $(i, l)$ , can be expressed through the equal-time Green's function during the simulation:

$$R_\sigma = 1 + (1 - \mathbf{g}_{ii}^\sigma(l)) \left( e^{-2\lambda\sigma s_i(l)} - 1 \right) \quad (4.1.34)$$

With this, we have collected all basic ingredients necessary to run a simulation.

## 4.2. Dual Fermion Perturbation Theory

Throughout the attached papers and in the last chapter, we use the DQMC approach discussed above to obtain data of a chosen *reference system*, which in turn is used to describe a more complex problem as accurately as possible. Generally, the simplest choice of a reference system is a non-interacting Hamiltonian, which is justified through the validity of Wick's theorem, allowing the straightforward evaluation of many-particle Green's functions. Methods such as the local density approximation within the density functional theory [71] consider an interacting, homogeneous electron gas as a reference. Further below, we also discuss the Dynamical Mean Field Theory (DMFT) [72, 73], which maps a lattice problem onto an interacting impurity problem coupled to a fermionic bath.

Here, based on the lecture notes in [74], we go through the basics of a more general approach which, based on the dual fermion path integral formalism [33], allows us to choose any reference system we deem appropriate. In the following, it is assumed that the reader is familiar with the path integral and action formalism. Extensive introductions on these topics can be found in [75, 76].

To be more specific, the system of interest is a doped Hubbard model which contains hopping terms between both nearest neighbours and next nearest neighbours:

$$H_\alpha = - \sum_{\substack{ij \\ \sigma}} t_{ij}^\alpha c_{i\sigma}^\dagger c_{j\sigma} + U \sum_i \left( n_{i\uparrow} - \frac{1}{2} \right) \left( n_{i\downarrow} - \frac{1}{2} \right) \quad (4.2.1)$$

The interaction term is written in a way that a chemical potential of  $\mu = 0$  corresponds to half-filling of the system. The factor  $\alpha$ , which can be either 0 or 1, determines whether next nearest neighbor hoppings and a shift in  $\mu$  is present in  $t_{ij}^\alpha$ :

$$t_{ij}^\alpha = \begin{cases} t & (i, j) \text{ are nearest neighbours,} \\ \alpha t' & (i, j) \text{ are next nearest neighbors,} \\ \alpha \mu & i = j, \\ 0 & \text{otherwise} \end{cases} \quad (4.2.2)$$

At the interesting regions within the doped square lattice Hubbard model, where  $d$ -wave superconductivity is expected, i.e. at  $U/t \approx 8$  and a temperature at  $k_B T/t \approx 0.1$ , the fermionic sign problem discussed earlier in the DQMC section renders any reasonable simulation impossible [77]. In addition, the exact influence of  $t'$ , which makes the problem even more complicated, is still an unresolved issue [78, 79, 80].

In order to tackle this problem, we make use of the fact that, on a bipartite lattice (e.g. a square lattice treated in this work), there is no sign problem for  $t' = 0$  at half filling (i.e. for  $\alpha = 0$ ). Thus, it is possible to obtain data on  $H_0$  with a very good accuracy, making it a very good reference system compared to the non-interacting case as it already contains strong local and nonlocal correlations. From this starting point, the  $t'$ - and  $\mu$ -terms are treated perturbatively.

With an action  $S_\alpha$  which corresponds to the problem  $H_\alpha$ , the partition function  $\mathcal{Z}_\alpha$  of a fermionic lattice can be expressed as a functional field integral over Grassmann variables  $(c^*, c)$ :

$$\mathcal{Z}_\alpha = \int \mathcal{D}[c^*, c] e^{-S_\alpha[c^*, c]} \quad (4.2.3)$$

Thermodynamic expectation values with respect to  $H_\alpha$  can also be expressed as functional integrals:

$$\langle \dots \rangle_\alpha = \frac{1}{\mathcal{Z}_\alpha} \int \mathcal{D}[c^*, c] \dots e^{-S_\alpha[c^*, c]} \quad (4.2.4)$$

For a periodic lattice with  $N \times N$  lattice sites, which will be used to represent an infinite lattice, and with the combined index for lattice site, imaginary time and spin  $|1\rangle = |i_1, \tau_1, \sigma_1\rangle$ , the action reads as:

$$S_\alpha[c^*, c] = - \sum_{12} c_1^* (\mathcal{G}_\alpha)_{12}^{-1} c_2 + \frac{1}{4} \sum_{1234} U_{1234} c_1^* c_2^* c_4 c_3 \quad (4.2.5)$$

$\mathcal{G}_\alpha$  is the *bare* Green's function with respect to  $H_\alpha$ . It can be calculated by diagonalizing the non-interacting  $H_\alpha$  (i.e.  $U = 0$ ), and then applying Eq.(2.3.8) or Eq.(2.3.9) for  $\tau$ - or  $i\omega_n$ -space, respectively. Since non-interacting Hamiltonians on periodic lattices are diagonalized through a Fourier transform,  $\mathcal{G}_\alpha$  can be obtained in real space afterwards through inverse Fourier transform.

We define the *perturbation matrix*  $\tilde{t}$  as the difference between the inverses of the bare Green's functions for  $\alpha = 0, 1$ :

$$\tilde{t} = \mathcal{G}_0^{-1} - \mathcal{G}_1^{-1} \quad (4.2.6)$$

With  $\tilde{t}$ , a connection between the actions  $S_1$  and  $S_0$  can be expressed as:

$$S_1[c^*, c] = S_0[c^*, c] + \sum_{12} c_1^* \tilde{t}_{12} c_2 \quad (4.2.7)$$

The next step is the transformation from strongly interacting fermions  $(c^*, c)$  to *dual fermions*  $(d^*, d)$  which are weakly correlated. The idea is that weakly correlated systems can be treated perturbatively with good accuracy. The new Grassmann variables come from the following Hubbard-Stratonovich transformation:

$$e^{-c_1^* \tilde{t}_{12} c_2} = \mathcal{Z}_t \int \mathcal{D}[d^*, d] e^{d_1^* \tilde{t}_{12}^{-1} d_2 + d_1^* d_1^* c_1 + c_1^* d_1} \quad (4.2.8)$$

In this notation, a summation over repeated indices is assumed. Furthermore, we have  $\mathcal{Z}_t = \det[-\tilde{t}]$  and  $\tilde{t}_{12}^{-1} \equiv (\tilde{t}^{-1})_{12}$ . Applying this transformation on the partition function yields:

$$\mathcal{Z} = \mathcal{Z}_0 \mathcal{Z}_t \int \mathcal{D}[d^*, d, c^*, c] e^{d_1^* \tilde{t}_{12}^{-1} d_2} \left\langle e^{d_1^* c_1 + c_1^* d_1} \right\rangle_0 \quad (4.2.9)$$

The Grassmann fields  $(c^*, c)$  can now be integrated out, and it can be shown [81] that the expectation value in Eq.(4.2.9) can be expressed as:

$$\left\langle e^{d_1^* c_1} + e^{c_1^* d_1} \right\rangle_0 = \exp \left[ \sum_{n=1}^{\infty} \frac{(-1)^n}{(n!)^2} \gamma_{1\dots n, n' \dots 1'}^{(2n)} d_1^* \dots d_n^* d_{n'} \dots d_{1'} \right] \quad (4.2.10)$$

The  $\gamma$ -terms are defined by connected correlators with respect to the reference system  $S_0$ :

$$\gamma_{1\dots n, n' \dots 1'}^{(2n)} = (-1)^n \langle c_1 \dots c_n c_{n'}^* \dots c_{1'}^* \rangle_{0c} \quad (4.2.11)$$

The first term ( $n = 1$ ) in Eq.(4.2.11) simply corresponds to the Green's function of the reference system, i.e.  $g_{12} = -\langle c_1 c_2^* \rangle_0$ . Aside from the bare Green's function  $\mathcal{G}_0$ , the functions of the reference system  $S_0$  are denoted by small letters. With a given  $g$ , and by looking at Eq.(4.2.9) again, one can find the *bare* Green's function of the dual fermions:

$$\tilde{G}_{12}^0 = (\tilde{t}^{-1} - g)_{12}^{-1} \quad (4.2.12)$$

For  $n = 2$ , the  $\gamma$ -terms correspond to two-particle interactions among the dual fermions, whose corresponding, connected vertex reads as:

$$\gamma_{1234} = \langle c_1 c_2 c_3^* c_4^* \rangle_0 - \langle c_1 c_4^* \rangle_0 \langle c_2 c_3^* \rangle_0 + \langle c_1 c_3^* \rangle_0 \langle c_2 c_4^* \rangle_0 \quad (4.2.13)$$

Within the two-particle approximation, the action of the dual fermions  $\tilde{S}$  can then be expressed as:

$$\tilde{S}[d^*, d] = - \sum_{12} d_1^* \left( \tilde{G}^0 \right)_{12}^{-1} d_2 + \frac{1}{4} \sum_{1234} \gamma_{1234} d_1^* d_2^* d_4 d_3 \quad (4.2.14)$$

It should be noted that the sign and order of operators in the two-particle term is chosen to be consistent with Eq.(4.2.5).

Next, we discuss how obtain a dual self-energy with the help of Monte Carlo methods such as the DQMC algorithm. The first step is to perform a simple run of the reference system in order to obtain the reference Green's function  $g$ . With  $g$  and the perturbation matrix  $\tilde{t}$ , the bare dual Green's function  $\tilde{G}^0$  can be built. Then, a second QMC run is started. As a reminder, within DQMC, the Hubbard interaction is decoupled through a Hubbard-Stratonovich transformation (see Eq.(4.1.12)) which introduces discrete Ising-variables  $\{s\}$ . Within this framework, the first order correction for the dual self-energy  $\tilde{\Sigma}^{(1)}$  can be expressed as:

$$\tilde{\Sigma}_{12}^{(1)} = \frac{1}{N_{\text{MC}}} \sum_{\{s\}} \sum_{34} \gamma_{1324}^d(\{s\}) \tilde{G}_{43}^0 \quad (4.2.15)$$

The sum  $\sum_{\{s\}}$  should be understood as a sum over all measurements during the Monte Carlo simulation, with  $N_{\text{MC}}$  being the total number of measurements. The density vertex  $\gamma^s$  (with spin indices written explicitly now) reads as:

$$\gamma_{1234}^d = \gamma_{1234}^{\uparrow\uparrow\uparrow\uparrow} + \gamma_{1234}^{\uparrow\uparrow\downarrow\downarrow} \quad (4.2.16)$$

Similarly to direct measurements of higher-order correlators in a DQMC simulation, the  $\gamma$ -terms are also obtained through the validity of the Wick-theorem for a fixed configuration  $\{s\}$ :

$$\gamma_{1234}(\{s\}) = \langle c_1 c_2 c_3^* c_4^* \rangle_{\{s\}} = \langle c_1 c_4^* \rangle_{\{s\}} \langle c_2 c_3^* \rangle_{\{s\}} - \langle c_1 c_3^* \rangle_{\{s\}} \langle c_2 c_4^* \rangle_{\{s\}} \quad (4.2.17)$$

A connection between the real and dual Green's functions ( $G$  and  $\tilde{G}$ , respectively) can be found by performing a variation on the logarithm of the partition function,  $\ln \mathcal{Z}$  (see Eq.(4.2.9)), with respect to the elements of the perturbation matrix  $\tilde{t}$  [82]:

$$G_{12} = \frac{\delta(\ln \mathcal{Z})}{\delta \tilde{t}_{21}} = -\tilde{t}_{12}^{-1} + \tilde{t}_{13}^{-1} \tilde{G}_{34} \tilde{t}_{42}^{-1} \quad (4.2.18)$$

If the dual self-energy  $\tilde{\Sigma}$  is known, and with the help of the Dyson equation, i.e.  $\tilde{G}^{-1} = (\tilde{G}^0)^{-1} - \tilde{\Sigma}$ , this expression can be rewritten as:

$$G_{12} = \left[ \left( g + \tilde{\Sigma} \right)^{-1} - \tilde{t} \right]_{12}^{-1} \quad (4.2.19)$$

With this, we have a full recipe on how to obtain an approximate Green's function  $G$  (in real space) of a doped Hubbard model which includes  $t'$ . However, for larger system sizes, the effort necessary to compute the sum  $\sum_{34} \dots$  in Eq.(4.2.15) quickly becomes a problem. To that end, one can make use of the fact that for periodic lattices, both  $\tilde{G}^0$  and  $\tilde{\Sigma}$  (after QMC summation) are translationally invariant, and Fourier transform the above equations.

We start with the transformed bare dual Green's function:

$$\tilde{G}_k^0 = \left( \tilde{t}_k^{-1} - g_k \right)^{-1} \quad (4.2.20)$$

$k \equiv (\mathbf{k}, \omega_n)$  is a combined index which includes the possible  $\mathbf{k}$ -vectors and Matsubara frequencies  $\omega_n$ .

In real space, after measuring a Green's function  $g_{12}(\{s\}) = -\langle c_1 c_2^* \rangle_{\{s\}}$ , the disconnected part of the vertex in Eq.(4.2.13) can be included by subtracting the Green's function  $g$  from the reference run:

$$\tilde{g}_{12}(\{s\}) = g_{12}(\{s\}) - g_{12} \quad (4.2.21)$$

In  $k$ -space, this expression reads as:

$$\tilde{g}_{kk'}(\{s\}) = g_{kk'}(\{s\}) - g_k \delta_{kk'} \quad (4.2.22)$$

It should be noted that, for a specific configuration of  $\{s\}$ , the Green's function  $g_{12}(\{s\})$  is not translationally invariant, and hence the change of indices  $(1, 2) \rightarrow (k, k')$ . The Green's function  $g$  from the reference run is both translationally invariant and has the fermionic symmetries in  $\tau$ -space, which is why it transforms to  $g_k \delta_{kk'}$ .

Taking into consideration that the bare dual Green's function also has all symmetries (and thus transforms as  $\tilde{G}_{12}^0 \rightarrow \tilde{G}_k^0 \delta_{kk'}$ ) and that the same holds for the dual self-energy after QMC-summation, Eq.(4.2.15) can be expressed in  $k$ -space:

$$\tilde{\Sigma}_k^{\uparrow(1)} = \frac{(-1)}{N_{\text{MC}} (\beta N)^2} \sum_{\{s\}} \sum_{k'} \left[ \tilde{g}_{kk}^{\uparrow\uparrow} \tilde{g}_{k'k'}^{\uparrow\uparrow} + \tilde{g}_{kk}^{\uparrow\uparrow} \tilde{g}_{k'k'}^{\downarrow\downarrow} - \tilde{g}_{kk'}^{\uparrow\uparrow} \tilde{g}_{k'k}^{\uparrow\uparrow} \right] \tilde{G}_{k'}^0 \quad (4.2.23)$$

The equation for the spin-down component  $\tilde{\Sigma}_k^{\downarrow(1)}$  is the same as above, but with flipped spins. In paramagnetic systems, one can average over the spins to reduce the Monte Carlo noise.

The real Green's function in  $k$ -space is obtained similarly to Eq.(4.2.19):

$$G_k = \left[ \left( g_k + \tilde{\Sigma}_k \right)^{-1} - \tilde{t}_k \right]^{-1} \quad (4.2.24)$$

The computational advantage of working in  $k$ -space is that in Eq.(4.2.23), there is only one sum over  $k'$  instead of the sums  $\sum_{34\dots}$  in real space. Furthermore, objects like the perturbation matrix  $\tilde{t}$  are very simple to express analytically in  $k$ -space. The price one has to pay is that the Green's functions  $g(\{s\})$  need to be Fourier transformed after every measurement during the Monte Carlo run. While this may be tedious for larger systems, it still saves a large amount of computation time.

### 4.3. DMFT and DCA

In this section, two more methods of obtaining approximate solutions of the Hubbard model are discussed. We start with the widely used *Dynamical Mean-Field Theory* (DMFT). A detailed introduction and a review can be found in [83] and [84], respectively. For our purposes, consider again the problem of a general one-band Hubbard model, with the chemical potential  $\mu$  included in the one-particle terms:

$$H = \sum_{\substack{ij \\ \sigma}} t_{ij} c_{i\sigma}^\dagger c_{j\sigma} + U \sum_i n_{i\uparrow} n_{i\downarrow} \quad (4.3.1)$$

As a reminder, after obtaining the dispersion  $\varepsilon_{\mathbf{k}}$  through Fourier transform (and assuming spin symmetry), the  $\mathbf{k}$ - and frequency-dependent Green's function can be expressed through the self-energy  $\Sigma(\mathbf{k}, i\omega_n)$ , i.e.:

$$G(\mathbf{k}, i\omega_n) = \frac{1}{i\omega_n - (\varepsilon_{\mathbf{k}} - \mu) - \Sigma(\mathbf{k}, i\omega_n)} \quad (4.3.2)$$

The local Green's function in real space, i.e.  $G_{ii}(i\omega_n)$ , plays an important role within the DMFT cycle, and reads as:

$$G_{ii}(i\omega_n) = \sum_{\mathbf{k}} G(\mathbf{k}, i\omega_n) = \sum_{\mathbf{k}} \frac{1}{i\omega_n - (\varepsilon_{\mathbf{k}} - \mu) - \Sigma(\mathbf{k}, i\omega_n)} \quad (4.3.3)$$

While the one-dimensional case ( $D = 1$ ) is the only one that can be solved exactly [85], considerations in the  $D \rightarrow \infty$  limit were the starting point of the DMFT which can be applied to the physically interesting cases with  $D = 2, 3$ . Specifically, the findings that the self-energy has no spatial fluctuations for  $D \rightarrow \infty$ , i.e.  $\Sigma = \Sigma(i\omega_n)$  only depends on the frequency, and that other problems such as the Falicov-Kimball model on a lattice can be mapped to an atomic problem within a dynamic field [86], led to the idea of mapping the Hubbard model to an Anderson impurity problem.

The Anderson impurity model was introduced [87] as a description of magnetic impurities embedded in metals. For a single impurity within one band, the Hamiltonian reads as:

$$H = \sum_{\mathbf{k}\sigma} \varepsilon_{\mathbf{k}} c_{\mathbf{k}\sigma}^\dagger c_{\mathbf{k}\sigma} + \sum_{\sigma} \varepsilon_{d,\sigma} d_{\sigma}^\dagger d_{\sigma} + U d_{\uparrow}^\dagger d_{\uparrow} d_{\downarrow}^\dagger d_{\downarrow} + \sum_{\mathbf{k},\sigma} V_{\mathbf{k}\sigma} \left( d_{\sigma}^\dagger c_{\mathbf{k}\sigma} + c_{\mathbf{k}\sigma}^\dagger d_{\sigma} \right) \quad (4.3.4)$$

The first term corresponds to a band with a dispersion  $\varepsilon_{\mathbf{k}}$ , while  $d_{\sigma}^{(\dagger)}$  annihilates (creates) an electron on the *impurity* with an on-site energy  $\varepsilon_{d,\sigma}$ . As the impurity is supposed to describe strongly localized orbitals, a local Hubbard interaction is assumed. Lastly, the terms with the prefactor  $V_{\mathbf{k}\sigma}$  describe a hopping of electrons between the impurity and the band. Assuming a chemical potential  $\mu$  and zero orbital energy for the impurity, the non-interacting impurity Green's function  $G_{d,\sigma}^0$  can be expressed

through the *hybridization function*  $\Delta_\sigma(i\omega_n)$ :

$$\Delta_\sigma(i\omega_n) = \sum_{\mathbf{k}} \frac{|V_{\mathbf{k}\sigma}|^2}{i\omega_n - \varepsilon_{\mathbf{k}}} \quad (4.3.5)$$

$$G_{d,\sigma}^0 = (i\omega_n + \mu - \Delta_\sigma(i\omega_n))^{-1} \quad (4.3.6)$$

In the interacting case, the impurity Green's function also contains a self-energy  $\Sigma_d(i\omega_n)$ .

The DMFT maps the Hubbard model onto such an impurity problem in a way that the full (interacting) impurity Green's function  $G_{d,\sigma}(i\omega_n)$  coincides with the local lattice Green's function  $G_{ii}(i\omega_n)$ , which is exact for  $D \rightarrow \infty$ . One starts with a guess for the impurity self-energy  $\Sigma_d(i\omega_n)$  (e.g. zero) and makes the approximation  $\Sigma(\mathbf{k}, i\omega_n) \approx \Sigma_d(i\omega_n)$ , from which the local lattice Green's function  $G_{ii,\sigma}(i\omega_n)$  can be calculated. Then, a new hybridization function (which acts as a dynamical mean field) is obtained via:

$$\Delta_\sigma(i\omega_n) = i\omega_n + \mu - G_{ii,\sigma}^{-1} - \Sigma_d(i\omega_n) \quad (4.3.7)$$

An impurity model with the new  $\Delta_\sigma(i\omega_n)$  as its hybridization function is then solved for a new impurity Green's function  $G_d$  and thus, a new impurity self-energy  $\Sigma_d$  via the Dyson-equation:

$$\Sigma_d(i\omega_n) = (G_d^0)^{-1}(i\omega_n) - (G_d)^{-1}(i\omega_n) \quad (4.3.8)$$

$\Sigma_d$  can then again be used to build a new local lattice Green's function  $G_{ii}(i\omega_n)$ , which restarts the cycle. This process is repeated until  $\Sigma_d(i\omega_n)$  is converged.

While the DMFT provided insight to many complicated problems, fully neglecting the spatial dependencies often becomes very inaccurate, especially for novel materials and models which are two-dimensional. Methods such as the *Dynamical Cluster Approximation* (DCA) [35, 88] tackle this restriction by systematically introducing a weak  $\mathbf{k}$ -dependency by, as the name suggests, mapping the problem onto a *cluster* of variable size instead of a single impurity. Here, we introduce the basics, following the notation of the summary found in [89].

Instead of neglecting all  $\mathbf{k}$ -dependencies, the Brillouin zone is divided into  $N_c$  equally sized patches which have a coarse-grained *cluster momentum*  $\mathbf{K}$  at their center. The patches are described by the following function:

$$\phi_{\mathbf{K}}(\mathbf{k}) = \begin{cases} 1 & \text{if } \mathbf{k} \text{ within the patch of } \mathbf{K} \\ 0 & \text{else} \end{cases} \quad (4.3.9)$$

The basic idea is that the actual lattice self-energy depends only weakly on  $\mathbf{k}$  and can be described by a cluster self-energy which depends on a small number of discrete  $\mathbf{K}$ :

$$\Sigma(\mathbf{k}, i\omega_n) \approx \Sigma_c(\mathbf{K}, i\omega_n) \quad (4.3.10)$$



We further introduce a coarse-grained Green's function  $\bar{G}$  which is obtained by taking the lattice Green's function  $G(\mathbf{k}, i\omega_n)$  and averaging out the  $\mathbf{k}$ -dependence not contained in the cluster:

$$\bar{G}(\mathbf{K}, i\omega_n) = \frac{N_c}{N} \sum_{\mathbf{k}} \phi_{\mathbf{K}}(\mathbf{k}) G(k, i\omega_n) = \frac{N_c}{N} \sum_{\mathbf{k}} \phi_{\mathbf{K}}(\mathbf{k}) \frac{1}{i\omega_n - (\varepsilon_{\mathbf{k}} - \mu) - \Sigma^{\text{DCA}}(\mathbf{k}, i\omega_n)} \quad (4.3.11)$$

The self-energy  $\Sigma^{\text{DCA}}(\mathbf{k}, i\omega_n)$  can be expressed through its cluster counterpart, using the patch function  $\phi_{\mathbf{K}}(\mathbf{k})$  to extend its dependency from  $\mathbf{K}$  to all  $\mathbf{k}$ :

$$\Sigma^{\text{DCA}}(k, i\omega_n) = \sum_{\mathbf{K}} \phi_{\mathbf{K}}(\mathbf{k}) \Sigma_c(\mathbf{K}, i\omega_n) \quad (4.3.12)$$

From  $\bar{G}$  and  $\Sigma_c$ , a non-interacting cluster Green's function can be built:

$$G_c^0 = [\bar{G}^{-1}(\mathbf{K}, i\omega_n) + \Sigma_c(\mathbf{K}, i\omega_n)]^{-1} \quad (4.3.13)$$

With this  $G_c^0$ , and assuming a Hubbard interaction with the strength  $U$ , a new cluster problem is built and solved with a method of choice. Once a new cluster Green's function  $G_c$  has been obtained, a new cluster self-energy follows as:

$$\Sigma_c(\mathbf{K}, i\omega_n) = (G_c^0)^{-1}(\mathbf{K}, i\omega_n) - (G_c)^{-1}(\mathbf{K}, i\omega_n) \quad (4.3.14)$$

From here, similarly to the DMFT, the cycle is restarted until the self-energy is converged. Indeed, one can easily recover the DMFT by setting  $N_c = 1$  which is the same as neglecting the  $\mathbf{k}$ -dependence. Although not used here, it should be noted that it is also possible to obtain self-energies which are smooth instead of constant within the patches, through interpolation schemes like the DCA<sup>+</sup>-method [90].

#### 4.4. CT-AUX

Within the DMFT and DCA formalism discussed in the previous section, an interacting impurity or cluster problem needs to be solved explicitly. Within the action formalism, after obtaining a non-interacting impurity or cluster Green's function  $G^0$ , and assuming a Hubbard interaction with the strength  $U$ , the action  $S$  and partition function  $\mathcal{Z}$  of the model can be expressed as:

$$S[\phi^*, \phi] = - \int_0^\beta \int_0^\beta d\tau d\tau' \sum_{\substack{ij \\ \sigma}} \phi_{i\sigma}^*(\tau) G_{ij,\sigma}^0(\tau - \tau') \phi_{j\sigma}(\tau') \\ + \int_0^\beta d\tau \sum_i U \phi_{i\uparrow}^*(\tau) \phi_{i\uparrow}(\tau) \phi_{i\downarrow}^*(\tau) \phi_{i\downarrow}(\tau) \quad (4.4.1)$$

$$\mathcal{Z} = \int \mathcal{D}[\phi^*, \phi] e^{-S[\phi^*, \phi]} \quad (4.4.2)$$

While methods which are very similar to the idea of the DQMC (see Ch.(4.1.2)) are available as impurity solvers [91], more recent developments were focused on so-called *continuous-time* Monte Carlo approaches [92] which do not suffer from the systematic error stemming from the Trotter discretization of the imaginary time. Thus, extrapolations of the discrete time steps, i.e.  $\Delta\tau \rightarrow 0$ , are not necessary. Specifically, we discuss the CT-AUX solver developed by the Gull group. The main paper [93] discusses the derivation for a single impurity model and explains generalizations at the end, while the short summary in [89] provides a derivation for clusters. Notation-wise, we will follow the latter.

Going back to a Hamiltonian formulation, the problem can be written as  $H = H_0 + V$ , with  $H_0$  containing the one-particle and Hubbard interaction terms, respectively. Following [94], by introducing a nonzero  $K$ , the partition function can be expressed as:

$$\mathcal{Z} = \text{Tr} \left( e^{-\beta H} \right) = e^{-K} \text{Tr} \left( e^{-\beta H_0} T_\tau \exp \left[ - \int_0^\beta d\tau (V(\tau) - K/\beta) \right] \right) \quad (4.4.3)$$

After expanding the time-ordered exponential into powers of  $K/\beta - V$ , the following auxiliary field decomposition is applied:

$$1 - \frac{\beta U}{K} \sum_i \left[ n_{i\uparrow} n_{i\downarrow} - \frac{1}{2} (n_{i\uparrow} + n_{i\downarrow}) \right] = \frac{1}{2N_c} \sum_i \sum_{s_i = \pm 1} e^{\gamma s_i (n_{i\uparrow} - n_{i\downarrow})} \quad (4.4.4)$$

$N_c$  denotes the number of cluster sites, while  $\gamma$  is defined by  $\cosh(\gamma) = 1 + U\beta N_c/2K$ . The partition function then reads as:

$$\mathcal{Z} = \sum_{n=0}^{\infty} \sum_{s_i \dots s_n = \pm 1} \int_0^\beta d\tau_1 \dots \int_{\tau_{n-1}}^\beta d\tau_n \left( \frac{K}{2\beta N_c} \right)^n Z_n(\{x, \tau, s\}_n) \quad (4.4.5)$$

For the expansion order  $n$  with auxiliary Ising spins  $s_1 \dots s_n$ , the term  $Z_n$  is:

$$Z_n(\{x, \tau, s\}_n) = Z_0 \prod_{\sigma} \det N_{\sigma}^{-1}(\{x, \tau, s\}_n) \quad (4.4.6)$$

$\{x, \tau, s\}_n$  denotes a specific configuration of  $n$  vertices with cluster site  $x$ , imaginary time  $\tau$  and Ising spin  $s$ . With  $\mathcal{G}_{\sigma}^0$  being the bare cluster Green's function,  $N_{\sigma}$  is a  $n \times n$  matrix with the entries defined as follows:

$$[N_{\sigma}^{-1}]_{ij} = \left( e^{\gamma(-1)^{\sigma} s_i} \right) \delta_{ij} - \mathcal{G}_{\sigma}^0(x_i, \tau_i; x_j, \tau_j) \quad (4.4.7)$$

In summary, the product of determinants of matrices  $N_{\sigma}$  defines the statistical weight of a configuration  $\{x, \tau, s\}_n$ .  $\mathcal{Z}$  can then be sampled by randomly creating or removing Ising spins  $s$  at random cluster sites  $x$  and imaginary times  $\tau$ . Although we do not discuss the details here, it should be noted that measurements can be done in a similar fashion as in the DQMC algorithm, since the auxiliary field decoupling here also leads to the validity of Wick's theorem.

---

## 5. Nonlocal Exchange Interactions in Strongly Correlated Electron Systems

### 5.1. Scope of the work and Statement of Contributions

In the first publication, we discuss the effects of extending the Hubbard model by a ferromagnetic Heisenberg term which represents the nonlocal exchange interaction (see Ch.(2.6)). Said exchange interactions were usually neglected due to the smallness of the respective integrals in three-dimensional solids, but as there is no reason to believe this translates to novel, two-dimensional materials, we thought it worthwhile to revisit the problem of a Hubbard-Heisenberg Hamiltonian on a square lattice.

Due to the complexity of the the problem, we applied the variational mapping discussed in Ch.(3.3.1) as a new approximation. After benchmarking on an exactly solvable 4-site model which illustrates that this method is more adequate than static mean-field theory, we applied it on a periodic, half-filled square lattice with the help of Determinantal QMC. The results show that our new method predicts a continuous transition of the sign of the spin-spin correlation between adjacent sites (i.e. antiferromagnetic vs. ferromagnetic ground state), where static mean-field theory wrongly predicts a first-order phase transition.

The calculations and substantial parts of the manuscript were done by me. After a few revisions between Malte Schüler and me, we revised the text a few more times with Tim Wehling and Gerd Czyscholl before submitting it to Physical Review B.

### 5.2. Actual Paper

Starting on the next page, we present the paper as published [36] in *Physical Review B*, on the 26th June 2020.

**Nonlocal exchange interactions in strongly correlated electron systems**Edin Kapetanović<sup>1,2</sup>, Malte Schüler<sup>1,2</sup>, Gerd Czycholl,<sup>1</sup> and Tim O. Wehling<sup>1,2</sup><sup>1</sup>*Institut für Theoretische Physik, Universität Bremen, Otto-Hahn-Allee 1, D-28359 Bremen, Germany*<sup>2</sup>*Bremen Center for Computational Materials Science, Universität Bremen, Am Fallturm 1a, D-28359 Bremen, Germany* (Received 19 November 2019; accepted 17 April 2020; published 26 June 2020)

We study the influence of ferromagnetic nonlocal exchange on correlated electrons in terms of an SU(2)-Hubbard-Heisenberg model and address the interplay of on-site interaction induced local moment formation and the competition of ferromagnetic direct and antiferromagnetic kinetic exchange interactions. In order to simulate thermodynamic properties of the system in a way that largely accounts for the on-site interaction driven correlations in the system, we advance the correlated variational scheme introduced in [M. Schüler *et al.*, *Phys. Rev. Lett.* **111**, 036601 (2013)] to account for explicitly symmetry broken electronic phases by introducing an auxiliary magnetic field. After benchmarking the method against exact solutions of a finite system, we study the SU(2) Hubbard-Heisenberg model on a square lattice. We obtain the  $U$ - $J$  finite temperature phase diagram of a SU(2)-Hubbard-Heisenberg model within the correlated variational approach and compare it to static mean-field theory. While the generalized variational principle and static mean-field theory yield transitions from dominant ferromagnetic to antiferromagnetic correlations in similar regions of the phase diagram, we find that the nature of the associated phase transitions differs between the two approaches. The fluctuations accounted for in the generalized variational approach render the transitions continuous, while static mean-field theory predicts discontinuous transitions between ferro- and antiferromagnetically ordered states.

DOI: [10.1103/PhysRevB.101.235165](https://doi.org/10.1103/PhysRevB.101.235165)**I. INTRODUCTION**

One of the most intensively studied and most fundamental models for the description of correlated electrons on a crystal lattice is the Hubbard model [1–5]. The central point of this model is to neglect all interactions aside from the local Coulomb repulsion between two electrons occupying the same lattice site. While the approximation of purely local interaction can pose a drastic simplification, the model is still capable of describing a wide range of phenomena from Mott-Hubbard metal-insulator transitions to unconventional superconductivity. This is why the model became a key for understanding the competition between itinerancy and localization due to interactions. Several recently emerging quantum materials challenged the Hubbard model paradigm and realize correlated electron physics likely governed by more complex interaction patterns.

First, in low-dimensional and insulating systems, the neglected nonlocal Coulomb interactions play a significant role due to reduced screening, and the Hubbard model can fail to provide an adequate description. It is well known by now that nonlocal Coulomb repulsion in the form of so-called density-density terms can drive the system towards a charge density wave (CDW) [6–8], effectively screen the local interaction [9], influence possibly existing tendencies towards superconductivity [10–12], and lead to a renormalization of Fermi velocities [13,14].

In systems like twisted bilayer graphene [15,16] or other twisted 2D materials [17], general four fermion interactions are likely steering the low-energy electrons [18] due to the intricate real space patterns of the low-energy electronic Wannier functions. Currently, very little is known about the

effects of general nonlocal four fermion interaction terms on electronic correlation phenomena. Among these are effects of, e.g., correlated hopping terms and importantly nonlocal exchange interactions  $J$ .

Traditionally,  $J$  has been neglected mostly based on the smallness of the direct exchange integral ( $J \sim 1/40$  eV for  $3d$  electrons) in comparison to the on-site repulsion ( $U \sim 10$  eV [1]). However, this argumentation can be misleading. Generally, in the strong coupling case with  $U \gg t$  exceeding the hopping  $t$  by far,  $J$  competes against the kinetic exchange given by  $-4t^2/U$ , which can be orders of magnitude smaller than the original  $U$ . As such, it is plausible that a small  $J$  is sufficient to push the system towards a ferromagnetic instability. So far, various studies [19–23], came to different conclusions, and we believe it is worth to revisit this issue with novel methods. Additionally, for novel, synthetic quantum materials like twisted bilayer graphene, where the electron correlations emerge beyond the atomic scale, it is very unclear why any estimates made for  $3d$ -electron materials should transfer to this case.

In this paper, we advance a theoretical approach to account for interaction terms beyond the on-site Hubbard paradigm. We consider the explicit example of the Hubbard-Heisenberg model, which supplements the Hubbard model with nonlocal exchange terms, and analyze the interplay of on-site repulsion and nonlocal exchange effects. This problem has so-far been addressed with different approaches: First, SU( $N$ ) generalizations of the Hubbard-Heisenberg model have been studied in the large- $N$  limit [24–26]. Secondly, the important SU(2)-case has been studied in terms of static Hartree-Fock mean-field theory (MFT) [27,28]. Calculations in the framework of the dynamical mean-field theory (DMFT) [23,29], which are

exact in infinite dimensions, yield a phase diagram similar to the one we present in this work. Here, we develop a variational approach to study the impact of quantum and thermal fluctuations on the interplay of local moment formation with ferromagnetic and antiferromagnetic spin correlations in the SU(2) Hubbard-Heisenberg model. In infinite dimensions, our method indeed coincides with the DMFT approach. However, within our approach, there is no systematical error linked to the dimension of the system, which makes it more suitable for application on low-dimensional materials.

The paper is structured as follows. In Sec. II A, we introduce the Hubbard-Heisenberg model. Section II B explains the generalization of the variational approach from Ref. [9] to account for explicitly symmetry broken phases and nonlocal exchange interactions: we map the Hubbard-Heisenberg Hamiltonian to an auxiliary Hamiltonian, which includes a renormalized Hubbard interaction and allows for breaking of the SU(2) spin symmetry by including an effective, external magnetic field in  $z$  direction. In Sec. II C, we then give the computational details of the simulations of this auxiliary system performed with determinantal quantum Monte Carlo (DQMC).

In Sec. III A, we compare the exact solution of a four-site Hubbard-Heisenberg cluster to approximate solutions from the variational approach developed here and to MFT for benchmarking purposes. Section III B discusses the phase diagram and thermodynamic properties of the SU(2) Hubbard-Heisenberg model on a square lattice. The phase diagrams obtained with the generalized variational principle and MFT are qualitatively similar. We find, however, that the fluctuations accounted for in the generalized variational approach render the transitions between ferro- and antiferromagnetically correlated states continuous, while MFT predicts discontinuous transitions. Furthermore, we illustrate and discuss the nonmonotonous influence of a small, direct exchange, on correlation functions such as the double occupancy.

## II. METHODS

### A. The Model Hamiltonian

Consider an extended Hubbard model for electrons on a lattice which includes nonlocal interactions:

$$H = \sum_{i,j,\sigma} t_{ij} c_{i\sigma}^\dagger c_{j\sigma} + U \sum_i n_{i\uparrow} n_{i\downarrow} + \frac{1}{2} \sum_{i \neq j, \sigma, \sigma'} V_{ij} n_{i\sigma} n_{j\sigma'} - \frac{1}{2} \sum_{i \neq j} J_{ij} \vec{S}_i \cdot \vec{S}_j. \quad (1)$$

Here,  $c_{i\sigma}^\dagger$  and  $c_{i\sigma}$  denote the creation and annihilation operators for an electron in a Wannier state on site  $i$  with the spin  $\sigma$ . The  $t_{ij}$  contain the hopping matrix elements and the on-site energies.  $U$  is the on-site interaction strength, while  $V_{ij}$  and  $J_{ij}$  are the nonlocal Coulomb repulsion and the exchange interaction, respectively.  $n_{i\sigma} = c_{i\sigma}^\dagger c_{i\sigma}$  denotes the occupation number operator, while  $\vec{S}_i$  represents the spin operator.

In previous papers [9,30], it was shown that the nonlocal Coulomb repulsion can be included in an effective Hubbard model with local interactions only, by renormalizing the on-site repulsion. While this mapping is an approximation,

especially regarding the charge correlations, it works well for describing the spin dynamics since the  $V$  term couples to the charge degrees of freedom. The nonlocal exchange, which we focus on, however, couples directly to the spin degrees of freedom. Thus, in this work, we assume that the nonlocal repulsion has already been absorbed into an effective Hubbard  $U$  and neglect the  $V$  terms. We restrict ourselves to a one-band model with only next-neighbor hopping and interactions on a square lattice, which corresponds to the following Hubbard-Heisenberg-Hamiltonian:

$$H = -t \sum_{\langle i,j \rangle, \sigma} (c_{i\sigma}^\dagger c_{j\sigma} + \text{H.c.}) + U \sum_i n_{i\uparrow} n_{i\downarrow} - J \sum_{\langle i,j \rangle} \vec{S}_i \cdot \vec{S}_j \quad (2)$$

Here, the  $\langle i, j \rangle$  denote pairs of nearest-neighbor sites.

### B. The variational principle

Our goal is to obtain an approximation to thermodynamic properties of the system defined in Eq. (2) by mapping it onto a simpler auxiliary system which is easier to handle. More precisely, we want to describe the properties of  $H$  by mapping it onto an effective Hamiltonian  $\tilde{H}$ :

$$\tilde{H} = -t \sum_{\langle i,j \rangle, \sigma} (c_{i\sigma}^\dagger c_{j\sigma} + \text{H.c.}) + \tilde{U} \sum_i n_{i\uparrow} n_{i\downarrow} - \tilde{B} \sum_i S_i^z. \quad (3)$$

The effective, magnetic field  $\tilde{B}$  has been introduced in order to implement ferromagnetic correlations, which stem from the Heisenberg-term in  $H$  and cannot be captured in the framework of a simple half-filled Hubbard model. While we intend to use the effective model in Eq. (3) as a variational ansatz, it should be noted that this reduction becomes exact in the limit of infinite dimensions since a mean-field decoupling can be applied to the Heisenberg-term. Such a model has been studied within DMFT before [23]. Keeping a renormalized on-site interaction  $\tilde{U}$  allows this auxiliary system to capture correlations which go beyond Hartree-Fock theory. As shown in Appendix A, setting  $\tilde{U} = 0$  is indeed equivalent to a mean-field description. A rationale behind introducing the auxiliary magnetic field  $\tilde{B}$  is the following: the Hubbard model with on-site interactions has different low-energy states *close* to the ground state. The auxiliary field  $\tilde{B}$  lowers those with desirable spin polarization in energy to achieve an optimized description of the full system.

For the mapping of the Hubbard Heisenberg model, Eq. (2), to the auxiliary Hubbard model in an external magnetic field, Eq. (3), we make use of the Peierls-Feynman-Bogoliubov variational principle [31–33].  $(\tilde{U}, \tilde{B})$  are variational parameters which are chosen so that the density operator  $\rho_{\tilde{H}}$  of the auxiliary system  $\tilde{H}$  approximates the real density operator  $\rho_H$  as good as possible. In order to do so, we minimize the following expression with respect to the parameters  $(\tilde{U}, \tilde{B})$ :

$$\Phi_H \leq \tilde{\Phi} = \langle H - \tilde{H} \rangle_{\tilde{H}} + \Phi_{\tilde{H}}, \quad (4)$$

Here,  $\Phi_H = -\frac{1}{\beta} \ln Z_H$  denotes the grand canonical potential<sup>1</sup> of the original Hamiltonian  $H$  with  $Z_H = \text{Tr}(e^{-\beta H})$  being the partition function while  $\Phi_{\tilde{H}}$  is the grand canonical potential of the auxiliary system.  $\langle A \rangle_{\tilde{H}} = \frac{1}{Z_{\tilde{H}}} \text{Tr}(A e^{-\beta \tilde{H}})$  expresses the expectation value of an operator  $A$  evaluated with the thermodynamic density operator of the effective Hamiltonian  $\tilde{H}$ . Evaluating the expression for  $\tilde{\Phi}$  in Eq. (4) leads to

$$\begin{aligned} \tilde{\Phi} = & (U - \tilde{U}) \sum_i \langle n_{i\uparrow} n_{i\downarrow} \rangle_{\tilde{H}} - J \sum_{(i,j)} \langle \vec{S}_i \cdot \vec{S}_j \rangle_{\tilde{H}} \\ & + \tilde{B} \sum_i \langle S_i^z \rangle_{\tilde{H}} + \Phi_{\tilde{H}}. \end{aligned} \quad (5)$$

### C. Quantum Monte Carlo: computational details

We solve the effective Hamiltonian  $\tilde{H}$  for different  $(\tilde{U}, \tilde{B})$  on a square lattice by performing determinantal quantum Monte Carlo (DQMC) [34] simulations with the quantum electron simulation toolbox (QUEST) code [35]. The raw data obtained from the simulation are available in Ref. [36]. We restrict our calculations to the half-filled case for which no sign problem exists even for  $\tilde{B} \neq 0$ . The temperature for all simulations presented in this work is set to  $\beta t = 10$ , which means that for a square lattice, the thermal energy is of the order of 1/40 of the free system bandwidth. This temperature is cold enough to observe correlations and to capture the interesting phase transitions, particularly the metal-insulator transition [37]. In order to deal with finite size effects, we performed calculations for different system sizes (i.e.,  $4 \times 4$ ,  $6 \times 6$ ,  $8 \times 8$ ,  $10 \times 10$ , and  $12 \times 12$ ) with periodic boundary conditions and extrapolate to the  $N \rightarrow \infty$  limit as described in Ref. [30].

In order to achieve good qualitative results, a rough estimate is to choose a discretization  $\Delta\tau \sim \sqrt{0.125/U}$  for the Trotter-Suzuki decomposition [38]. For  $U = 6$ , which is the highest value that we use for the mapping, this leads to  $\Delta\tau \approx 0.144$ . In order to minimize the remaining Trotter error, instead of simulating the system only at  $\Delta\tau = 0.1$ , we also simulate  $\Delta\tau = 0.2$ . This allows for an extrapolation  $\Delta\tau \rightarrow 0$ , since the Trotter error is known to scale with  $\mathcal{O}(\Delta\tau^2)$ . In Appendix B, we provide an example which justifies the extrapolation with only two data points.

For each data point for  $(\tilde{U}, \tilde{B})$  with 28 data points  $\tilde{U}/t = 0-6$  and 48 data points for  $\tilde{B}/t = 0-4$ , the simulation is run with 10 000 warmup sweeps and 30 000 measurement sweeps. In order to significantly reduce the Monte Carlo noise, we smooth the data with a two-dimensional Savitzky-Golay filter, as further explained in Appendix C 1.

While the double occupancies and the spin-related expectation values appearing in Eq. (5) can be directly measured within DQMC, determining the grand canonical potential  $\Phi_{\tilde{H}}$  of the effective system requires a coupling constant integration. Since

$$-\frac{\partial \Phi_{\tilde{H}}}{\partial \tilde{B}} = \sum_i \langle S_i^z \rangle_{\tilde{H}}, \quad \frac{\partial \Phi_{\tilde{H}}}{\partial \tilde{U}} = \sum_i \langle n_{i\uparrow} n_{i\downarrow} \rangle_{\tilde{H}}.$$

<sup>1</sup>Free energy in the canonical case.

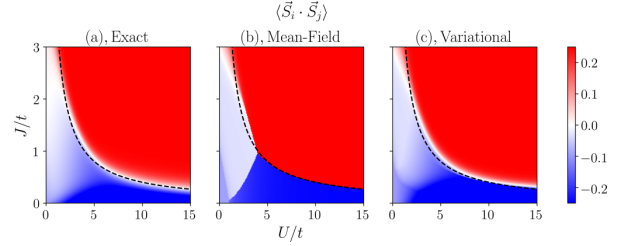


FIG. 1. Spin-spin correlation between next neighbors on a four-site model. The  $4t^2/U$  line is where the transition is expected analytically in the strong- $U$  limit. (a) Exact diagonalization. (b) Mean-field treatment which allows ferromagnetic and antiferromagnetic ordering. (c) Variational approach.

$\Phi_{\tilde{H}}$  can be determined (up to a constant) by integrating with respect to  $(\tilde{U}, \tilde{B})$ :

$$\begin{aligned} \Phi_{\tilde{H}}(\tilde{U}, \tilde{B}) = & \sum_i \int_0^{\tilde{U}} dU' \langle n_{i\uparrow} n_{i\downarrow} \rangle_{\tilde{H}}(U', 0) \\ & - \sum_i \int_0^{\tilde{B}} dB' \langle S_i^z \rangle_{\tilde{H}}(\tilde{U}, B') + \Phi_{\tilde{H}}(0, 0). \end{aligned} \quad (6)$$

The constant  $\Phi_{\tilde{H}}(0, 0)$  corresponds to the grand canonical potential of a tight-binding model, which may be evaluated analytically. However, this constant is not relevant when searching for the minima of  $\tilde{\Phi}$ .

## III. RESULTS

### A. Benchmarking: four-site model

To assess merit and shortcomings of the variational method suggested, here, we perform benchmark calculations for a system which can also be solved exactly. In the following, we compare solutions of the Hubbard-Heisenberg Hamiltonian, Eq. (2), on a four-site cluster obtained with exact diagonalization, the Hartree-Fock approximation and with the generalized variational principle explained in Sec. II B.

We treat the system at half filling by setting the chemical potential to  $\mu = U/2$ . Figure 1 then shows the total spin-spin correlation between next neighbors  $\langle \vec{S}_i \cdot \vec{S}_j \rangle$  obtained by the three different approaches: exact diagonalization, a spin-unrestricted mean-field treatment which allows for both ferromagnetic and antiferromagnetic solutions (see Appendix A) and the variational approach which uses the effective Hamiltonian  $\tilde{H}$  [Eq. (3)]. Before analyzing the data, it is important to note that for the strong-coupling case ( $U \gg t$ ), the behavior of the system is known, as the Hubbard model becomes equivalent to a Heisenberg model [39] with an antiferromagnetic kinetic exchange coupling  $-4t^2/U$  between nearest-neighbor spins. In our case, the kinetic exchange competes with the ferromagnetic direct exchange  $J$  and one obtains

$$H \stackrel{U \gg t}{\approx} -\left(J - \frac{4t^2}{U}\right) \sum_{(i,j)} \vec{S}_i \cdot \vec{S}_j.$$

From this, it is easy to see that the nearest-neighbor spin-spin correlations should change sign at  $J = 4t^2/U$  in the large- $U$

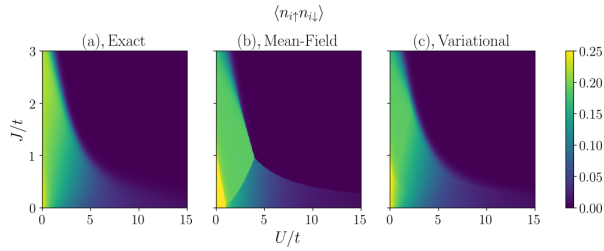


FIG. 2. Double occupancy on a four-site model. (a) Exact diagonalization. (b) Hartree-Fock mean-field treatment which allows ferromagnetic and antiferromagnetic ordering. (c) Variational approach.

limit. A  $4t^2/U$  line is plotted as a dashed, black curve inside the pictures.

The exact solution in Fig. 1(a) shows continuous transitions from positive to negative nearest-neighbor spin-spin correlations. As expected, antiferromagnetic correlations dominate where  $J$  is small, while a large  $J$  leads to ferromagnetic correlations. One should keep in mind, however, that the finite size of the system prohibits actual antiferromagnetic or ferromagnetic ordering in the exact solution. This differs from the other approximative cases where symmetry breaking is explicitly allowed. The MFT treatment in Fig. 1(b) correctly predicts a competition between direct and kinetic exchange in the strong- $U$  limit, however fails to capture the correct order of the transition as the system undergoes a first-order phase transition from the Néel to the ferromagnetic state (and vice versa), which does not occur in the exact solution.

The spin-spin correlations as calculated with the variational approach [Fig. 1(c)] are in much closer agreement with the exact solution [Fig. 1(a)] than the MFT results [Fig. 1(b)]. It should be noted, that, similarly to the mean-field result, a small step (i.e., a first-order transition) is still visible for intermediate  $U$ , which is an artifact of the method itself. This problem is, however, much less severe than in the mean-field treatment. In the  $U = 0$  case, the variational approach and the MFT become equivalent. Both yield the same result in this case, as it must be.

The double occupancy, as obtained from the exact solution, MFT and the variational approach, is shown in Fig. 2. The transitions seen in the spin-spin correlation functions manifest themselves also in the  $U$ - $J$  dependence of the double occupancies. In the exact solution, it is visible that both the Hubbard  $U$  and the direct exchange  $J$ , by themselves, tend to reduce the double occupancy, and thus localize the electrons. However, kinetic (antiferromagnetic) and direct (ferromagnetic) exchange can cancel each other, which leads to nonmonotonous behavior when both interactions are present.

This can be seen more clearly from the lineplots of the spin-spin correlation function and the double occupancy shown in Fig. 3. For both values of  $U$ , the variational approach approximates the exact solution much closer than the MFT treatment. One important thing to consider is the spin-spin correlation for a strong Hubbard  $U$  [Fig. 3(b)]. For small  $J$ , MFT describes the antiferromagnetic correlations by explicitly going into a Néel state, which leads to a value of  $\langle \vec{S}_i \cdot \vec{S}_j \rangle = -\frac{1}{4}$  for spin  $-\frac{1}{2}$  fermions (i.e., electrons). However,

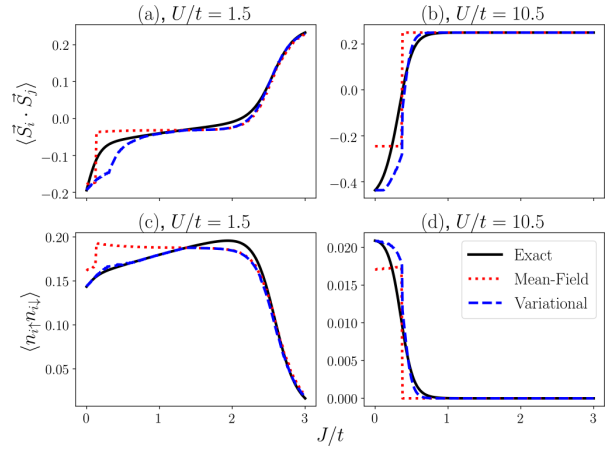


FIG. 3. Correlation functions for two different, fixed values  $U$ , depending on  $J$ . The black line shows the exact solution. The red dotted line stems from the mean-field solution, while the blue dashed lines come from our variational approach. [(a) and (b)] Next-neighbor spin-spin correlation. [(c) and (d)] Double occupancy.

antiferromagnetic correlations are, as shown in the plot, much stronger. Since the auxiliary system  $\tilde{H}$  is a correlated problem due to the on-site interaction  $\tilde{U}$ , it is capable of capturing such behavior.

## B. Hubbard-Heisenberg model on the square lattice

In the following, we study the spin-spin correlation functions and the double occupancies of the Hubbard-Heisenberg model on the square lattice obtained in MFT and with the generalized variational approach.

Figure 4(a) shows the nearest-neighbor spin-spin correlation function, depending on  $U$  and  $J$  obtained from MFT. Qualitatively, it behaves similarly to the mean-field solution of the four-site model, where the transition from dominantly antiferromagnetic to ferromagnetic spin-correlations are continuous for small  $U$ , while a discontinuity appears with increasing  $J$  for larger  $U \gtrsim 3$ . The transition does not occur

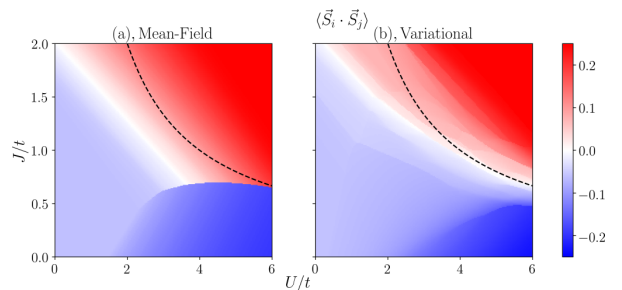


FIG. 4. Spin-spin correlation of the Hubbard-Heisenberg model between next neighbors on a half-filled square lattice, obtained from extrapolated data ( $N \rightarrow \infty$ ) at  $\beta t = 10$ . The  $4t^2/U$  line is where the transition is expected analytically in the strong- $U$  limit. (a) Hartree-Fock mean-field treatment which allows ferromagnetic and antiferromagnetic ordering. (b) Variational approach.



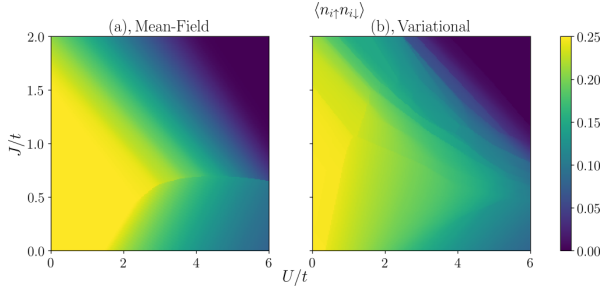


FIG. 5. Double occupancy of the Hubbard-Heisenberg model on a half-filled square lattice, obtained from extrapolated data ( $N \rightarrow \infty$ ) at  $\beta t = 10$ . (a) Hartree-Fock mean-field treatment which allows ferromagnetic and antiferromagnetic ordering. (b) Variational approach.

at the  $4t^2/U$  line in the parameter regime of  $U < 6$  shown, here. At stronger on-site repulsion,  $U > 7$  MFT does however recover the transition at  $J \approx 4t^2/U$  as expected in the strong coupling limit (see Appendix A).

Figure 4(b) shows the  $U$  and  $J$  dependence of the spin-spin correlation function, obtained from the variational principle. The spin-spin correlation functions obtained within mean-field theory and with the variational principle are similar regarding the global shape of predominantly ferromagnetically and antiferromagnetically correlated regions. Differences occur however at a quantitative level. First, in the variational principle, the crossover point  $\langle \vec{S}_i \cdot \vec{S}_j \rangle = 0$  from antiferro- to ferromagnetic correlations approaches the strong-coupling expectation of  $J = 4t^2/U$  already at much smaller on-site interaction  $U/t \approx 3$  than in the MFT case. Furthermore, the  $J$ -induced crossover from predominant antiferromagnetic to ferromagnetic spin correlations is smoother than in MFT. While several smaller steps are still appearing in the spin-spin correlation function calculated with the variational principle, we find that these steps are within our estimated errors [see Appendix C 3).

Furthermore, a step is still visible even at  $U = 0$ , where our results should coincide with the MFT. Since there is no systematic Trotter error for  $U = 0$ , this clearly hints that the steps stem from finite size effects which remain even after extrapolating to  $N \rightarrow \infty$ . This leads us to the conclusion that, within our variational framework, the transition into the area with ferromagnetic correlations with increasing  $J$  is smooth.

Figure 5 shows the double occupancy in MFT (a) and within the variational framework (b) depending on  $U$  and  $J$ . Qualitatively, as is the case for the spin-spin correlations, both results are roughly similar. However, the transition between states with different expectation values of the double occupancies is smooth within the variational approach, whereas MFT gives again a discrete step for  $U/t \gtrsim 3$ . Notably, as illustrated in a line plot in Fig. 6, the influence of  $J$  on the double occupancy is nonmonotonous, which we also observed for the four-site cluster (see Fig. 2). While both the  $J$  and the  $U$  terms in  $H$  support the formation of local magnetic moments and thus reduce the double occupancy, the interplay between the two can lead to a higher value. At  $U/t = 3$  in Fig. 6, where the Mott-Heisenberg picture (competition between direct exchange  $J$  and kinetic exchange  $-4t^2/U$ ) is not appropriate,

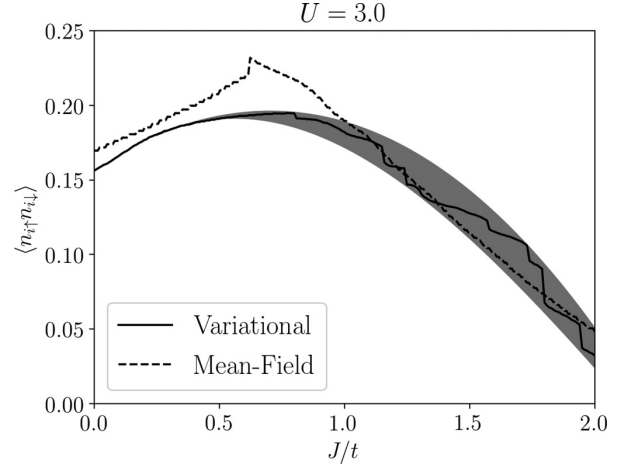


FIG. 6. Double occupancy of the Hubbard-Heisenberg model as function of nearest-neighbor Heisenberg exchange  $J$  at a fixed  $U/t = 3$ . The shaded, grey area is meant to mark uncertainties resulting from finite size effects in the DQMC data.

this can be understood as a competition between Heisenberg-type ferromagnetism and Slater-type antiferromagnetism. A  $J$  which is of the order of the hopping amplitude  $t$  can lead to a nonnegligible difference in the double occupancy and other correlation functions.

Qualitatively, our phase diagrams look similar to what is known from DMFT calculations [23,29]. This stems from the fact that, in infinite dimensions, and assuming that the local interaction remains unchanged ( $\tilde{U} = U$ ), the effective Hamiltonian  $\tilde{H}$  corresponds to the DMFT problem. The spatial correlations neglected in DMFT (and taken into account in this work) lead to quantitative differences only. However, the accuracy of the variational approach presented here does not systematically depend on the system dimension, which makes it more suitable for application on low-dimensional problems. Additionally, allowing renormalization of the local interaction allows the discussion of screening effects. Thus our work complements what is known from DMFT by providing improvements which are necessary for describing low-dimensional materials.

#### IV. CONCLUSIONS AND OUTLOOK

In this work, we investigated the properties of a Hubbard-Heisenberg model, which interpolates between many mechanisms for magnetism, i.e., the Slater, Stoner, and Heisenberg picture. For the realistic  $SU(2)$  case, we presented the  $U$ - $J$  phase diagram for a half-filled square lattice which goes beyond static mean-field theory, by employing a Hubbard model with broken spin symmetry as an effective Hamiltonian through the use of the Feynman-Peierls-Bogoliubov variational principle. While both interactions present in the system lead to the formation of local magnetic moments, the interplay between the two (e.g., the competition between Slater-type antiferromagnetism and Heisenberg-type ferromagnetism) can lead to nonmonotonous behavior in properties such as the double occupancy. Compared to the discrete

transitions between areas with dominant antiferromagnetic and ferromagnetic correlations, obtained within the Hartree-Fock mean-field treatment, the variational approach leads to continuous transitions. While direct Monte Carlo simulations of the lattices are strongly restricted due to the sign problem, other approaches (e.g., dynamical mean-field theory, dynamical cluster approximations, cluster dynamical mean-field approaches) where the problem is less severe may allow the investigation of doped systems.

### ACKNOWLEDGMENTS

This work has been performed within the research program of the DFG Research Training Group *Quantum Mechanical Materials Modeling* (QM<sup>3</sup>) (Project P3). We thank Erik van Loon for many insightful discussions. The authors furthermore acknowledge the North-German Supercomputing Alliance (HLRN) (Project ID: hbp00046) for providing resources and the computing time necessary for carrying out the DQMC simulations.

### APPENDIX A: MEAN-FIELD SOLUTIONS

The mean-field solutions for the four-site model and the square lattice can in principle be obtained by the decoupling of the interaction terms in the original Hamiltonian [Eq. (2)]. Here, however, we use the variational principle (which leads to a completely analogous solution) by employing a noninteracting, effective Hamiltonian  $\tilde{H}$  which allows both for ferro- and antiferromagnetism through two effective fields:

$$\begin{aligned} \tilde{H} = & -t \sum_{(i,j),\sigma} (a_{i\sigma}^\dagger b_{j\sigma} + \text{H.c.}) - \tilde{B}_1 \sum_i (S_{ia}^z + S_{ib}^z) \\ & - \tilde{B}_2 \sum_i (S_{ia}^z - S_{ib}^z). \end{aligned} \quad (\text{A1})$$

Notably, the staggered magnetic field with the magnitude  $\tilde{B}_2$  breaks translational symmetry due to the induced Néel order. Hence, the original square lattice is divided into two sublattices, leading to two distinct fermionic operators for the respective sublattices. The parameters ( $\tilde{B}_1$ ,  $\tilde{B}_2$ ) are chosen variationally for each set of original ( $U$ ,  $J$ ).

We can solve the effective, noninteracting Hamiltonian analytically through simple Fourier transform of the fermionic operators and find (with the lattice constant set to  $a = 1$ ) the following four bands:

$$\varepsilon_{1,2}^\sigma(\vec{k}) = -\frac{\tilde{B}_1 \sigma}{2} \pm \sqrt{\left(\frac{\tilde{B}_2}{2}\right)^2 + \left(4t \cos\left(\frac{k_x}{\sqrt{2}}\right) \cos\left(\frac{k_y}{\sqrt{2}}\right)\right)^2}.$$

From this, all relevant expectation values can be computed exactly, either directly through the derivatives of the grand potential or through Wick factorization. If we then write out the variational equation [Eq. (4)] explicitly, we obtain the following expression which needs to be minimized with respect to ( $\tilde{B}_1$ ,  $\tilde{B}_2$ ):

$$\begin{aligned} \tilde{\Phi} = & U \sum_i \langle n_{i\uparrow}^a n_{i\downarrow}^a + n_{i\uparrow}^b n_{i\downarrow}^b \rangle_{\tilde{H}} - J \sum_{(i,j)} \langle \vec{S}_i^a \cdot \vec{S}_j^b \rangle_{\tilde{H}}, \\ & + \tilde{B}_1 \sum_i \langle S_{ia}^z + S_{ib}^z \rangle_{\tilde{H}} + \tilde{B}_2 \sum_i \langle S_{ia}^z - S_{ib}^z \rangle_{\tilde{H}} + \Phi_{\tilde{H}}. \end{aligned} \quad (\text{A2})$$

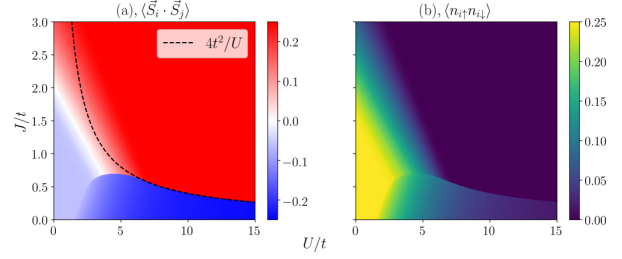


FIG. 7. Mean-field solutions for a half filled square lattice. (a) Next-neighbor spin-spin correlation with the  $4t^2/U$  line. (b) Double occupancy.

As mentioned above, employing a noninteracting effective  $\tilde{H}$  within the variational framework is completely analogous to performing a decoupling of  $H$  which allows for ferro- and antiferromagnetic solutions. Figure 7 shows, again, the spin-spin correlation and double occupancy, for a greater parameter range than in Sec. III. The transition between Néel and ferromagnetic order, which is analytically expected at the  $J = 4t^2/U$  line in the strong- $U$  regime, can be seen clearly.

### APPENDIX B: TROTTER EXTRAPOLATION

In this section, we provide an example in order to justify the Trotter extrapolation which was performed with only two data points ( $\Delta\tau = 0.1$  and  $0.2$ ). The error is known to scale with  $\mathcal{O}(\Delta\tau^2)$ . Consider again the exactly solvable four-site model which was treated in Sec. III A, for the specific case of  $J = 0$ , i.e. a four-site Hubbard model at half filling. In order to compare to the exact results obtained from exact diagonalization, we simulated the model within DQMC at four different Trotter discretizations. The simulations are performed with 15 000 warmup sweeps and 30 000 measurement sweeps for  $U = 0-8$ , at 80 equidistant data points. Furthermore, the obtained data are smoothed with a Savitzky-Golay filter using third order polynomials and a window length of  $w = 7$  data points.

Figure 8(a) shows the double occupancy of the model depending on  $U$ , obtained from ED, DQMC for varying Trotter steps. The systematic error which depends on  $\Delta\tau$  is clearly

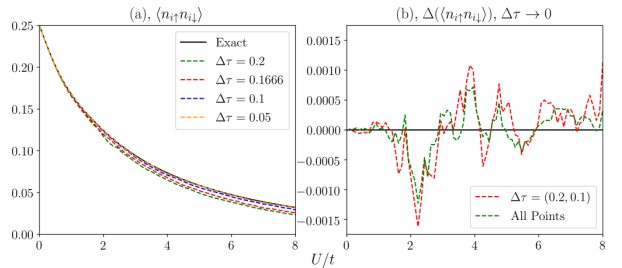


FIG. 8. (a) Double occupancy of a four-site Hubbard model at half filling, obtained from ED, DQMC for a set of Trotter steps. (b) Total error in the double occupancy after extrapolation  $\Delta\tau \rightarrow 0$ . One extrapolation was performed with the two data points used throughout this work, the other included all Trotter steps from (a). The temperature is set to  $\beta t = 10$

visible. Figure 8(b) shows the error in the double occupancy after extrapolating  $\Delta\tau \rightarrow 0$  for two different sets of  $\Delta\tau$ . The red curve is obtained by extrapolating only with the two data points used throughout this work, the green one includes all points. After extrapolating, the systematic error is diminished in both cases, and only the statistical noise remains, which is visible as the extrapolated curves oscillate slightly around 0. Using additional Trotter steps in the extrapolation merely leads to a reduced statistical noise due to a higher number of samples, which justifies our extrapolation with two points only.

### APPENDIX C: ERROR ESTIMATION

The calculations in this work are prone to a variety of different error sources, which need to be addressed separately. First, we discuss the variational principle itself, where the exact benchmarking data provide some insight. Secondly, we turn our attention to the results obtained from DQMC, i.e., the statistical error, the finite size extrapolation, and the integration errors which occur when computing the free energy.

#### 1. Systematic and statistical errors of DQMC

The most obvious error source when using Monte Carlo methods is the statistical error due to a finite number of samplings. As mentioned before, we carried out simulations on an equidistant  $48 \times 48$  grid for  $\tilde{U}/t = 0-10$  and  $\tilde{B}/t = 0-4$ , with 10 000 warmup and 30 000 measurement sweeps. The error can be drastically reduced by making use of an appropriate filter. Similarly to another work [40] done in our group which also relies on DQMC, we make use of a two-dimensional Savitzky-Golay filter [41] which, in a box width of  $w_{\tilde{U}}$  and  $w_{\tilde{B}}$ , fits a two-dimensional polynomial of the form

$$p(\tilde{U}, \tilde{B}) = \sum_{nm} c_{nm} \tilde{U}^n \tilde{B}^m$$

to the data. The polynomials are of third order, and box widths are both set to  $w = 1.0$ . Additionally, data, which is close to the original starting point  $(\tilde{U}_0, \tilde{B}_0)$ , are given additional weight through a tricubic weighting function  $(1-d^3)^3$ , where the distance  $d$  is defined as  $d = \max\{|\tilde{U} - \tilde{U}_0|/w_{\tilde{U}}, |\tilde{B} - \tilde{B}_0|/w_{\tilde{B}}\}$ .

Another important error source to address is the integration procedure [see Eq. (6)] when computing the grand potential  $\Phi_{\tilde{H}}$  of the effective system. While the remaining statistical errors tend to cancel itself out when integrating, the remaining Trotter error might be magnified again.

In order to estimate the errors of the whole mapping procedure, we set  $H = \tilde{H}$ , mapping the effective Hamiltonian to itself,  $(U, B) \rightarrow (\tilde{U}, \tilde{B})$ . Obviously, in the absence of errors, the parameters  $(U, B)$  should not change. Figure 9 shows both the absolute errors of  $(\tilde{U}, \tilde{B})$  and the correlation functions (i.e., the double occupancy and the spin-spin correlation) which are necessary for the mapping.

#### 2. Finite size error of DQMC

As mentioned above, we carried out simulations of the Hamiltonian in Eq. (3) on a square lattice with periodic bound-

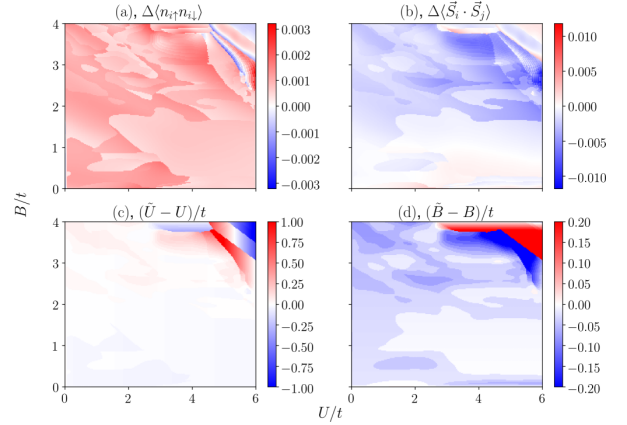


FIG. 9. Absolute errors which stem from the integration procedure and the remaining Trotter error. (a) Double occupancy. (b) Spin-spin correlation. (c) On-site interaction. (d) Magnetic field.

ary conditions, with system sizes of  $L = 4, 6, 8, 10$ , and 12 lattice sites in one direction. The data is then extrapolated to  $N \rightarrow \infty$  by plotting it against  $1/N^2$  (with  $N = L^2$  being the total number of lattice sites) and fitting a line.

In order to assess the errors which remain after the extrapolation, it should be noted that finite size effects will be the strongest when the system is free of interactions, i.e.,  $\tilde{U} = 0$ , since the Hubbard- $U$  generally tends to localize the electrons. Furthermore, in this case, the error from the Trotter decomposition is nonexistent since there is no interaction which needs to be decoupled. The noninteracting case, where the finite size error is the most severe, can be solved analytically, which allows us to compare our data to the exact solution.

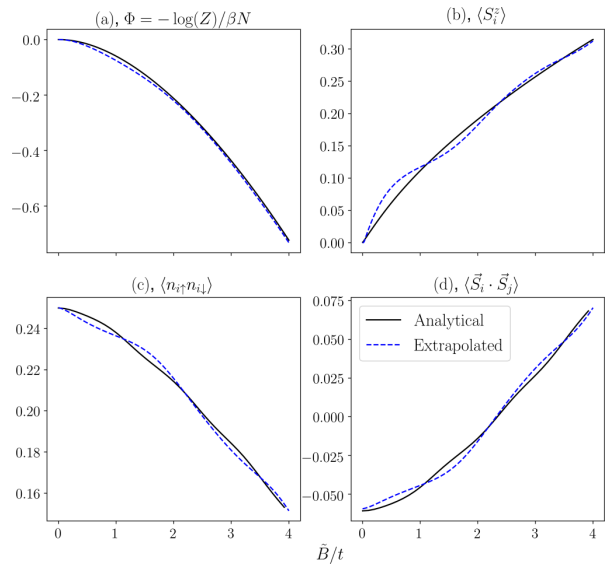


FIG. 10. (a) Analytical (black line) and extrapolated (blue, dashed line) grand potential  $\Phi$  of  $\tilde{H}$  with  $\tilde{U} = 0$ . (b) Magnetization, computed as the derivative of  $\Phi$  with respect to  $\tilde{B}$ . (c) Double occupancy. (d) Next-neighbor spin-spin correlation.

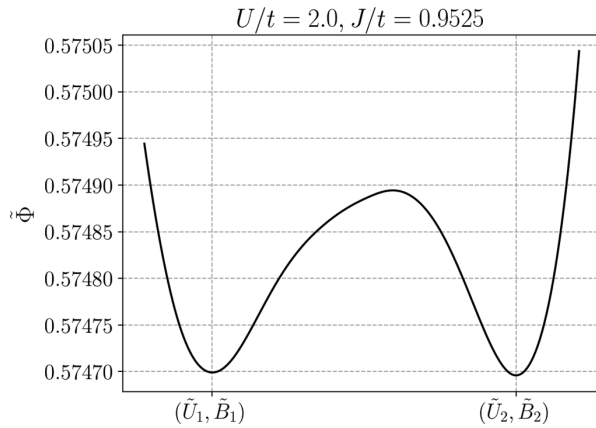


FIG. 11. Functional  $\tilde{\Phi}$ , along the line connecting the two minima at  $(\tilde{U}, \tilde{B})_1 \approx (1.11, 0.34)$  and  $(\tilde{U}, \tilde{B})_2 \approx (1.02, 0.88)$ , for fixed  $(U, J) = (2.0, 0.9525)$ .

Figure 10(a) shows the exact grand potential (per lattice site) of  $\tilde{H}$  on a half-filled square lattice and the grand potential

obtained by integrating over the smoothed and extrapolated DQMC data. Qualitatively, they are in very good agreement. However, when computing observables like the magnetization [Fig. 10(b)] by calculating the derivatives, the small, remaining oscillations become clearly visible.

### 3. Error estimation at the steps

While there are clear hints that the steps are an artifact which stems from remaining finite size effects, we additionally demonstrate that the steps are within our estimated error bars. As a representative example, we pick the step which is visible in Fig. 4(b) at  $U/t \approx 2.0$  and  $J/t \approx 0.95$ . The step itself stems from the existence of two minima in the functional  $\tilde{\Phi}$ , which are located at  $(\tilde{U}, \tilde{B})_1 \approx (1.11, 0.34)$  and  $(\tilde{U}, \tilde{B})_2 \approx (1.02, 0.88)$ .

Figure 11 shows a line plot of the functional  $\tilde{\Phi}$  in the  $(\tilde{U}, \tilde{B})$  plane along the line connecting two minima. The potential barrier between the minima has a height of  $h_{\tilde{\Phi}} < 0.0002$ . However, we estimate that the error for  $\tilde{\Phi}$  is on a scale  $\Delta\tilde{\Phi} \sim 0.05$ , which is clearly larger than the barrier height. Thus the transition is smooth within our error bars.

- [1] J. Hubbard, *Proc. R. Soc. London A* **276**, 238 (1963).  
 [2] J. Hubbard, *Proc. R. Soc. London A* **277**, 237 (1964).  
 [3] J. Hubbard, *Proc. R. Soc. London A* **281**, 401 (1964).  
 [4] M. C. Gutzwiller, *Phys. Rev. Lett.* **10**, 159 (1963).  
 [5] J. Kanamori, *Prog. Theor. Phys.* **30**, 275 (1963).  
 [6] H. Terletska, T. Chen, and E. Gull, *Phys. Rev. B* **95**, 115149 (2017).  
 [7] R. A. Bari, *Phys. Rev. B* **3**, 2662 (1971).  
 [8] Y. Zhang and J. Callaway, *Phys. Rev. B* **39**, 9397 (1989).  
 [9] M. Schüler, M. Rösner, T. O. Wehling, A. I. Lichtenstein, and M. I. Katsnelson, *Phys. Rev. Lett.* **111**, 036601 (2013).  
 [10] S. Onari, R. Arita, K. Kuroki, and H. Aoki, *Phys. Rev. B* **70**, 094523 (2004).  
 [11] D. Sénéchal, A. G. R. Day, V. Bouliane, and A.-M. S. Tremblay, *Phys. Rev. B* **87**, 075123 (2013).  
 [12] A. Reymbaut, M. Charlebois, M. F. Asiani, L. Fratino, P. Sémon, G. Sordi, and A.-M. S. Tremblay, *Phys. Rev. B* **94**, 155146 (2016).  
 [13] D. C. Elias, R. V. Gorbachev, A. S. Mayorov, S. V. Morozov, A. A. Zhukov, P. Blake, L. A. Ponomarenko, I. V. Grigorieva, K. S. Novoselov, F. Guinea, and A. K. Geim, *Nat. Phys.* **7**, 701 (2011).  
 [14] H.-K. Tang, J. N. Leaw, J. N. B. Rodrigues, I. F. Herbut, P. Sengupta, F. F. Assaad, and S. Adam, *Science* **361**, 570 (2018).  
 [15] Y. Cao, V. Fatemi, S. Fang, K. Watanabe, T. Taniguchi, E. Kaxiras, and P. Jarillo-Herrero, *Nature (London)* **556**, 43 (2018).  
 [16] Y. Cao, V. Fatemi, A. Demir, S. Fang, S. L. Tomarken, J. Y. Luo, J. D. Sanchez-Yamagishi, K. Watanabe, T. Taniguchi, E. Kaxiras, R. C. Ashoori, and P. Jarillo-Herrero, *Nature (London)* **556**, 80 (2018).  
 [17] F. Wu, T. Lovorn, E. Tutuc, I. Martin, and A. H. MacDonald, *Phys. Rev. Lett.* **122**, 086402 (2019).  
 [18] M. Koshino, N. F. Q. Yuan, T. Koretsune, M. Ochi, K. Kuroki, and L. Fu, *Phys. Rev. X* **8**, 031087 (2018).  
 [19] J. E. Hirsch, *Phys. Rev. B* **40**, 2354 (1989).  
 [20] J. E. Hirsch, *Phys. Rev. B* **40**, 9061 (1989).  
 [21] J. C. Amadon and J. E. Hirsch, *Phys. Rev. B* **54**, 6364 (1996).  
 [22] R. Strack and D. Vollhardt, *Phys. Rev. Lett.* **72**, 3425 (1994).  
 [23] D. Vollhardt, N. Blümer, K. Held, M. Kollar, J. Schlipf, and M. Ulmke, *Z. Phys. B* **103**, 283 (1996).  
 [24] I. Affleck and J. B. Marston, *Phys. Rev. B* **37**, 3774 (1988).  
 [25] J. B. Marston and I. Affleck, *Phys. Rev. B* **39**, 11538 (1989).  
 [26] C. H. Chung, J. B. Marston, and R. H. McKenzie, *J. Phys.: Condens. Matter* **13**, 5159 (2001).  
 [27] A. B. Eriksson, T. Einarsson, and S. Östlund, *Phys. Rev. B* **52**, 3662 (1995).  
 [28] W. Czart and S. Robaszkiewicz, *Acta Phys. Pol. A* **109**, 577 (2006).  
 [29] J. Wahle, N. Blümer, J. Schlipf, K. Held, and D. Vollhardt, *Phys. Rev. B* **58**, 12749 (1998).  
 [30] M. Schüler, E. G. C. P. van Loon, M. I. Katsnelson, and T. O. Wehling, *Phys. Rev. B* **97**, 165135 (2018).  
 [31] R. Peierls, *Phys. Rev.* **54**, 918 (1938).  
 [32] R. P. Feynman, *Statistical Mechanics* (W. A. Benjamin, Reading, MA, 1972).  
 [33] N. N. Bogolyubov, *Dokl. Akad. Nauk SSSR* **119**, 244 (1958).  
 [34] R. Blankenbecler, D. J. Scalapino, and R. L. Sugar, *Phys. Rev. D* **24**, 2278 (1981).  
 [35] QUEST code, <https://code.google.com/archive/p/quest-qmc/>.  
 [36] E. Kapetanović, M. Schüler, G. Czycholl, and T. O. Wehling, <http://doi.org/10.5281/zenodo.3503424>.  
 [37] T. Schäfer, F. Geles, D. Rost, G. Rohringer, E. Arrighini, K. Held, N. Blümer, M. Aichhorn, and A. Toschi, *Phys. Rev. B* **91**, 125109 (2015).  
 [38] R. R. dos Santos, *Braz. J. Phys.* **33**, 36 (2003).  
 [39] C. L. Cleveland and R. Medina A., *Am. J. Phys.* **44**, 44 (1976).  
 [40] M. Schüler, E. G. C. P. van Loon, M. I. Katsnelson, and T. O. Wehling, *SciPost Phys.* **6**, 67 (2019).  
 [41] A. Savitzky and M. J. E. Golay, *Anal. Chem.* **36**, 1627 (1964).

## 6. Charge correlation, doublon-holon binding and screening in the doped Hubbard model

### 6.1. Scope of the work and Statement of Contributions

In the Hubbard model, the competition between kinetic and Coulomb interaction energy lead to a complicated phase diagram. For the doped square lattice, we investigate the spatial distribution of the electrons and find an emergence of exciton complexes such as two empty sites bound to a doubly occupied site. We discuss this in detail for a  $4 \times 4$  periodic lattice (solved via Determinantal QMC) and with results from exact diagonalization of smaller clusters, which both lead to similar results.

In the second part, through the variational approach discussed in Ch.(3.3.2), we investigate how such excitations affect the screening of nonlocal Coulomb interactions. To that end, we make use of the DQMC scheme and the Dynamical Cluster approximation to solve the Hubbard model for a large parameter grid of interactions and fillings. Both methods yield the result that the screening increases when hole-doping away from half filling, which implies that, when downfolding a complex structure to simple Hubbard models, doping-dependent interactions are necessary for an accurate description.

The DCA and DQMC calculations both for the first and second part and the necessary implementations explained in Ch.(6.3) have been done by me, while Guglielmo Nicola Gigante provided the results from Exact Diagonalization shown in the first part. Malte Schüler gave general input on how to deal with the screening problem considered in the second part. The text itself is mostly written by Erik van Loon and me, with a few revisions done together with Tim Wehling and Malte Schüler.

### 6.2. Actual Paper

Starting on the next page, we show the paper as presented on arXiv [38], on the 09th September 2024.

# Charge correlation, doublon-holon binding and screening in the doped Hubbard model

Edin Kapetanović,<sup>1</sup> Guglielmo Nicola Gigante,<sup>2</sup> Malte Schüler,<sup>3,4</sup> Tim O. Wehling,<sup>1,5</sup> and Erik van Loon<sup>2</sup>

<sup>1</sup>*Institute of Theoretical Physics, Universität Hamburg, D-22607 Hamburg, Germany*

<sup>2</sup>*NanoLund and Division of Mathematical Physics, Department of Physics, Lund University, Professorsgatan 1, Lund, Sweden*

<sup>3</sup>*Institut für Theoretische Physik, Universität Bremen, Otto-Hahn-Allee 1, D-28359 Bremen*

<sup>4</sup>*Bremen Center for Computational Materials Science, Universität Bremen, Am Fallturm 1a, D-28359 Bremen*

<sup>5</sup>*The Hamburg Centre for Ultrafast Imaging, Luruper Chaussee 149, D-22761 Hamburg, Germany*

(Dated: September 10, 2024)

Electronic correlations arise from the competition between the electrons' kinetic and Coulomb interaction energy and give rise to a rich phase diagram and many emergent quasiparticles. The binding of doubly-occupied and empty sites into a doublon-holon exciton is an example of this in the Hubbard model. Unlike traditional excitons in semiconductors, in the Hubbard model it is the kinetic energy which provides the binding energy. Upon doping, we find the emergence of exciton complexes, such as a holon-doublon-holon trion. The appearance of these low-lying collective excitations make screening more effective in the doped system. As a result, Hubbard-based modelling of correlated materials should use different values of  $U$  for the doped system and the insulating parent compound, which we illustrate using the cuprates as an example.

## I. INTRODUCTION

Although the Coulomb interaction between electrons is fundamentally repulsive, its final effect can be attractive and bound many-electron quasiparticles and phase transitions resulting from the Coulomb interaction are at the heart of condensed matter physics. In magnetism, the combination of the Coulomb interaction and the antisymmetry of the wavefunction generates the exchange interactions responsible for magnetic phases [1]. In semiconductors, working with valence band holes changes the sign of the Coulomb interaction and explains the binding of excitons and more complex emergent quasiparticles such as trions [2]. The spatial structure of the Coulomb interaction leads to charge-density waves [3, 4] and Wigner crystallization [5], where a non-uniform ground state minimizes the Coulomb energy. On the other hand, the dynamic structure of the phonon-screened Coulomb interaction leads to the effective attraction between Cooper pairs in BCS superconductivity [6]. Finally, for unconventional superconductors, it is postulated that collective electronic excitations take over the role of phonons and provide the pairing glue [7].

The essential elements of several Coulomb-driven emergent phenomena show up in the Hubbard model [8–10] and its extensions, for example metal-insulator transitions [11], magnetism [12–14], charge-density waves [15] and unconventional superconductivity [16]. Although the model is generically hard to solve [17], there has been tremendous numerical progress in recent years [16, 18, 19], especially when it comes to the determination of ground state properties of the square lattice Hubbard model. It has an antiferromagnetic ground state at zero temperature and half-filling (one electron per site), which is destroyed by Mermin-Wagner fluctuations at  $T > 0$  [14], but with very strong antiferromagnetic correlations still present.

This antiferromagnetic ground state at half-filling forms a starting point for understanding the effect of doping. If the repulsive interaction  $U$  is large, doping introduces holes into an antiferromagnetic background, while double occupancy remains forbidden. One of the insights coming from the  $t$ - $J$  model [20] is that these holes can propagate as pairs of empty sites (holon-pairs) without disturbing the antiferromagnetic ordering. This pair binding has been suggested as a possible mechanism for unconventional superconductivity. When  $U$  is similar to the bandwidth, double occupancy is suppressed but not completely forbidden (e.g., 5% double occupancy at  $U/t = 8$ , half-filling and low temperature [21]) and the  $t$ - $J$  approximation is no longer valid. The presence of doublons (doubly occupied sites) and their possible contribution to binding should now be considered. Do doublons repel or attract holons? This question of doublon-holon binding becomes more important as doping increases, since more and more holons are present in the ground state. Apart from doublon-holon pairs, it is even possible to form higher-order exciton complexes.

With hole doping, the empty sites also tend to order spatially, e.g., in the form of stripes [22, 23]. The Hubbard interaction is not sensitive to the spatial structure of the holons, so it must be the kinetic energy that drives this ordering. At the same time, the appearance of these phases with non-homogeneous electron density raises questions about the applicability of the Hubbard model, i.e., the neglect of nonlocal Coulomb interactions. For a non-uniform ordered phase, these explicitly contribute to the total energy. Zheng et al. [23] estimate an energy difference of  $0.01t$  between vertical stripes and uniform superconducting states in the Hubbard model, and hole densities that differ by roughly 0.1 electron/site. With  $\Delta E \approx V \Delta n_i \Delta n_j$ , and given that  $V \approx 2t$  in the cuprates [24], the potential energy difference between charge-ordered and uniform phases due to the nonlocal

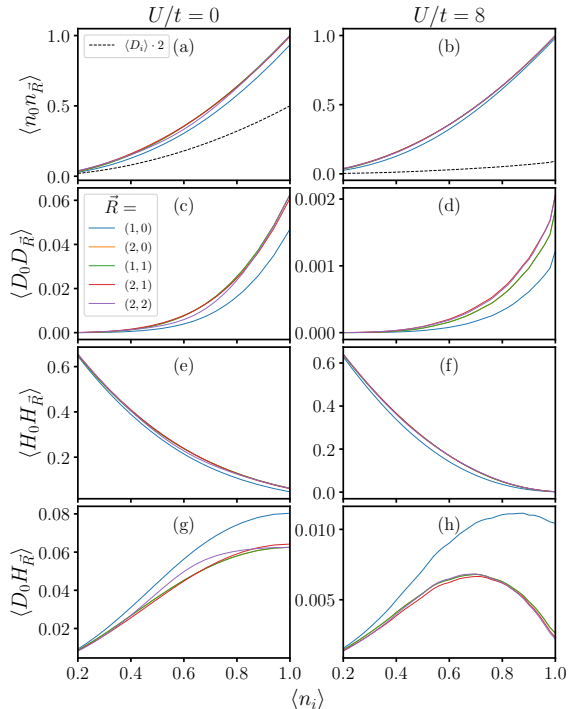


FIG. 1. Spatial charge correlations in the Hubbard model, DQMC on a  $4 \times 4$  periodic cluster at  $\beta t = 2$ . (a-b) Density-density, (c-d) doublon-doublon, (e-f) hole-hole (g-h) doublon-hole. Plots for intermediate values, i.e.  $U/t = 2, 4, 6$  are provided in the Appendix (Fig 6).

Coulomb interaction has the same order of magnitude and cannot simply be ignored. This has motivated the study of the effect of nonlocal interactions on charge ordering [25–27] and superconductivity [28–30].

The impact of nonlocal Coulomb interactions can already be assessed based on knowledge of the correlation functions in the Hubbard model, using a variational principle [31]. Essentially, the charge correlations of the Hubbard model show how the nonlocal Coulomb interactions effectively screens the Hubbard interaction. This approach has been applied extensively to half-filled systems [31–34], but the doped case has received less attention until now, due to the numerical difficulty caused by the Monte Carlo sign problem.

Here, we study the charge fluctuations in the doped Hubbard model using Quantum Monte Carlo. First, we quantify the presence of charge correlations as a function of doping and interaction strength. Then, we proceed with the spatial correlation between doublons and holes, to investigate if there are signs of exciton binding at the four-particle level. We focus on the regime up to  $U \leq W$ , where doublons are sufficiently present and where Quantum Monte Carlo studies of the doped system are numerically feasible. Finally, we study how screen-

ing is affected by doping, and the implications for the doping-dependence of the effective local interaction [31] in correlated materials modelling.

## II. SOLVING THE HUBBARD MODEL

We consider the Hubbard model on the square lattice, in the grand canonical ensemble, i.e.,

$$H_{\text{Hub}} = -t \sum_{\langle i,j \rangle, \sigma} (c_{i\sigma}^\dagger c_{j\sigma} + h.c.) + U \sum_i n_{i\uparrow} n_{i\downarrow} - \mu \sum_i n_i. \quad (1)$$

Here,  $c_{i\sigma}^{(\dagger)}$  denotes the annihilation (creation) operator for an electron on site  $i$  with spin  $\sigma$ ,  $n_{i\sigma}$  is the corresponding occupation number operator,  $n_i = n_{i\uparrow} + n_{i\downarrow}$  the total occupation number. The physical parameters are the nearest-neighbor hopping  $t$ , the on-site or Hubbard interaction  $U$  and the chemical potential  $\mu$ . We consider the hole-doped case, i.e.,  $\langle n_i \rangle \leq 1$  and  $\mu \leq \mu_{1/2} = U/2$ .

We study this model at finite temperature using Quantum Monte Carlo simulations, namely the Determinantal Quantum Monte Carlo method [35] (DQMC) as implemented in the QUEST code [36] and the Dynamical Cluster Approximation [37] (DCA) using a CT-AUX solver [38], see Appendix A for further details. The size of the simulation cell is an important limitation for both methods, but since the finite size effects are handled in different ways, both methods are complementary. We restrict ourselves to a  $4 \times 4$  periodic square lattice within DQMC due to the severity of the Monte Carlo sign problem, and to an 8-site and 16-site dynamical cluster within DCA. The charge-correlation functions of interest can be obtained directly from the respective clusters.

For both methods, raw Monte Carlo data is obtained on a dense grid in  $(U-\mu)$  space, and is then smoothed by a Savitzky-Golay filter [39]. This filter mitigates the problem with noise when numerically evaluating derivatives, as needed later for the determination of effective Hubbard interactions. To facilitate the comparison between different values of  $U$ , the data is mapped from  $\mu$  to  $\langle n \rangle$  in the figures. More details about the computations can be found in the Appendix B, which also contains Exact Diagonalization results obtained using EDLib [40] as a reference.

## III. CHARGE FLUCTUATIONS

Figure 1(a-b) shows the density-density correlation  $\langle n_0 n_{\vec{R}} \rangle$  and the double occupancy (i.e.,  $\vec{R} = 0$ ). Both increase with  $\langle n \rangle$ , as expected. The main effect of  $U$  is to suppress the double occupancy, while the other charge correlation functions are weakly enhanced: with fewer doubly occupied sites, there are also fewer empty sites, so the *instantaneous* charge distribution is more homogeneous. Comparing the different values of  $\vec{R}$  (colored

lines) shows that the nearest-neighbor correlation function is always smaller than the ones further away. Avoiding charges on neighboring sites allows for more hopping processes and therefore lowers the kinetic energy.

Knowing that there are doubly-occupied sites, we continue with their spatial distribution. Figure 1(c-d) shows that doublons repel each other, since the doublon-doublon correlation function is smaller for neighboring sites than for sites further apart. This effect is already present at  $U = 0$ , where  $\langle D_i D_j \rangle = \langle n_{i\sigma} n_{j\sigma} \rangle^2$ . Even with the overall suppression of the number of doubly occupied sites by  $U$ , doublons still repel and are unlikely to sit on neighboring sites, since that is bad for the kinetic energy. Similarly, Figure 1(e-f) shows that holons are less likely to occupy neighboring sites. In both cases, by increasing  $U$ , the charge localizes and correlations beyond nearest neighbor are weakly dependent on distance.

On the other hand, doublons and holons are more likely to occupy neighboring sites, as shown in Fig. 1(g-h). Again, this effect is already present at  $U = 0$ , but it is enhanced by  $U$ , especially for  $\langle n \rangle > 0.7$ . In a real-space strong-coupling picture, putting doublons and holons next to each other maximizes the kinetic energy gain. In other words, virtual hopping of one electron to a neighboring site is the main mechanism creating doublons in a doped antiferromagnet (see Figure 2), and the kinetic energy provides the binding for this doublon-holon exciton. Of the spatial correlation functions considered here, the doublon-holon binding is by far the strongest effect.

#### IV. VARIATIONAL APPROACH TO NONLOCAL COULOMB INTERACTIONS

Going beyond the Hubbard approximation, two-dimensional materials have nonlocal Coulomb interactions of substantial magnitude, and these directly affect the charge-correlation function. Here, we consider the extended Hubbard model with nearest-neighbor Coulomb interaction  $V$ ,

$$H_{\text{eHub}} = H_{\text{Hub}} + V \sum_{\langle i,j \rangle} n_i n_j$$

Note that it is also possible to write the nonlocal interaction in terms of fluctuations away from half-filling, i.e.,  $V \sum_{\langle i,j \rangle} (n_i - 1)(n_j - 1)$ . This formulation is equivalent up to shifts in the chemical potential and total energy, and can simplify pictorial arguments substantially.

Using the Peierls-Feynman-Bogoliubov Variational principle [41–43], it is possible to map [31] the extended Hubbard model onto a regular Hubbard model with modified parameters  $\tilde{U}$ ,  $\tilde{\mu}$ , which are variational and should be chosen so that the density operator of the effective Hamiltonian  $\tilde{H}$  approximates the real density operator as well as possible, as illustrated in Fig. 2.

Although Quantum Monte Carlo works in the grand canonical ensemble, one usually adjusts the chemical po-

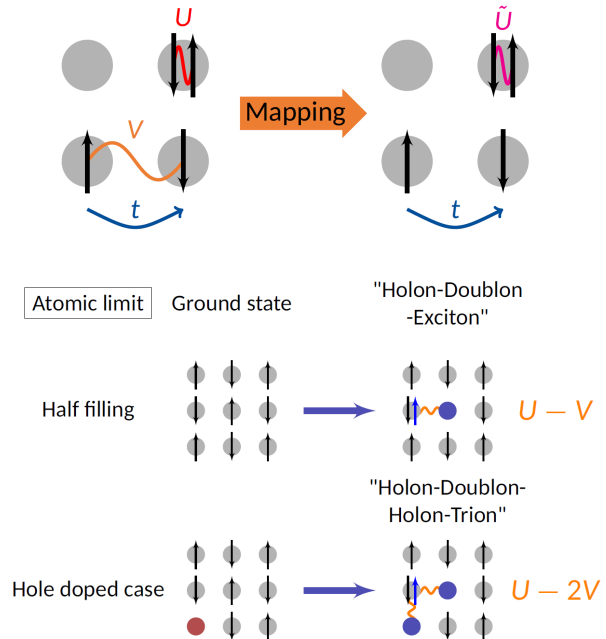


FIG. 2. Extended Hubbard model can be mapped onto an effective model with local interactions only. The value of  $\tilde{U}$ , given by Eq. (2) is based on the excitations in the model. In the antiferromagnetic ground state in the atomic limit, at half-filling the basic excitation is the creation of a holon-doublon exciton, while the formation of holon-doublon-holon trions is possible in the doped system.

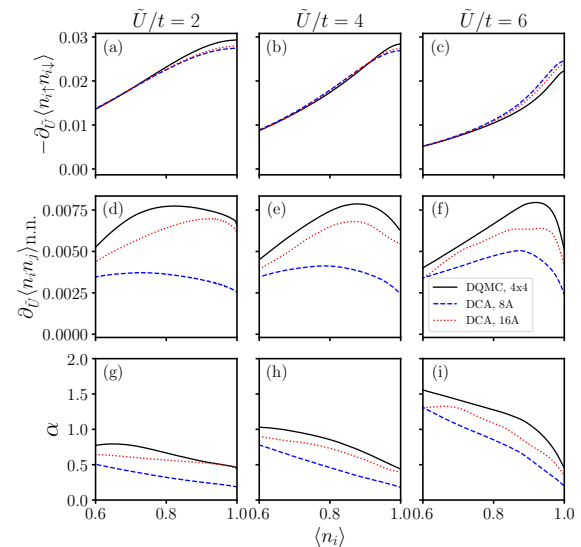


FIG. 3. Screening factor  $\alpha$  and the  $\tilde{U}$ -derivatives of the double occupancy and the next-neighbor density-density correlation vs. filling  $\langle n_i \rangle$  at  $\beta t = 2$ , for different  $\tilde{U}$ . For the square lattice, DCA and DQMC lead to qualitatively similar results.



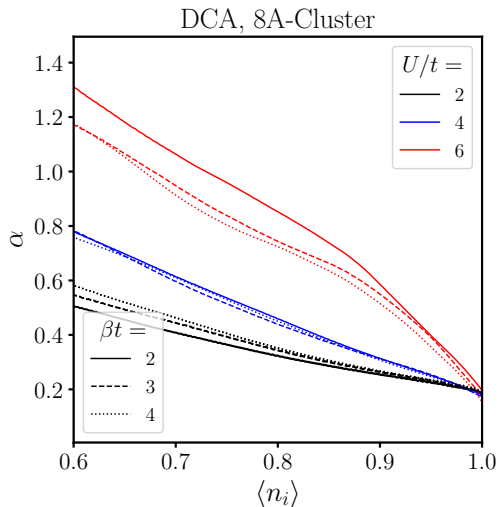


FIG. 4. Screening factor  $\alpha$  for different inverse temperatures  $\beta$ :  $\beta t = 2$  (full),  $\beta t = 3$  (dashed) and  $\beta t = 4$  (dotted), obtained using 8-Site Cluster (DCA).

tential to obtain a desired filling. Thus, for the variational approach, we choose  $\tilde{\mu}$  as a function of  $\tilde{U}$  in order to obtain a fixed filling ( $\langle n_i \rangle_{\tilde{H}} = \text{const.}$ ), and  $\tilde{U}$  remains as the sole variational parameter. Then, the effective local interaction  $\tilde{U}$  is given by [31, 44]:

$$\tilde{U} = U - \alpha(\tilde{U}), V \quad (2)$$

$$\alpha(\tilde{U}) = -\frac{Z}{2} \frac{\partial_{\tilde{U}} \langle n_i n_j \rangle_{\tilde{H}}}{\partial_{\tilde{U}} \langle n_{i\uparrow} n_{i\downarrow} \rangle_{\tilde{H}}}. \quad (3)$$

$\alpha$  is the *screening factor* which determines how strongly the nonlocal Coulomb interaction effectively changes the local one. It is the central quantity in the variational approach and only depends on the properties of the effective Hubbard model, so it can be extracted from the available Quantum Monte Carlo data.

The interpretation of the renormalized Hubbard interaction is that it relates the cost of creating a doublon-holon excitation in both models, taking into account the spatial correlation between them. The value of  $\tilde{U}$  is chosen so that the “typical” doublon excitation has the same cost as in the extended Hubbard model Eq. (IV). At half filling and strong coupling,  $\tilde{U} = U - V$  [31], i.e.  $\alpha = 1$ , corresponding to a strongly bound nearest-neighbor doublon-holon exciton, as shown in Fig. 2. Previous studies have shown [44] that  $\alpha < 1$  at smaller  $U$  and half-filling, since the doublon-holon pair is more delocalized, as is also visible in Fig. 1(g-h).

For the doped system, Figure 3 shows the  $\tilde{U}$ -derivatives that make up the numerator and denominator of Eq. (3) as well as the screening factor  $\alpha$ . The behaviour is qualitatively similar in DQMC and 8-site and 16-site DCA, showing that the observed mechanisms are robust with

respect to finite-size errors. Importantly, the screening factor  $\alpha$  *increases* when doping the system away from half-filling, and  $\alpha > 1$  for a large range of filling at the largest shown value of  $U$ .

In order to gain a physical understanding of the observed increase in screening upon doping, we go back to the atomic limit, as shown in Fig. 2. Whereas half-filling has the nearest-neighbor doublon-holon exciton forming from a uniform background as the elementary excitation ( $\alpha = 1$ ), the doped system already has holes present in the ground state, so the created doublon-holon pair can bind to an existing holon and form a holon-doublon-holon trion. This costs energy  $U - 2V$ , which is less than  $U - V$  for a normal exciton, and which would lead to  $\alpha \approx 2$  if it was the only relevant process. The observed  $\alpha$  is an indicator of the relative statistical importance of holon-doublon excitons ( $\alpha = 1$ ) and higher-order holon-doublon exciton complexes ( $\alpha = 2$  for the trion). As the system is doped away from half-filling, the number of holes present in the ground state increases, and therefore also the probability of forming the compound quasiparticles, as visible in Fig 3. The presence of these lower-lying excitations explains why the additional presence of holes leads to a more effective screening process. At very strong doping, this picture of a uniform antiferromagnetic background eventually breaks down, and we would expect  $\alpha$  to decrease again since in the limit  $\langle n \rangle \rightarrow 0$  there are no electrons to do the screening.

Since the variational principle is based on the free energy, the screening factor  $\alpha$  depends on temperature via the correlation functions entering Eq. (3). The temperature-dependence of the double occupancy has been studied in detail [21, 32, 45, 46]. In  $\alpha$ , this leads to visible differences between  $T = t/2$  and  $T = t/3$ , but smaller differences going to  $T = t/4$ , as shown in the DCA results of Figure 4. Thus, while the numerical sign problem prohibits us from performing Monte Carlo simulations of the doped model at low temperature, it is reasonable to assume that the effect of increased screening when doping the system away from half filling remains also at lower temperature. As a complementary method, we have performed exact diagonalization calculations at  $T = 0$ , as shown in the Appendix.

## V. CONCLUSIONS AND OUTLOOK

In conclusion, the presence of holes in the doped Hubbard model makes spatial charge correlations omnipresent, even at strong coupling. One of the main effects is the binding of doublon-holon excitons on neighboring sites, an effective non-local interaction between charged particles that arises from the kinetic energy in the Hubbard model. In terms of screening, the doped Hubbard model has an additional screening process in the form of holon-doublon-holon coupling, due to the holes in the antiferromagnetic background. This leads to screening factors  $\alpha > 1$  in the mapping to an effective Hubbard

model, and thus to lower effective interactions.

Concretely, it means that a lower value of  $U$  should be used to model the doped cuprates than to model their half-filled parent compounds, if the modelling is done at the level of the Hubbard model, i.e., with non-local Coulomb interactions integrated out. Estimates of  $t$ ,  $U$  and  $V$  for the cuprates [24] in a downfolded one-band model give a local interaction  $U/t \approx 10$ , while  $V \approx U/4$ . At half-filling, this value of  $U/t$  is large enough to put the system in the strong coupling limit with  $\alpha \approx 1$ , leading to an effective local interaction  $\tilde{U}/t = (U - V)/t = 7.5$ . If, however, as our data suggests, it is possible that  $\alpha \approx 1.5$  for the doped case due to additional trionic screening channel, then the appropriate interaction for Hubbard model studies of the doped system would instead be roughly  $\tilde{U}/t \approx 6.25$ , which is a substantial reduction.

### ACKNOWLEDGMENTS

This work has been performed within the research program of the DFG Research Training Group *Quantum Mechanical Materials Modeling* (QM<sup>3</sup>) (Project P3). Furthermore, the work has been funded by the Cluster of Excellence ‘‘Advanced Imaging of Matter’’ of the Deutsche Forschungsgemeinschaft (DFG) - EXC 2056. EvL acknowledges support from the Swedish Research Council (Vetenskapsrådet, VR) under grant 2022-03090 and by eSENCE, a strategic research area for e-Science, grant number eSENCE@LU 9:1. G.N.G. acknowledges the Wallenberg Center for Quantum Technology (WACQT) for financial support via the EDU-WACQT program funded by Marianne and Marcus Wallenberg Foundation. We thank Emanuel Gull for providing the CT-AUX code, and EK thanks Xinyang Dong for help at properly compiling it. The authors gratefully acknowledge the computing time made available to them on the high-performance computer Lise at the NHR Center ZIB (HLRN at the time). These centers are jointly supported by the Federal Ministry of Education and Research and the state governments participating in the NHR. Further computations were performed using resources provided by LUNARC, The Centre for Scientific and Technical Computing at Lund University through projects LU 2023/2-37, 2024/2-24 and 2023/17-14.

### Appendix A: Computational details

In order to obtain the screening factor  $\alpha(\tilde{U})$  (see Fig 3 4), we solved the Hubbard Hamiltonian  $\tilde{H}(H_{\text{Hub}})$ , Eq. (1), on an equidistant  $41 \times 41$  data grid ( $\tilde{U}/t \in [0, 8]$ ,  $\tilde{\mu}/t \in [-8, 0]$ ) for a temperature of  $\beta t = 2$  within two different approaches: Determinantal Quantum Monte Carlo (DQMC) and the Dynamical Cluster approximation (DCA).

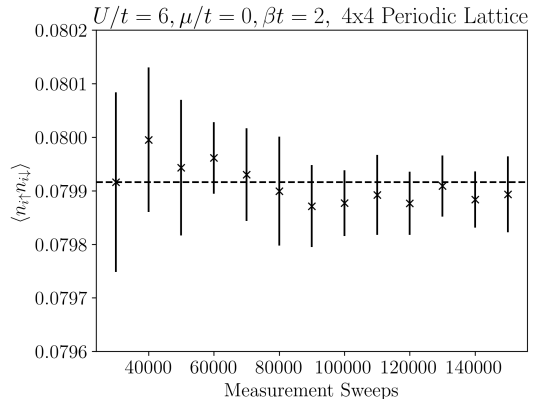


FIG. 5. DQMC, QUEST code: Result for the double occupancy  $\langle n_{i\uparrow}n_{i\downarrow} \rangle$  with error bars for different numbers of measurement sweeps.

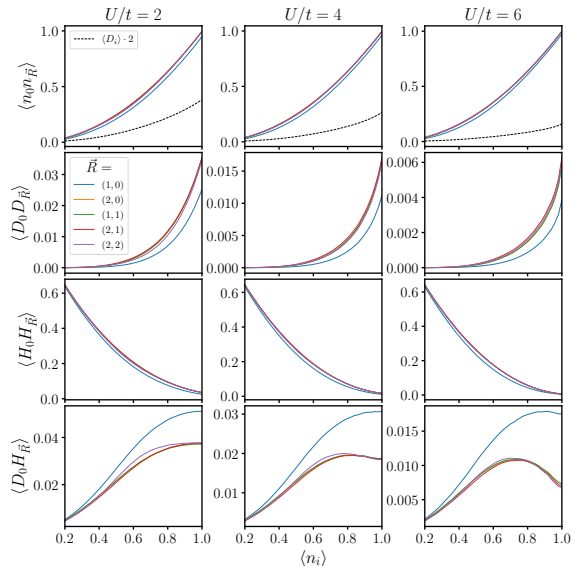


FIG. 6. Spatial charge correlations (same as in Fig 1, but for  $U/t = 2, 4, 6$ ) in the Hubbard model, DQMC on a  $4 \times 4$  periodic cluster at  $\beta t = 2$ .

#### a. DQMC

The DQMC simulations have been performed with the QUEST code [36] on a  $4 \times 4$  periodic lattice. The systematic error from the Trotter-Suzuki decomposition ( $\mathcal{O}(\Delta\tau^2)$ ) can be minimized by choosing an appropriately small Trotter step ( $\Delta\tau \sim \sqrt{0.125/\tilde{U}}$ ) [47]. For the highest value of  $\tilde{U}/t = 8$  considered here, this estimate would lead to  $\Delta\tau \sim 0.125$ . In order to keep the systematic error at a minimum, we choose  $\Delta\tau = 0.05$  for the big simula-

tions from which  $\alpha$  is obtained, and  $\Delta\tau = 0.02$  for the calculations of the four-particle correlators.

For each data point, the simulation is run with 10000 warmup sweeps and 30000 measurement sweeps. Since the system thermalizes quickly at the temperature considered, rather short simulations already yield appropriate results. As an example, Fig. 5 shows, for a specific data point, that the correlation functions (here: the double occupancy) obtained from 30000 measurement sweeps are within error bars of simulations which are 5 times longer. Thus, for the purpose of evaluating accurate derivatives, a dense parameter grid combined with filtering is the more important aspect compared to the simulation time within QUEST.

### b. DCA

For the DCA approach, we use the CT-AUX code of Ref. [38]. Here, we find the necessary correlation functions by solving dynamical clusters with 8 and 16 sites. The simulations were performed in a timed manner, i.e. 25 minutes runtime (8 CPUs) for each data point and iteration step respectively. Within the self-consistency cycle, we allow for up to 8 iterations, which is, at the given temperature, more than sufficient. Fig. 8 illustrates for a single data point (8-site cluster), at 2  $k$ -points, how the Matsubara Green's function behaves from iteration to iteration. The top left and right plots show the spin-averaged  $G_k^{\sigma}(\tau)$  after iteration steps  $N$ , while the bottom pictures show the difference in the Green's function between iterations. In this case, already at 2 steps within the cycle, further iterations no longer cause significant changes.

### c. Filtering and Interpolation

The central quantity presented within this work, the screening factor  $\alpha(\tilde{U})$ , depends on derivatives of  $\tilde{U}$ -dependent correlation functions. Such derivatives are difficult to obtain from noisy data, which is inherent in any Monte Carlo method. As such, proper filtering of our data is necessary.

Here, similar to previous works [33, 34], we make use of a two-dimensional Savitzky-Golay filter [39] which, in a box width of  $w_{\tilde{U}}$  and  $w_{\tilde{\mu}}$ , fits a two-dimensional polynomial of the following form to the data:

$$p(\tilde{U}, \tilde{\mu}) = \sum_{nm} c_{nm} \tilde{U}^n \tilde{\mu}^m$$

The polynomials are of third order, and the box widths are set to  $w = 1.5$  for the DQMC and the 8-site DCA data, while it is set to  $w = 2.0$  for the 16-site DCA data due to higher noise. Additionally, data which is

close to the original starting point  $(\tilde{U}_0, \tilde{\mu}_0)$ , is given additional weight through a tricubic weighting function  $(1 - d^3)^3$  where the distance  $d$  is defined as  $d = \max\left\{|\tilde{U} - \tilde{U}_0|/w_{\tilde{U}}, |\tilde{\mu} - \tilde{\mu}_0|/w_{\tilde{\mu}}\right\}$ .

After filtering the data, we use two-dimensional cubic interpolation to extend our parameter grid from 41x41 to 401x401, which makes it more convenient to evaluate derivatives.

Within the derivation for Eq.(3), we chose  $\tilde{\mu}$  as a function of  $\tilde{U}$  in order to obtain a fixed filling, i.e.  $\langle n_i \rangle_{\tilde{H}} = \text{const.}$ . As such, as the last step before evaluating derivatives of correlation functions and thus,  $\alpha(\tilde{U})$ , we use the fillings  $\langle n_i \rangle$  obtained from the simulations to transform the  $\tilde{\mu}$ -axis to an  $\langle n_i \rangle$ -axis.

## Appendix B: Exact Diagonalization

To verify our numerical results, we have also performed exact diagonalization (ED) simulations of a  $4 \times 2$  ribbon with periodic boundary conditions in both directions (i.e., a donut), using EDLib [40]. We extract the relevant correlation functions from the ground state wavefunctions in a particular sectors ( $N_{\uparrow}, N_{\downarrow}$ ). The Exact Diagonalization is complementary to the QMC in several ways, it is performed at  $T = 0$  directly and with fixed particle number, instead of the grand canonical ensemble used in QMC. It is sign-problem free and can be done at any  $U$ . On the other hand, the scaling of the computational effort with system size is much worse than in QMC.

Figure 9 shows the results of the ED, which can be compared with Fig. 1. Note that the  $4 \times 2$  geometry with periodic boundary conditions in both directions leads to a difference between the  $\vec{R} = (0, 1)$  and  $\vec{R} = (1, 0)$  correlation functions, since hopping along the short direction is enhanced. Thus, to optimize the kinetic energy, doublon excitons preferentially align along this axis. In this way, the broken rotational symmetry of the system actually provides strong evidence for the kinetic energy as the mechanism for the binding. A similar mechanism has been discussed in  $t - J$ -bilayers [48].

Apart from the special  $\vec{R} = (0, 1)$  in the  $4 \times 2$  cluster, the results at  $U/t = 8$  are qualitatively similar and even quantitatively close to Fig. 1, even though there is a difference in cluster size and statistical ensemble. This shows that generic mechanisms of the Hubbard model are responsible for these effects. In ED, we can also increase  $U$  further, to  $U/t = 16$ . The density-dependence of the curves does not change, but the overall magnitude of the doublon correlators decreases substantially due to the decrease in the number of doublons. This shows that the  $U/t = 8$  QMC results in the main text already give a good impression of what happens at strong coupling.

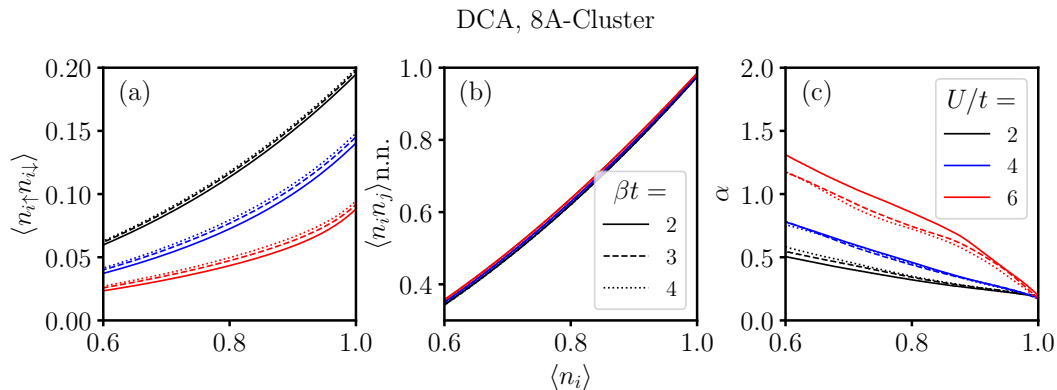


FIG. 7. Double occupancy, next-neighbor density-density correlation and the resulting screening factor  $\alpha$  as a function of interaction strength  $U$ , inverse temperature  $\beta$  and filling  $\langle n_i \rangle$ , obtained using a 8-Site Cluster in DCA, c.f. Fig. 4 in the main text.

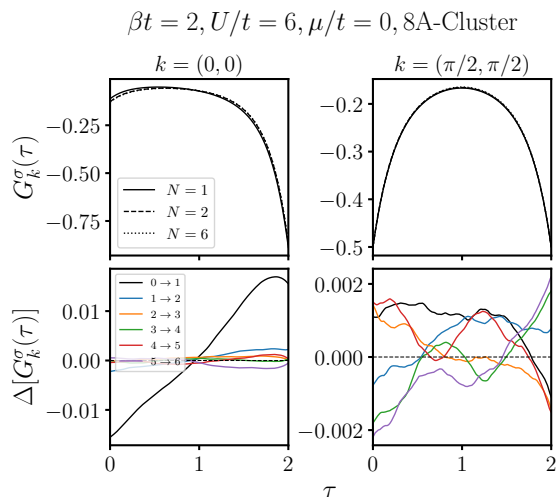


FIG. 8. DCA, CT-AUX solver: Top pictures: Spin-averaged Green's function  $G_k^\sigma(\tau)$  at different iteration steps within the self-consistency cycle. Bottom: Differences  $\Delta(G_k^\sigma(\tau))$  between Green's functions at different steps.

- 
- [1] A. Szilva, Y. Kvashnin, E. A. Stepanov, L. Nordström, O. Eriksson, A. I. Lichtenstein, and M. I. Katsnelson, *Rev. Mod. Phys.* **95**, 035004 (2023).  
 [2] M. A. Lampert, *Phys. Rev. Lett.* **1**, 450 (1958).  
 [3] E. Tosatti and P. W. Anderson, *Japanese Journal of Applied Physics* **13**, 381 (1974).  
 [4] P. Hansmann, T. Ayrál, L. Vaugier, P. Werner, and S. Biermann, *Phys. Rev. Lett.* **110**, 166401 (2013).  
 [5] E. Wigner, *Phys. Rev.* **46**, 1002 (1934).  
 [6] J. R. Schrieffer, *Theory of superconductivity* (CRC press, 2018).  
 [7] M. R. Norman, *Science* **332**, 196 (2011).  
 [8] J. Hubbard, *Proc. Roy. Soc. Lond. A* **276**, 238 (1963).  
 [9] J. Hubbard, *Proc. Roy. Soc. Lond. A* **277**, 237 (1964).  
 [10] J. Hubbard, *Proc. Roy. Soc. Lond. A* **281**, 401 (1964).  
 [11] M. Imada, A. Fujimori, and Y. Tokura, *Rev. Mod. Phys.* **70**, 1039 (1998).  
 [12] J. Kanamori, *Progress of Theoretical Physics* **30**, 275 (1963).  
 [13] M. C. Gutzwiller, *Phys. Rev. Lett.* **10**, 159 (1963).  
 [14] T. Schäfer, F. Geles, D. Rost, G. Rohringer, E. Arrigoni, K. Held, N. Blümer, M. Aichhorn, and A. Toschi, *Phys.*

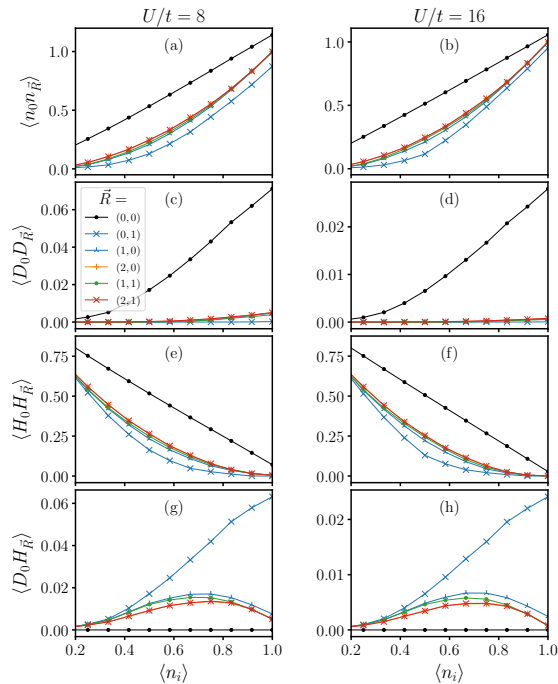


FIG. 9. Spatial charge correlations in the Hubbard model, ED on a  $4 \times 2$  periodic cluster at  $T = 0$ . (a-b) Density-density, (c-d) doublon-doublon, (e-f) hole-hole (g-h) doublon-hole.

- Rev. B **91**, 125109 (2015).
- [15] Y. Zhang and J. Callaway, Phys. Rev. B **39**, 9397 (1989).
- [16] H.-C. Jiang and T. P. Devereaux, Science **365**, 1424 (2019).
- [17] M. Troyer and U.-J. Wiese, Phys. Rev. Lett. **94**, 170201 (2005).
- [18] M. Qin, C.-M. Chung, H. Shi, E. Vitali, C. Hubig, U. Schollwöck, S. R. White, and S. Zhang (Simons Collaboration on the Many-Electron Problem), Phys. Rev. X **10**, 031016 (2020).
- [19] T. Schäfer, N. Wentzell, F. Šimkovic, Y.-Y. He, C. Hille, M. Klett, C. J. Eckhardt, B. Arzhang, V. Harkov, F.-M. Le Régent, A. Kirsch, Y. Wang, A. J. Kim, E. Kozik, E. A. Stepanov, A. Kauch, S. Andergassen, P. Hansmann, D. Rohe, Y. M. Vilch, J. P. F. LeBlanc, S. Zhang, A.-M. S. Tremblay, M. Ferrero, O. Parcollet, and A. Georges, Phys. Rev. X **11**, 011058 (2021).
- [20] P. W. Anderson, Science **235**, 1196 (1987).
- [21] J. P. F. LeBlanc, A. E. Antipov, F. Becca, I. W. Bulik, G. K.-L. Chan, C.-M. Chung, Y. Deng, M. Ferrero, T. M. Henderson, C. A. Jiménez-Hoyos, E. Kozik, X.-W. Liu, A. J. Millis, N. V. Prokof'ev, M. Qin, G. E. Scuseria, H. Shi, B. V. Svistunov, L. F. Tocchio, I. S. Tupitsyn, S. R. White, S. Zhang, B.-X. Zheng, Z. Zhu, and E. Gull (Simons Collaboration on the Many-Electron Problem), Phys. Rev. X **5**, 041041 (2015).
- [22] D. Poilblanc and T. M. Rice, Phys. Rev. B **39**, 9749 (1989).
- [23] B.-X. Zheng, C.-M. Chung, P. Corboz, G. Ehlers, M.-P. Qin, R. M. Noack, H. Shi, S. R. White, S. Zhang, and G. K.-L. Chan, Science **358**, 1155 (2017).
- [24] M. Hirayama, Y. Yamaji, T. Misawa, and M. Imada, Phys. Rev. B **98**, 134501 (2018).
- [25] H. Terletska, T. Chen, and E. Gull, Phys. Rev. B **95**, 115149 (2017).
- [26] R. A. Bari, Phys. Rev. B **3**, 2662 (1971).
- [27] Y. Zhang and J. Callaway, Phys. Rev. B **39**, 9397 (1989).
- [28] S. Onari, R. Arita, K. Kuroki, and H. Aoki, Phys. Rev. B **70**, 094523 (2004).
- [29] D. Sénéchal, A. G. R. Day, V. Bouliane, and A.-M. S. Tremblay, Phys. Rev. B **87**, 075123 (2013).
- [30] A. Reymbaut, M. Charlebois, M. F. Asiani, L. Fratino, P. Sémon, G. Sordi, and A.-M. S. Tremblay, Phys. Rev. B **94**, 155146 (2016).
- [31] M. Schüler, M. Rösner, T. O. Wehling, A. I. Lichtenstein, and M. I. Katsnelson, Phys. Rev. Lett. **111**, 036601 (2013).
- [32] M. Schüler, E. G. C. P. van Loon, M. I. Katsnelson, and T. O. Wehling, Phys. Rev. B **97**, 165135 (2018).
- [33] M. Schüler, E. G. C. P. van Loon, M. I. Katsnelson, and T. O. Wehling, SciPost Phys. **6**, 67 (2019).
- [34] E. Kapetanović, M. Schüler, G. Czyczoll, and T. O. Wehling, Phys. Rev. B **101**, 235165 (2020).
- [35] R. Blankenbecler, D. J. Scalapino, and R. L. Sugar, Phys. Rev. D **24**, 2278 (1981).
- [36] Quest code, <https://code.google.com/archive/p/quest-qmc/>.
- [37] M. H. Hettler, A. N. Tahvildar-Zadeh, M. Jarrell, T. Pruschke, and H. R. Krishnamurthy, Phys. Rev. B **58**, R7475 (1998).
- [38] E. Gull, P. Werner, O. Parcollet, and M. Troyer, Europhysics Letters **82** (2008), 57003.
- [39] A. Savitzky and M. J. E. Golay, Analytical Chemistry **36**, 1627 (1964), <https://doi.org/10.1021/ac60214a047>.
- [40] S. Isakov and M. Danilov, Computer Physics Communications **225**, 128 (2018).
- [41] R. Peierls, Phys. Rev. **54**, 918 (1938).
- [42] R. P. Feynman, *Statistical Mechanics* (Reading, Mass. : W. A. Benjamin, 1972).
- [43] N. N. Bogoliubov, Dokl. Akad. Nauk SSSR **119**, 244 (1958).
- [44] E. G. C. P. van Loon, M. Schüler, M. I. Katsnelson, and T. O. Wehling, Phys. Rev. B **94**, 165141 (2016).
- [45] A. Sushcheyev and S. Wessel, Phys. Rev. B **106**, 155121 (2022).
- [46] S. Roy, S. Pervaiz, T. Paiva, and N. Trivedi, Signatures of metal to insulator crossover in the repulsive Fermi Hubbard model through static correlations (2024), arXiv:2403.13054 [cond-mat.str-el].
- [47] R. R. dos Santos, Braz. J. Phys. **33** (2003).
- [48] A. Bohrdt, L. Homeier, I. Bloch, E. Demler, and F. Grusdt, Nature Physics **18**, 651 (2022).

### 6.3. Implementations in the QUEST code

In the paper, static correlators such as e.g.  $\langle n_{i\uparrow}n_{i\downarrow}n_{j\uparrow}n_{j\downarrow} \rangle$  have been evaluated within the DQMC scheme. In order to measure such four-particle correlators, a few modifications were necessary in the QUEST-code (unmodified version is found in [41]), which are discussed in detail here.

The first step in measuring higher-order correlators within the DQMC algorithm is doing the Wick-factorization, as Wick's theorem is valid (see Ch.(4.1.2)) for a fixed configuration of auxiliary Ising-fields. The factorizations of all necessary correlators are provided in Ch.(2.2.3).

Static properties are measured through the subroutines in the **DQMC\_Phy0**-module. The only necessary changes are thus in the **dqmc\_phy0.F90**-file in the SRC-folder of QUEST. First, indices for all variables that are measured with their full  $(i, j)$ -dependency must be declared at the top in the following way:

```

75  ! Array
76  integer, parameter :: narrays = 13
77
78  ! Index of the array variables
79  integer, parameter :: IMEAS = 0
80  integer, parameter :: IGFUN = 1
81  integer, parameter :: IGFUP = 2
82  integer, parameter :: IGFDN = 3
83  integer, parameter :: ISPXX = 4
84  integer, parameter :: ISPZZ = 5
85  integer, parameter :: IAVSP = 6
86  integer, parameter :: IDEN0 = 7
87  integer, parameter :: IDEN1 = 8
88  integer, parameter :: IPAIR = 9
89  integer, parameter :: ITEST = 10
90  integer, parameter :: IDODO = 11
91  integer, parameter :: IDOHO = 12
92  integer, parameter :: IHOHO = 13

```

**narrays** defines the number of variables, and the last three indices are for the four-particle correlators. Notation-wise, the names **DODO**, **DOHO**, **HOHO** stand for the doublon-doublon, doublon-holon and holon-holon correlators, respectively.

The next change is in the definition of the custom type **Phy0**, which contains pointers to all static measurements. Entries must be made as follows:

```

180  !Pointers to AllProp
181  real(wp), pointer :: G_fun(:, :) ! Green's function
182  real(wp), pointer :: Gf_up(:, :) ! Green's function
183  real(wp), pointer :: Gf_dn(:, :) ! Green's function
184  real(wp), pointer :: SpinXX(:, :) ! XX Spin correlation function
185  real(wp), pointer :: SpinZZ(:, :) ! ZZ Spin correlation function
186  real(wp), pointer :: AveSpin(:, :) ! Ave Spin correlation function
187  real(wp), pointer :: Den0(:, :) ! Density-density correlation
188  real(wp), pointer :: Den1(:, :) ! up-up (0) and up-dn (1)
189  real(wp), pointer :: Pair(:, :) ! on-site pairing
190  real(wp), pointer :: Test(:, :)
191
192  ! Entries for the four-particle correlators
193  real(wp), pointer :: DoDo(:, :) ! Doublon-Doublon
194  real(wp), pointer :: DoHo(:, :) ! Doublon-Holon
195  real(wp), pointer :: HoHo(:, :) ! Holon-Holon

```

In the **DQMC\_Phy0\_Init**-subroutine, all variables must be initialized:

## 6 CHARGE CORRELATION, DOUBLON-HOLON BINDING AND SCREENING IN THE DOPED HUBBARD MODEL

---

```
258  !Pointers to beginning of each array
259  P0%IARR(IMEAS) = 1
260  do i = 1, narrays + 1
261    P0%IARR(i) = P0%nmeas + 1 + (i - 1) * P0%nClass
262  enddo
263
264  P0%meas    => P0%AllProp(P0%IARR(IMEAS):P0%IARR(IMEAS + 1) - 1, :)
265  P0%G_fun  => P0%AllProp(P0%IARR(IGFUN):P0%IARR(IGFUN + 1) - 1, :)
266  P0%Gf_up  => P0%AllProp(P0%IARR(IGFUP):P0%IARR(IGFUP + 1) - 1, :)
267  P0%Gf_dn  => P0%AllProp(P0%IARR(IGFDN):P0%IARR(IGFDN + 1) - 1, :)
268  P0%SpinXX => P0%AllProp(P0%IARR(ISPXX):P0%IARR(ISPXX + 1) - 1, :)
269  P0%SpinZZ => P0%AllProp(P0%IARR(ISPZZ):P0%IARR(ISPZZ + 1) - 1, :)
270  P0%AveSpin => P0%AllProp(P0%IARR(IAVSP):P0%IARR(IAVSP + 1) - 1, :)
271  P0%Den0   => P0%AllProp(P0%IARR(IDEN0):P0%IARR(IDEN0 + 1) - 1, :)
272  P0%Den1   => P0%AllProp(P0%IARR(IDEN1):P0%IARR(IDEN1 + 1) - 1, :)
273  P0%Pair   => P0%AllProp(P0%IARR(IPAIR):P0%IARR(IPAIR + 1) - 1, :)
274  P0%Test   => P0%AllProp(P0%IARR(ITEST):P0%IARR(ITEST + 1) - 1, :)
275
276
277  ! Four-Particle Correlators
278  P0%DoDo   => P0%AllProp(P0%IARR(IDODO):P0%IARR(IDODO + 1) - 1, :)
279  P0%DoHo   => P0%AllProp(P0%IARR(IDOHO):P0%IARR(IDOHO + 1) - 1, :)
280  P0%HoHo   => P0%AllProp(P0%IARR(IHOHO):P0%IARR(IHOHO + 1) - 1, :)
```

```
295  ! Initialize
296  P0%meas    = ZERO
297  P0%stgn    = ZERO
298  P0%G_fun   = ZERO
299  P0%Gf_up   = ZERO
300  P0%Gf_dn   = ZERO
301  P0%SpinXX  = ZERO
302  P0%SpinZZ  = ZERO
303  P0%AveSpin = ZERO
304  P0%Den0    = ZERO
305  P0%Den1    = ZERO
306  P0%Pair    = ZERO
307  ! Four-Particle Correlators
308  P0%Test    = ZERO
309  P0%DoDo    = ZERO
310  P0%DoHo    = ZERO
311  P0%HoHo    = ZERO
312
```

In the subroutine `DQMC_Phy0_Free`, which deallocates used space at the end of the program, additional entries are made:

```

354     nullify(P0%meas)
355     nullify(P0%G_fun, P0%Gf_up, P0%Gf_dn)
356     nullify(P0%SpinXX, P0%SpinZZ, P0%AveSpin)
357     nullify(P0%Den0, P0%Den1)
358     nullify(P0%Pair)
359     nullify(P0%Test)
360     !
361     nullify(P0%DoDo)
362     nullify(P0%DoHo)
363     nullify(P0%HoHo)
364
365     deallocate(P0%AllProp, P0%sign)

```

QUEST groups the averages from a set number of measurements in bins. The routine `DQMC_Phy0_Avg` performs the averaging within a bin, which must also be done for our four-particle correlators:

```

419     n = P0%nClass
420     call blas_dscal(n, factor, P0%G_fun (1:n, idx), 1)
421     call blas_dscal(n, factor, P0%Gf_up (1:n, idx), 1)
422     call blas_dscal(n, factor, P0%Gf_dn (1:n, idx), 1)
423     call blas_dscal(n, factor, P0%SpinXX(1:n, idx), 1)
424     call blas_dscal(n, factor, P0%SpinZZ(1:n, idx), 1)
425     call blas_dscal(n, factor, P0%Den0 (1:n, idx), 1)
426     call blas_dscal(n, factor, P0%Den1 (1:n, idx), 1)
427     call blas_dscal(n, factor, P0%Pair (1:n, idx), 1)
428     call blas_dscal(n, factor, P0%Test (1:n, idx), 1)
429     ! Four-Particle Correlators
430     call blas_dscal(n, factor, P0%DoDo (1:n, idx), 1)
431     call blas_dscal(n, factor, P0%DoHo (1:n, idx), 1)
432     call blas_dscal(n, factor, P0%HoHo (1:n, idx), 1)
433

```

At the end of the `DQMC_Phy0_Print`-subroutine, which prints the output, the following additional calls are made at the end:

```

516     ! Four-Particle Corr's
517     call DQMC_Print_RealArray(0, nClass, "Doublon-Doublon correlator:", &
518         S%clabel, P0%DoDo(:, avg:avg), P0%DoDo(:, err:err), OPT)
519
520     call DQMC_Print_RealArray(0, nClass, "Doublon-Holon correlator:", &
521         S%clabel, P0%DoHo(:, avg:avg), P0%DoHo(:, err:err), OPT)
522
523     call DQMC_Print_RealArray(0, nClass, "Holon-Holon correlator:", &
524         S%clabel, P0%HoHo(:, avg:avg), P0%HoHo(:, err:err), OPT)

```

`DQMC_Phy0_GetErr` estimates the error by applying the Jackknife-algorithm on the binned results. The additional calls are:



## 6 CHARGE CORRELATION, DOUBLON-HOLON BINDING AND SCREENING IN THE DOPED HUBBARD MODEL

---

```
644      ! =====
645      ! Four-Particle Corr's
646      do i = 1, P0%nClass
647          data = P0%DoDo(i, 1:n)
648          call DQMC_SignJackKnife(n, P0%DoDo(i, avg), P0%DoDo(i, err), &
649              data, y, sgn, sum_sgn)
650      end do
651
652      do i = 1, P0%nClass
653          data = P0%DoHo(i, 1:n)
654          call DQMC_SignJackKnife(n, P0%DoHo(i, avg), P0%DoHo(i, err), &
655              data, y, sgn, sum_sgn)
656      end do
657
658      do i = 1, P0%nClass
659          data = P0%HoHo(i, 1:n)
660          call DQMC_SignJackKnife(n, P0%HoHo(i, avg), P0%HoHo(i, err), &
661              data, y, sgn, sum_sgn)
662      end do
663      ! =====
```

Finally, in the `DQMC_Phy0_Meas`-subroutine, the actual measurements are done. First, all observables are initialized to zero:

```
786      ! Initialization
787      ! Here we use avg bin as a temp variable
788      P0%meas(:,tmp) = ZERO
789
790      P0%G_fun(:,tmp) = ZERO
791      P0%Gf_up(:,tmp) = ZERO
792      P0%Gf_dn(:,tmp) = ZERO
793      P0%Den0(:,tmp) = ZERO
794      P0%Den1(:,tmp) = ZERO
795      P0%SpinXX(:,tmp) = ZERO
796      P0%SpinZZ(:,tmp) = ZERO
797      P0%Pair(:,tmp) = ZERO
798      P0%Test(:,tmp) = ZERO
799      ! Four-Particle Corr's
800      P0%DoDo(:,tmp) = ZERO
801      P0%DoHo(:,tmp) = ZERO
802      P0%HoHo(:,tmp) = ZERO
```

Then, the Wick-factorized (see Ch.(2.2.3)) correlators need to be coded up:

```

1056      ! Measurement of the Four-Particle Corr's
1057
1058      ! Kronecker-Delta
1059      if (i .eq. j) then
1060         kd = ONE
1061      else
1062         kd = ZERO
1063      end if
1064
1065      ! Occupations of Site i and j
1066      niup = (ONE - G_up(i,i))
1067      nidn = (ONE - G_dn(i,i))
1068      !
1069      njup = (ONE - G_up(j,j))
1070      njdn = (ONE - G_dn(j,j))
1071
1072      ! Tmp variables
1073      tmp1 = niup * nidn * njup * njdn
1074      tmp2 = niup * njup * (kd - G_dn(j,i)) * G_dn(i,j)
1075      tmp3 = nidn * njdn * (kd - G_up(j,i)) * G_up(i,j)
1076      tmp4 = (kd - G_up(j,i)) * G_up(i,j) * (kd - G_dn(j,i)) * G_dn(i,j)
1077      ! Sum
1078      tmp5 = tmp1 + tmp2 + tmp3 + tmp4
1079      !
1080      tmp6 = niup * njup + (kd - G_up(j,i)) * G_up(i,j)
1081      tmp7 = nidn * njdn + (kd - G_dn(j,i)) * G_dn(i,j)
1082
1083      ! Doublon-Doublon Correlator
1084      P0%DoDo(k,tmp) = P0%DoDo(k,tmp) + tmp5
1085
1086      ! Doublon-Holon Correlator
1087      P0%DoHo(k,tmp) = P0%DoHo(k,tmp) + ( niup*nidn - nidn*tmp6 - niup*tmp7 + tmp5 )
1088
1089      ! Holon-Holon Correlator
1090      P0%HoHo(k,tmp) = P0%HoHo(k,tmp) + ( ONE - (niup + nidn + njup + njdn) + niup*nidn + njup*njdn &
1091      + niup*njdn + nidn*njup + tmp6 + tmp7 &
1092      - (nidn + njdn)*tmp6 - (niup + njup)*tmp7 &
1093      + tmp5 )
1094
1095
1096      ! =====
1097

```

Since the final, averaged result is translationally invariant, QUEST saves the measurement depending on distinct distance classes  $d = |\mathbf{R}_i - \mathbf{R}_j|$  instead of the full  $(i, j)$ -dependence. As such, the measurements are normalized by the number of lattice vectors leading to a specific distance (**S%F(i)** in the next picture). Afterwards, the measurements are put into the correct bin. We add the respective statements for the new correlators:

```

1118      ! Average
1119      P0%meas(:,tmp) = P0%meas(:,tmp) / n
1120      do i = 1, P0%nClass
1121         P0%G_fun(i, tmp) = P0%G_fun(i, tmp) / S%F(i) * HALF
1122         P0%Gf_up(i, tmp) = P0%Gf_up(i, tmp) / S%F(i)
1123         P0%Gf_dn(i, tmp) = P0%Gf_dn(i, tmp) / S%F(i)
1124         P0%SpinXX(i, tmp) = P0%SpinXX(i, tmp) / S%F(i)
1125         P0%SpinZZ(i, tmp) = P0%SpinZZ(i, tmp) / S%F(i)
1126         P0%Den0(i, tmp) = P0%Den0(i, tmp) / S%F(i) * HALF
1127         P0%Den1(i, tmp) = P0%Den1(i, tmp) / S%F(i)
1128         P0%Pair(i, tmp) = P0%Pair(i, tmp) / S%F(i) * HALF
1129         P0%Test(i, tmp) = P0%Test(i, tmp) / S%F(i)
1130         ! Four-Particle Corr's
1131         P0%DoDo(i, tmp) = P0%DoDo(i, tmp) / S%F(i)
1132         P0%DoHo(i, tmp) = P0%DoHo(i, tmp) / S%F(i)
1133         P0%HoHo(i, tmp) = P0%HoHo(i, tmp) / S%F(i)
1134      end do
1135

```

## 6 CHARGE CORRELATION, DOUBLON-HOLON BINDING AND SCREENING IN THE DOPED HUBBARD MODEL

```

1142 ! Accumulate result to P0(:, idx)
1143 sgn = sgnup * sgndn
1144 P0%meas(:, idx) = P0%meas(:, idx) + P0%meas(:, tmp) * sgn
1145
1146 m = P0%nClass
1147 call blas_daxpy(m, sgn, P0%G_fun (1:m,tmp), 1, P0%G_fun (1:m,idx), 1)
1148 call blas_daxpy(m, sgn, P0%Gf_up (1:m,tmp), 1, P0%Gf_up (1:m,idx), 1)
1149 call blas_daxpy(m, sgn, P0%Gf_dn (1:m,tmp), 1, P0%Gf_dn (1:m,idx), 1)
1150 call blas_daxpy(m, sgn, P0%SpinXX(1:m,tmp), 1, P0%SpinXX(1:m,idx), 1)
1151 call blas_daxpy(m, sgn, P0%SpinZZ(1:m,tmp), 1, P0%SpinZZ(1:m,idx), 1)
1152 call blas_daxpy(m, sgn, P0%Den0 (1:m,tmp), 1, P0%Den0 (1:m,idx), 1)
1153 call blas_daxpy(m, sgn, P0%Den1 (1:m,tmp), 1, P0%Den1 (1:m,idx), 1)
1154 call blas_daxpy(m, sgn, P0%Pair (1:m,tmp), 1, P0%Pair(1:m,idx), 1)
1155 call blas_daxpy(m, sgn, P0%Test (1:m,tmp), 1, P0%Test(1:m,idx), 1)
1156 ! Four-Particle Corr's
1157 call blas_daxpy(m, sgn, P0%DoDo (1:m,tmp), 1, P0%DoDo(1:m,idx), 1)
1158 call blas_daxpy(m, sgn, P0%DoHo (1:m,tmp), 1, P0%DoHo(1:m,idx), 1)
1159 call blas_daxpy(m, sgn, P0%HoHo (1:m,tmp), 1, P0%HoHo(1:m,idx), 1)
1160
1161 P0%sign(P0_SGN, idx) = P0%sign(P0_SGN, idx) + sgn
1162 P0%sign(P0_SGNUP, idx) = P0%sign(P0_SGNUP, idx) + sgnup
1163 P0%sign(P0_SGNDN, idx) = P0%sign(P0_SGNDN, idx) + sgndn
1164 P0%cnt = P0%cnt + 1
1165

```

Although not used in the paper, the code will also compute the Fourier transform and Eigenmodes of all correlators. In order to print them in the output, `DQMC_Phy0_PrintFT` needs additional statements:

```

1465 ! Four-Particle Corr's
1466 FTptr => P0%AllPropFT(P0%IARRFT(IDODO):P0%IARRFT(IDODO+1)-1,:)
1467 call DQMC_Print_RealArray(0, nakg*(na+1)/2, "FT of Doublon-Doublon correlator:", &
1468 clabel, FTptr(:, avg:avg), FTptr(:, err:err), OPT)
1469
1470 FTptr => P0%AllPropFT(P0%IARRFT(IDOHO):P0%IARRFT(IDOHO+1)-1,:)
1471 call DQMC_Print_RealArray(0, nakg*(na+1)/2, "FT of Doublon-Holon correlator:", &
1472 clabel, FTptr(:, avg:avg), FTptr(:, err:err), OPT)
1473
1474 FTptr => P0%AllPropFT(P0%IARRFT(IHOHO):P0%IARRFT(IHOHO+1)-1,:)
1475 call DQMC_Print_RealArray(0, nakg*(na+1)/2, "FT of Holon-Holon correlator:", &
1476 clabel, FTptr(:, avg:avg), FTptr(:, err:err), OPT)
1477

```

```

1580 ! Four-Particle Corr's
1581 Nmptr => P0%AllPropEigVec(:, :, IDODO)
1582 call DQMC_Print_EigenMode(na, nkg, "Eigenmodes of the Doublon-Doublon correlator:", &
1583 Nmptr, OPT)
1584
1585 Nmptr => P0%AllPropEigVec(:, :, IDOHO)
1586 call DQMC_Print_EigenMode(na, nkg, "Eigenmodes of the Doublon-Holon correlator:", &
1587 Nmptr, OPT)
1588
1589 Nmptr => P0%AllPropEigVec(:, :, IHOHO)
1590 call DQMC_Print_EigenMode(na, nkg, "Eigenmodes of the Holon-Holon correlator:", &
1591 Nmptr, OPT)
1592

```

The QUEST library can then be compiled as usual. The standard `geom`-binary (for usage, see the original documentation on [41]) will now yield additional entries in the output file. Assuming a periodic 4x4 square lattice, which has six inequivalent distances between sites, the new entries read as:

```

127 =====
128 Doublon-Doublon correlator:
129 0 0 0.0000 0.0000 0.0000 016 0.11892324E+00 +- 0.24407654E-03
130 0 0 1.0000 0.0000 0.0000 064 0.85661897E-02 +- 0.40538600E-04
131 0 0 2.0000 0.0000 0.0000 032 0.12799845E-01 +- 0.64496824E-04
132 0 0 1.0000 1.0000 0.0000 064 0.12796585E-01 +- 0.52204910E-04
133 0 0 2.0000 1.0000 0.0000 064 0.13253806E-01 +- 0.53323673E-04
134 0 0 2.0000 2.0000 0.0000 016 0.11136814E-01 +- 0.12874797E-03
135 =====
136 Doublon-Holon correlator:
137 0 0 0.0000 0.0000 0.0000 016 -0.73322041E-19 +- 0.11267435E-18
138 0 0 1.0000 0.0000 0.0000 064 0.29728168E-01 +- 0.57700896E-04
139 0 0 2.0000 0.0000 0.0000 032 0.15608612E-01 +- 0.91357199E-04
140 0 0 1.0000 1.0000 0.0000 064 0.15629028E-01 +- 0.80219734E-04
141 0 0 2.0000 1.0000 0.0000 064 0.15488217E-01 +- 0.73212708E-04
142 0 0 2.0000 2.0000 0.0000 016 0.15638530E-01 +- 0.75690251E-04
143 =====
144 Holon-Holon correlator:
145 0 0 0.0000 0.0000 0.0000 016 0.11892324E+00 +- 0.24407654E-03
146 0 0 1.0000 0.0000 0.0000 064 0.85661897E-02 +- 0.40538600E-04
147 0 0 2.0000 0.0000 0.0000 032 0.12799845E-01 +- 0.64496824E-04
148 0 0 1.0000 1.0000 0.0000 064 0.12796585E-01 +- 0.52204910E-04
149 0 0 2.0000 1.0000 0.0000 064 0.13253806E-01 +- 0.53323673E-04
150 0 0 2.0000 2.0000 0.0000 016 0.11136814E-01 +- 0.12874797E-03

```

From this, the results in the paper have been obtained. As mentioned above, the Fourier transforms are also available.

## 7. Overcoming the fermionic QMC sign problem through Dual Fermion Perturbation Theory

In Ch.(4.1.2), where the Determinantal Quantum Monte Carlo method is introduced, it is mentioned that the determinants which constitute the statistical weights are not positive definite, leading to the famous fermionic sign problem which strongly restricts the applicability of *all* fermionic QMC methods. The absolute values of the statistical weights are still taken for measurements, but one has to divide them by the *average sign*  $\langle S \rangle$ , quickly rendering simulations impossible once it starts deviating strongly from  $\langle S \rangle \simeq 1$ . Aside from specific points such as the particle-hole symmetric, half-filled Hubbard model where  $\langle S \rangle = 1$ , the sign deteriorates exponentially with the inverse temperature  $\beta$ , the interaction strength  $U$  and the number of lattice sites  $N$ . Adding a hopping  $t'$  between next-nearest neighbours makes the problem even worse.

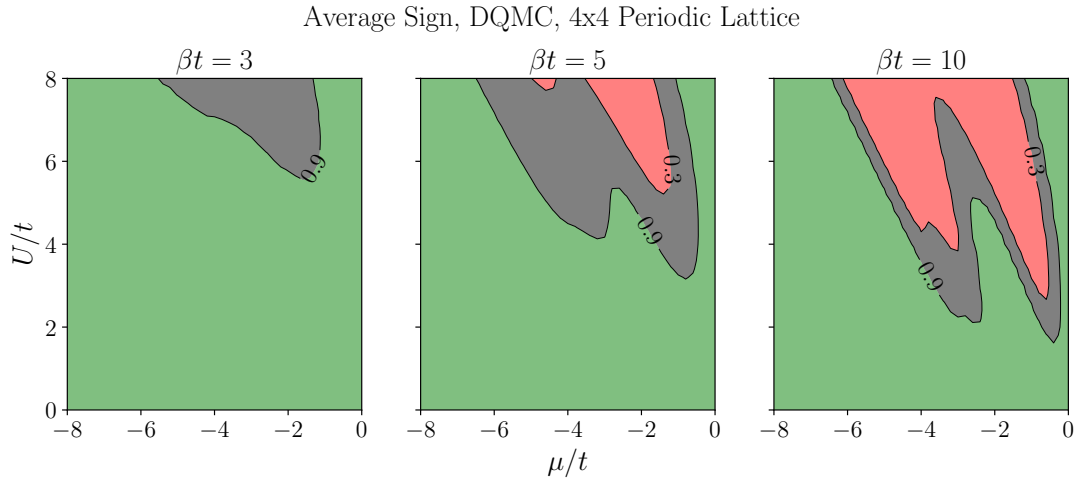


Figure 7.0.1: Average Sign (DQMC) of the square lattice Hubbard model ( $t' = 0$ ) for three temperatures on a  $(U, \mu)$ -grid:  $\langle S \rangle > 0.9$  (green),  $\langle S \rangle = 0.9 \dots 0.3$  (gray),  $\langle S \rangle < 0.3$  (red).

From the DQMC data obtained in Ch.(6), Fig.(7.0.1) shows a contour plot of how the average sign changes when cooling the system. In the green area of the parameter space where  $\langle S \rangle > 0.9$ , simulations can be done without problems. The gray area marks a crossover where the sign falls down to  $\langle S \rangle = 0.3$ , making simulations increasingly difficult but, depending on the system size, not necessarily impossible. Within the red area, simulations become exceedingly difficult even for the rather small 4x4-lattice, and almost impossible for larger systems. Unfortunately, the interesting area with strong coupling and a filling of  $\langle n_i \rangle \approx 0.75 \dots 0.95$  electrons per lattice site, where  $d$ -wave superconductivity is suspected, always lies in the red zone unless we stay at very high temperatures. In order to study these areas of the parameter space, new

methods are necessary.

In Ch.(4.2), we introduced a Dual Fermion Perturbation theory which allows for an arbitrary choice of a reference system from where a perturbation of choice is developed. In the results presented later in this chapter, we choose the half-filled Hubbard model, which does not suffer from the sign problem, and can thus be solved very accurately even for large  $U$ , as the reference point. Illustrated by Fig.(7.0.2), both a next-nearest neighbor hopping  $t'$  and a shift in chemical potential  $\mu$  is taken as the perturbation.

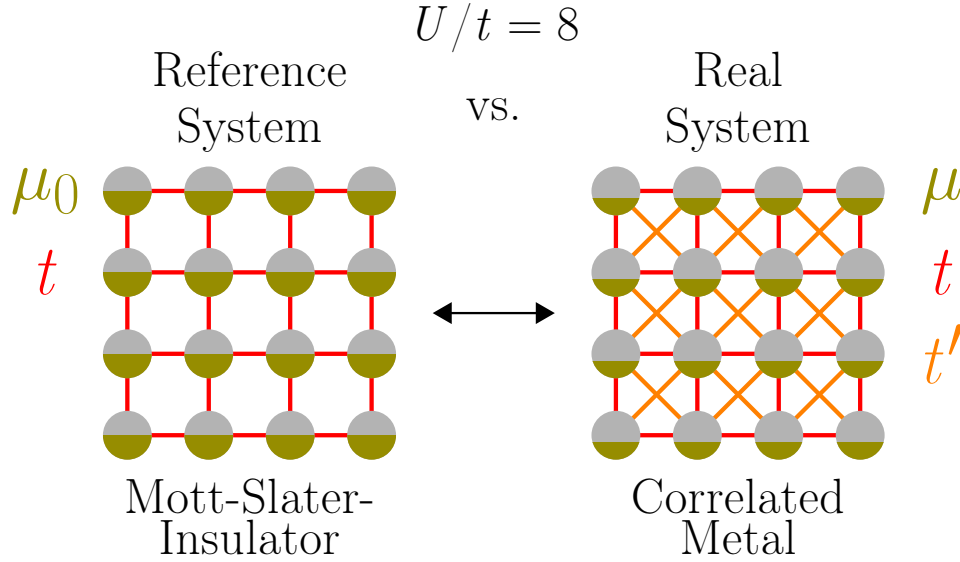


Figure 7.0.2: Half-filled Reference System vs. Real, doped System with  $t'$  which is developed perturbatively.

It should be noted that any point in the green area (and the gray area, with a bit of additional effort) in Fig.(7.0.1) can serve as a proper starting point. Indeed, it is a long-term goal to verify findings in the red area by arriving at the same solution from multiple sides within the parameter space.

In this chapter, we present a FORTRAN-implementation which realizes this Dual Fermion approach efficiently by making use of the QUEST-library [41] for the DQMC simulations.

### 7.1. Time-Dependent measurements in QUEST

Before discussing our own implementations, it is necessary to understand how the default QUEST [41] performs time-dependent measurements. Within the standard **ggeom**-program in the package (**ggeom.F90**-file), after initializing, warming up and setting a configuration of auxiliary fields, measurements are done as follows:

```

102      ! Fetch a random slice for measurement
103      call ran0(1, randn, Hub%seed)
104      slice = ceiling(randn(1)*Hub%L)
105      write(*,'(a,3i6)') ' Measurement Sweep, bin, iter, slice : ', i, j, slice
106
107      if (comp_tdm > 0) then
108          ! Compute full Green's function
109          call DQMC_Gtau_LoadA(tau, TAU_UP, slice, Hub%G_up%sgn)
110          call DQMC_Gtau_LoadA(tau, TAU_DN, slice, Hub%G_dn%sgn)
111          ! Measure equal-time properties
112          call DQMC_Hub_FullMeas(Hub, tau%nnb, tau%A_up, tau%A_dn, tau%sgnup, tau%sgndn)
113          ! Measure time-dependent properties
114          call DQMC_TDM1_Meas(tm, tau)

```

As a reminder, for a fixed set of fields, the Green's function  $g_{ij}^\sigma(l, l') = +\langle c_{i\sigma}(l)c_{j\sigma}^\dagger(l') \rangle$  (the positive sign is common QMC convention) is neither translationally invariant nor does it have the fermionic symmetry in the imaginary time, and thus depends on two time slice indices  $(l, l')$  with the time discretization  $\tau = 0 \dots (L-1)\Delta\tau$ . If the input parameter is set as **nOrth** = 1, **DQMC\_Gtau\_LoadA** will compute the Green's functions for **all** possible combinations of  $(l, l')$  and lattice sites  $(i, j)$ . As such, the size of the  $A$ -matrix ( $N$  lattice sites and  $L$  time slices) is  $N^2 \times L^2$ .

**DQMC\_TDM1\_Meas**, which is found in the **dqmc\_tdm1.F90**-file and obtains measurements from the  $A$ -matrix, contains a complicated double loop over time indices:

```

382  blocks: do i0 = 1, tau%nb
383      do dtau = 0, tau%nb-1
384          it = mod(i0+dtau-1,tau%nb) + 1
385
386          ! Stored value
387          call DQMC_Gtau_DumpA(tau, TAU_UP, it, i0)
388          if (tau%comp_dn .or. .not.tau%neg_u) &
389              call DQMC_Gtau_DumpA(tau, TAU_DN, it, i0)
390
391          jt = tau%it_up; j0 = tau%i0_up
392          call DQMC_TDM1_Compute(T1, upt0, up0t, dnt0, dn0t, up00, uptt, dn00, dnnt, jt, j0)
393
394          ! Decrement index tau%it. If north is even do only north/2-1 decrements.
395          do dt = 1, m-1+k
396              call DQMC_change_gtau_time(tau, TPLUS, TAU_UP)
397              if (tau%comp_dn) then
398                  call DQMC_change_gtau_time(tau, TPLUS, TAU_DN)
399              elseif (.not.tau%neg_u) then
400                  call DQMC_Gtau_CopyUp(tau)
401              endif
402
403          jt = tau%it_up; j0 = tau%i0_up
404          call DQMC_TDM1_Compute(T1, upt0, up0t, dnt0, dn0t, up00, uptt, dn00, dnnt, jt, j0)
405      enddo
406
407      if (m .gt. 0) then
408          call DQMC_Gtau_DumpA(tau, TAU_UP, it, i0)
409          if (tau%comp_dn .or. .not.tau%neg_u) &
410              call DQMC_Gtau_DumpA(tau, TAU_DN, it, i0)
411      endif
412      ! Increment index tau%it
413      do dt = 1, m
414          call DQMC_change_gtau_time(tau, TMINUS, TAU_UP)
415          if (tau%comp_dn) then
416              call DQMC_change_gtau_time(tau, TMINUS, TAU_DN)
417          elseif (.not.tau%neg_u) then
418              call DQMC_Gtau_CopyUp(tau)
419          endif
420          jt = tau%it_up; j0 = tau%i0_up
421          call DQMC_TDM1_Compute(T1, upt0, up0t, dnt0, dn0t, up00, uptt, dn00, dnnt, jt, j0)
422      enddo
423
424  enddo
425

```

For **nOrth** = 1, the incrementing and decrementing of indices does not occur since  $A$  already contains everything, and only the top part is relevant. Specifically, **DQMC\_Gtau\_DumpA** will load a subblock of  $(\mathbf{it}, \mathbf{i0})$ , which corresponds to  $(l, l')$ , and the respective Green's function can then be accessed via the pointers **upt0**, **up0t** . . . . The notation is as follows:

- $\text{upt0}(i,j) \Leftrightarrow g_{i,j}^\uparrow(l, l') \Leftrightarrow \langle c_{i\uparrow}(l) c_{j\uparrow}^\dagger(l') \rangle$
- $\text{up0t}(i,j) \Leftrightarrow g_{i,j}^\uparrow(l', l) \Leftrightarrow \langle c_{i\uparrow}(l') c_{j\uparrow}^\dagger(l) \rangle$
- $\text{up00}(i,j) \Leftrightarrow g_{i,j}^\uparrow(l', l') \Leftrightarrow \langle c_{i\uparrow}(l') c_{j\uparrow}^\dagger(l') \rangle$
- $\text{uptt}(i,j) \Leftrightarrow g_{i,j}^\uparrow(l, l) \Leftrightarrow \langle c_{i\uparrow}(l) c_{j\uparrow}^\dagger(l) \rangle$

Of course, the same notation applies to the spin-down Green's function (e.g. **dnt0** instead of **upt0**). Before we discuss what happens for **nOrth**  $\neq$  1, we take a look at how Green's functions are computed in **DQMC\_TDM1\_Compute**. Generally, if



## 7 OVERCOMING THE FERMIONIC QMC SIGN PROBLEM THROUGH DUAL FERMION PERTURBATION THEORY

---

the full  $(l, l')$ -dependence is available, there are two contributions to the final Green's function which depends on time differences only. Assuming  $l > l'$ , one could take the current  $g^\uparrow(l, l')$  (upt0) and put it into the  $(l - l')$ 'th time index of the final result. However,  $-g^\uparrow(l', l)$  (-up0t) also gives a contribution when shifting the time index by  $\beta$  (i.e. by  $L$ ).  $-g^\uparrow(l', l)$  is saved into the  $(L - (l - l'))$ 'th time slice. For  $l < l'$ , the same argument holds, but the other way around. Before computing anything, depending on  $l - l'$ , the subroutine defines the correct time slots at the top. If  $l = l'$ , only  $+\mathbf{upt0}$  is taken as a contribution:

```

484 dt = it - i0
485 if (dt .gt. 0) then
486   ! it > i0
487   dt1 = dt
488   dt2 = T1%L - dt
489   factor = 0.25d0
490 elseif (dt .lt. 0) then
491   ! it < i0
492   dt1 = dt + T1%L
493   dt2 = -dt
494   factor = -0.25d0
495 else
496   dt1 = 0
497   dt2 = 0
498   factor = 0.5d0
499 endif

```

After some overhead, the Spin-Up Green's function can then be measured as:

```

514 value1 => T1%properties(IGFUP)%values(:, dt1, T1%tmp)
515 value2 => T1%properties(IGFUP)%values(:, dt2, T1%tmp)
516 do i = 1, T1%properties(IGFUP)%n
517   do j = 1, T1%properties(IGFUP)%n
518     ! k is the distance index of site i and site j
519     k = T1%properties(IGFUP)%D(i, j)
520     value1(k) = value1(k) + 2*factor*upt0(i, j)
521     value2(k) = value2(k) - 2*factor*up0t(i, j)
522   end do
523 end do

```

The prefactor 2 and the **factor**-variable ensure correct normalization. Although we are only interested in the Green's function, it should be noted that the measurements of two-particle correlators works by Wick-factorization. A simple example is the Spin-XX correlator  $\langle S_i^x(\tau) S_j^x(0) \rangle$ , with  $S_i^x = c_{i\uparrow}^\dagger c_{i\downarrow} + c_{i\downarrow}^\dagger c_{i\uparrow}$ . Setting  $l' = 0$  for readability, the correlator factorizes into:

$$\begin{aligned} \langle S_i^x(l) S_j^x(0) \rangle &= - \left( \langle c_{j\uparrow}(0) c_{i\uparrow}^\dagger(l) \rangle \langle c_{i\downarrow}(l) c_{j\downarrow}^\dagger(0) \rangle + \langle c_{j\downarrow}(0) c_{i\downarrow}^\dagger(l) \rangle \langle c_{i\uparrow}(l) c_{j\uparrow}^\dagger(0) \rangle \right) \\ &\equiv - (\text{up0t}(j,i) * \text{dnt0}(i,j) + \text{dn0t}(j,i) * \text{upt0}(i,j)) \end{aligned}$$

In the program, this translates to:

```

536 value1 => T1%properties(ISPXX)%values(:, dt1, T1%tmp)
537 value2 => T1%properties(ISPXX)%values(:, dt2, T1%tmp)
538 do i = 1, T1%properties(ISPXX)%n
539     do j = 1, T1%properties(ISPXX)%n
540         ! k is the distance index of site i and site j
541         k = T1%properties(ISPXX)%D(i,j)
542         value1(k) = value1(k) - (up0t(j,i)*dnt0(i,j) &
543             + dn0t(j,i)*upt0(i,j))/2
544         value2(k) = value2(k) - (up0t(i,j)*dnt0(j,i) &
545             + dn0t(i,j)*upt0(j,i))/2
546     end do
547 end do

```

Now, we take a look at what happens when  $\mathbf{nOrth} \neq 1$ . Then, the calculation of the Green's function from scratch only occurs for a subset of  $(l, l')$ -indices. From there, in order to obtain the whole time-dependency, the index  $l$  is shifted through all possibilities via the B-matrices (see Eq.(4.1.29)).

For the extreme case of  $\mathbf{nOrth} = L$ , only one exact Green's function is evaluated at the random time slice used for equal-time measurements. We can keep track of the index-shifts by printing them every time the Green's function is computed (i.e. right before every call of `DQMC_TDM1_Compute`). The output for  $L = 20$  would be:

```

nOrth =          20
Number of times in A (tau%nb):          1
Time indices in A (tau%tau_up):         2
Values of k and m:           0          10
Double loop starts here...
=====
Starting point:
Indices (tau%it_up, tau%i0_up):         2          2
=====
Incrementing tau%it...
Indices (tau%it_up, tau%i0_up):         3          2
Indices (tau%it_up, tau%i0_up):         4          2
Indices (tau%it_up, tau%i0_up):         5          2
Indices (tau%it_up, tau%i0_up):         6          2
Indices (tau%it_up, tau%i0_up):         7          2
Indices (tau%it_up, tau%i0_up):         8          2
Indices (tau%it_up, tau%i0_up):         9          2
Indices (tau%it_up, tau%i0_up):        10          2
Indices (tau%it_up, tau%i0_up):        11          2
=====
Decrementing tau%it...
Indices (tau%it_up, tau%i0_up):         1          2
Indices (tau%it_up, tau%i0_up):        20          2
Indices (tau%it_up, tau%i0_up):        19          2
Indices (tau%it_up, tau%i0_up):        18          2
Indices (tau%it_up, tau%i0_up):        17          2
Indices (tau%it_up, tau%i0_up):        16          2
Indices (tau%it_up, tau%i0_up):        15          2
Indices (tau%it_up, tau%i0_up):        14          2
Indices (tau%it_up, tau%i0_up):        13          2
Indices (tau%it_up, tau%i0_up):        12          2

```

The Green's function at the time slice  $l, l' = 2$ , which was picked randomly, serves as a starting point, and  $l$  is shifted through all possible values. Choosing  $\mathbf{nOrth} = L/2$

## 7 OVERCOMING THE FERMIONIC QMC SIGN PROBLEM THROUGH DUAL FERMION PERTURBATION THEORY

---

instead of  $L$  leads to  $2 \times 2 = 4$  starting points from which indices are shifted. For our example above,  $\mathbf{nOrth} = 10$ , and the output reads as:

```

=====
Starting point (tau%it_up, tau%i0_up):          2          2
Incrementing tau%it...
Indices (tau%it_up, tau%i0_up):          3          2
Indices (tau%it_up, tau%i0_up):          4          2
Indices (tau%it_up, tau%i0_up):          5          2
Indices (tau%it_up, tau%i0_up):          6          2
Decrementing tau%it...
Indices (tau%it_up, tau%i0_up):          1          2
Indices (tau%it_up, tau%i0_up):         20          2
Indices (tau%it_up, tau%i0_up):         19          2
Indices (tau%it_up, tau%i0_up):         18          2
Indices (tau%it_up, tau%i0_up):         17          2
=====
Starting point (tau%it_up, tau%i0_up):         12          2
Incrementing tau%it...
Indices (tau%it_up, tau%i0_up):         13          2
Indices (tau%it_up, tau%i0_up):         14          2
Indices (tau%it_up, tau%i0_up):         15          2
Indices (tau%it_up, tau%i0_up):         16          2
Decrementing tau%it...
Indices (tau%it_up, tau%i0_up):         11          2
Indices (tau%it_up, tau%i0_up):         10          2
Indices (tau%it_up, tau%i0_up):          9          2
Indices (tau%it_up, tau%i0_up):          8          2
Indices (tau%it_up, tau%i0_up):          7          2
=====
Starting point (tau%it_up, tau%i0_up):         12         12
Incrementing tau%it...
Indices (tau%it_up, tau%i0_up):         13         12
Indices (tau%it_up, tau%i0_up):         14         12
Indices (tau%it_up, tau%i0_up):         15         12
Indices (tau%it_up, tau%i0_up):         16         12
Decrementing tau%it...
Indices (tau%it_up, tau%i0_up):         11         12
Indices (tau%it_up, tau%i0_up):         10         12
Indices (tau%it_up, tau%i0_up):          9         12
Indices (tau%it_up, tau%i0_up):          8         12
Indices (tau%it_up, tau%i0_up):          7         12
=====
Starting point (tau%it_up, tau%i0_up):          2         12
Incrementing tau%it...
Indices (tau%it_up, tau%i0_up):          3         12
Indices (tau%it_up, tau%i0_up):          4         12
Indices (tau%it_up, tau%i0_up):          5         12
Indices (tau%it_up, tau%i0_up):          6         12
Decrementing tau%it...
Indices (tau%it_up, tau%i0_up):          1         12
Indices (tau%it_up, tau%i0_up):         20         12
Indices (tau%it_up, tau%i0_up):         19         12
Indices (tau%it_up, tau%i0_up):         18         12
Indices (tau%it_up, tau%i0_up):         17         12
=====

```

This benefit of these groupings is that shifting time indices with the B-matrices is considerably faster than evaluating all Green's functions from scratch. Also, the size of

the  $A$ -matrix is kept low, which saves memory space. It should be noted that, although this scheme is enough to collect contributions for the final Green's function, it does not give the **full**  $(l, l')$ -dependence that we need for the Dual Fermion method unless **nOrth** = 1. Only the time index **it** is shifted through all possibilities through the subroutine **DQMC\_change\_gtau\_time**, by passing the arguments **TPLUS** or **TMINUS**. However, the subroutine also accepts **ZPLUS** and **ZMINUS** as an arguments for shifting **i0**, which could be implemented in a later version of our package.

### 7.2. Implementations for the Dual-Fermion Approach

In [95], the current version of a FORTRAN-package which was developed in this thesis is available. Its purpose is to make use of the QUEST library in order to realize the Dual Fermion Perturbation Theory discussed in Ch.(4.2) (hence, the naming *DFPT*) via the DQMC method. We do not give a full code documentation here, but rather discuss the relevant parts and give an introduction on how to use it. Furthermore, a few first results are provided, and necessary future implementations are explained.

#### 7.2.1. Compilation

Compiling the programs can be done simply by running **make** in the top folder. Before that, in the Makefile, the compilers (both sequential and MPI) need to be defined:

```
9 # Fortran-Compilers, sequential and MPI
10 FC_SEQ = gfortran
11 FC_MPI = mpif90
```

Also, a LAPACK-library (e.g. OpenBLAS [96]), FFTW [97], QUEST and the standard C++ library need to be specified:

```
30 # Top directory of QUEST and the library
31 QUEST_DIR = (...)
32 DQMCLIB = $(QUEST_DIR)/libdqmc.a
33
34 # BLAS/LAPACK (OpenBLAS or MKL)
35 libOpenBLAS = (...) /OpenBLAS-0.3.23/libopenblas.a
36 LAPACKLIB = $(libOpenBLAS)
37
38 # Standard C++ library
39 CXXLIB = -lstdc++
40
41 # FFTW
42 FFTW_DIR = (...) /fftw-3.3.10/build
43 FFTW_INC = $(FFTW_DIR)/include/
44 FFTW_LIB = $(FFTW_DIR)/lib/libfftw3.a
```

After the compilation, two binaries (**build\_ref** and **dfpt\_mpi**), which are explained in the following subchapters, can be found in the **bin**-folder.

### 7.2.2. Building the Reference System

The first step for realizing the Dual Fermion method is to obtain the Green's function of the system which we choose as a reference (denoted by small  $g$  in Ch.(4.2)). This can already be done with the standard **ggeom**-program of QUEST. Indeed, the program **build\_ref** which we provide is just a simplified version. More specifically, the time-dependent measurements are done with the **DFPT\_Meas\_Ref\_G** instead of **DQMC\_TDM1\_Meas**:

```

117      ! Fetch a random slice for measurement
118      call ran0(1, randn, Hub%seed)
119      slice = ceiling(randn(1)*Hub%L)
120      write(*, '(a,31o)') ' Measurement Sweep, bin, iter, slice : ', i, j, slice
121
122      if (comp_tdm > 0) then
123          ! Compute full Green's function
124          call DQMC_Gtau_LoadA(tau, TAU_UP, slice, Hub%G_up%sgn)
125          call DQMC_Gtau_LoadA(tau, TAU_DN, slice, Hub%G_dn%sgn)
126          ! Measure equal-time properties
127          call DQMC_Hub_FullMeas(Hub, tau%nnb, tau%A_up, tau%A_dn, tau%sgnup, tau%sgndn)
128          ! Measure time-dependent properties
129          !call DQMC_TDM1_Meas(tm, tau)
130          ! Modified DQMC_TDM1_Meas: Only measure g(tau)!
131          call DFPT_Meas_Ref_G(tm, tau)
132      else if (comp_tdm == 0) then
133          call DQMC_Hub_Meas(Hub, slice)
134      endif

```

The only difference is that **DFPT\_Meas\_Ref\_G** computes the Green's function only, while **DQMC\_TDM1\_Meas** also (unnecessarily) measures all other time dependent properties. An additional call to **DFPT\_Print\_Ref\_G** saves the Green's function (Spin-Up, Spin-Down and the average) in the format used afterwards into the files **GF\_up\_ref.txt**, **GF\_dn\_ref.txt** and **GF\_av\_ref.txt**. For the purpose of sanity checking between the first and second run, a few simulation parameters are also saved in **ref\_params.txt**. Aside from this, the program is only a faster version of **ggeom** and has exactly the same usage (we refer here to the original documentation), and the standard outputs are also kept for debugging purposes.

### 7.2.3. Second Run - Perturbation Theory

After an initial `build_ref`-run with the desired parameters, the `dfpt_mpi`-program reads in the generated reference Green's functions and perturbation and does a second QMC run with the aim of obtaining the ( $\mathbf{k}$ - and frequency-dependent) first-order dual self-energy  $\tilde{\Sigma}^{(1)}(\mathbf{k}, i\omega_n)$ .

The perturbation  $(\mu, t')$  can be set in the file `pert_params.txt` which, together with the reference Green's functions, should be in the folder where the program is run:

```

1 -0.2
2 -1.0
3
4 # tp
5 # mu

```

Figure 7.2.1: Input file `pert_params.txt` for the `dfpt_mpi`-program.

We will first discuss the following part in the initialization block:

```

171 ! Build Matrix for FT from (R,R') to (k,k')
172 call build_FT_matrix(F1,F2,r_vecs,k_vecs,N)
173
174 ! Initialize Reference G and Read from Files
175 num_d = tm%properties(1)%nclass
176 allocate(ref_GF_d_tau(num_d, 0:L-1, 3))
177 call DFPT_Read_Ref_G(tm, ref_GF_d_tau)
178
179 ! Extend Reference G from (D,tau)- to full spatial (i,j,tau)-dependence
180 allocate(ref_GF_ij_tau(N,N,0:L-1,3))
181 call DFPT_Extend_Ref_G_ij(ref_GF_d_tau,ref_GF_ij_tau,tm)
182
183 ! Extend to full (tau,tau')-dependence (used for the subtraction)
184 allocate(ref_GF_full(N*L,N*L))
185 call DFPT_Extend_Ref_G_ttp(ref_GF_ij_tau,tm,ref_GF_full)
186
187 ! Initialize the array for measured GFs (and g_tilde) in the same shape
188 allocate(GF_up_full(N*L,N*L))
189 allocate(GF_dn_full(N*L,N*L))
190 GF_up_full = ZERO
191 GF_dn_full = ZERO
192
193 ! Get indexing for "minus" k
194 allocate(mk(N*L))
195 call DFPT_minusk(mk, N, L)
196
197 ! FT from (i,j,tau) -> (k,k',tau) for Reference GF
198 allocate(ref_GF_kkp_tau(N,N,0:L-1,3))
199 call GF_R_to_K(ref_GF_ij_tau,ref_GF_kkp_tau,F1,F2,L)
200

```

Figure 7.2.2: Initialization block in `dfpt_mpi.F90`.

`DFPT_Read_Ref_G` reads in the reference Green's functions  $g_d(\tau)$ , which are saved depending on distinct distances  $d = |\mathbf{R}_i - \mathbf{R}_j|$ . For example, on a periodic 4x4 lattice, only six distinct  $d$  exist. Using the translational invariance of  $g$ , the full  $g_{ij}(\tau)$  is obtained through `DFPT_Extend_Ref_G_ij`, which makes use of the fact

that QUEST already has a matrix  $d(i, j)$  which gives the correct index for each pair of lattice sites:

```

871  ! Number of sites and time slices
872  L = T1%L
873  N = T1%properties(1)%n
874
875  do it = 0, L-1
876      do ii = 1, N
877          do jj = 1, N
878              D = T1%properties(1)%D(ii,jj)
879              ref_GF_ij(ii,jj,it,1) = ref_GF(D,it,1)
880              ref_GF_ij(ii,jj,it,2) = ref_GF(D,it,2)
881              ref_GF_ij(ii,jj,it,3) = ref_GF(D,it,3)
882          end do
883      end do
884  end do

```

Figure 7.2.3: Snippet from the subroutine `DFPT_Extend_Ref_G_ij` in `dfpt_tools.f90`.

Afterwards, with the subroutine `DFPT_Extend_Ref_G.ttp`, the fermionic symmetry in the imaginary time is used to obtain the full  $g_{ij}(l, l')$  from  $g_{ij}(\tau)$ , where  $(l, l')$  are time slices within the discretization of the DQMC algorithm. With  $N$  lattice sites and  $L$  time slices,  $g_{ij}(l, l')$  is saved as a two-dimensional array with the dimension  $(N \times L, N \times L)$  where the two indices  $(i, l)$  correspond to one combined index  $i + l \cdot N$ :



## 7 OVERCOMING THE FERMIONIC QMC SIGN PROBLEM THROUGH DUAL FERMION PERTURBATION THEORY

---

```

992 N = tm%properties(1)%n
993 L = tm%L
994 V = N*L
995 allocate(gtmp(-L+1:L-1))
996
997 do i1 = 1, N
998   do i2 = 1, N
999     do iL = 0, L-1
1000      ! For now, take the spin-averaged Reference GF (last index = 1)
1001      gtmp(iL) = ref_GF_ij(i1,i2,iL,1)
1002     end do
1003     ! Reflect G (due to symmetry) for negative arguments
1004     do iL = 1, L-1
1005      gtmp(-iL) = - gtmp(L-iL)
1006     end do
1007
1008     ! Put into correct slot of the big array
1009     do iL1 = 0, L-1
1010      jks = i1 + iL1 * N
1011      do iL2 = 0, L-1
1012       iks = i2 + iL2 * N
1013       ref_GF_full(iks,jks) = - gtmp(iL2 - iL1)
1014      end do
1015     end do
1016   end do
1017 end do
1018
1019 end do
1020
1021

```

Figure 7.2.4: Snippet from the subroutine **DFPT\_Extend\_Ref\_G\_ttp** in **dfpt\_tools.f90**.

For later use, the program also obtains  $g_{\mathbf{k}\mathbf{k}'}(\tau)$  through spatial Fourier transform in **GF\_R\_to\_K**. With these ingredients collected, and after reading in the perturbation parameters, the next important step is to build the bare dual Green's function  $\tilde{G}^0$  in  $k = (\mathbf{k}, i\omega_n)$ -space. In order to avoid divisions by very small numbers or zero, we rewrite Eq.(4.2.20):

$$\tilde{G}_k^0 = (\tilde{t}_k^{-1} - g_k)^{-1} = \tilde{t}_k (1 - \tilde{t}_k g_k)^{-1}$$

In  $(\mathbf{k}, i\omega_n)$ -space in a periodic system, the perturbation matrix  $\tilde{t}_k$  (assuming hoppings and shifts in the chemical potential as the perturbation) can be expressed generally as the difference in perturbed and unperturbed dispersions ( $\varepsilon_{\mathbf{k}}^0$  and  $\varepsilon_{\mathbf{k}}^1$ , respectively). Eq.(4.2.6) then reads as:

$$\tilde{t}_{\mathbf{k}} = \mathcal{G}_0^{-1}(\mathbf{k}, i\omega_n) - \mathcal{G}_1^{-1}(\mathbf{k}, i\omega_n) = (i\omega_n - \varepsilon_{\mathbf{k}0}) - (i\omega_n - \varepsilon_{\mathbf{k}}^1) = \varepsilon_{\mathbf{k}}^1 - \varepsilon_{\mathbf{k}}^0 \quad (7.2.1)$$

For the periodic square lattice, with  $(t', \mu)$  as the perturbation, we use the dispersion evaluated in Eq.(2.4.10)) and obtain:

$$\tilde{t}_{\mathbf{k}} = -\mu - 4t' \cos(k_x) \cos(k_y)$$

With these considerations in mind,  $\tilde{G}_{\mathbf{k}}^0(i\omega_n)$  is built by calling the **DFPT\_build\_dual\_G0**-subroutine:

```

921 ! Change Sign of reference GF (due to QMC notation) and transform to Matsubara Freq's
922 write(*,'(A20)') 'G_k_ref(iom)'
923 do kk = 1, N
924 ! For now: Spin-Average of ref. GF (last index 1) (assume spin-symmetry)
925 ref_GF_av(:) = ref_GF_kkp_tau(kk, kk, :, 1)
926 ! Change notation here so that: ctaudata(1) = - G_ref(tau=0)
927 do ll = 0, L-1
928 ctaudata(ll+1) = - ref_GF_av(ll)
929 end do
930 ! Matsubara
931 call nfourier(ctaudata, comdata, 0, L, Nom, dtau)
932
933 !write(*,'(3X,A3,3X,A1,6X,A4)') 'iom', 'k', 'gkw0'
934 do iom = 0, Nom
935 gkw0(kk, iom) = comdata(iom)
936 !write(*,'(2I5,2F15.10)') iom, kk, gkw0(kk, iom)
937 end do
938
939 end do
940

```

Figure 7.2.5: Snippet 1 from the subroutine `DFPT_build_dual_G0` in `dfpt_tools.f90`: Transformation of  $g_{\mathbf{k}}(\tau)$  to  $g_{\mathbf{k}}(i\omega_n)$ .

```

941 ! Now: Calculate Dual G0 in (k, iω)-space
942 !write(*,'(A20)') 'G_k_dual(iom)'
943 do kk = 1, N
944 ! Perturbation (μ and t'-dispersion)
945 tdk(kk) = - mu - 4.0_wp * tp * cos(k_vecs(kk,1)) * cos(k_vecs(kk,2))
946 do iom = 0, Nom
947 Gkwdf(kk, iom) = tdk(kk) / ( ONE - gkw0(kk, iom) * tdk(kk) )
948 !write(*,'(2I5,2F15.10)') iom, kk, Gkwdf(kk, iom)
949 end do
950 !write(*,'(2I5,2F15.10)')
951 end do
952
953 dual_g0(:, :) = Gkwdf(:, :)
954
955 !
956 ! Put the dual G0 into the format G(volume) that is used later
957 !
958 do kk = 1, N
959 ! Positive Frequencies
960 do ll = 0, L/2 - 1
961 idx = kk + ll * N
962 dual_g0_full(idx) = dual_g0(kk, ll)
963 end do
964
965 ! Negative Frequencies
966 do ll = L/2, L-1
967 idx = kk + ll * N
968 dual_g0_full(idx) = conjg(dual_g0(kk, L-1-ll ))
969 end do
970 end do
971

```

Figure 7.2.6: Snippet 2 from the subroutine `DFPT_build_dual_G0` in `dfpt_tools.f90`: Building the bare dual Green's function  $\tilde{G}_{\mathbf{k}}^0(i\omega_n)$  for a periodic square lattice.

## 7 OVERCOMING THE FERMIONIC QMC SIGN PROBLEM THROUGH DUAL FERMION PERTURBATION THEORY

First, the subroutine obtains  $g_{\mathbf{k}}(i\omega_n)$  through the `nfourier`-function, which uses a natural spline interpolation and an analytical expression of the integral in Eq.(2.3.6) to get the transformation  $\tau \rightarrow i\omega_n$ . Afterwards,  $\tilde{G}_{\mathbf{k}}^0(i\omega_n)$  is built with the same  $(N \times L)$ -indexing as the reference Green's function.

Now, the loops with the Monte Carlo sweeps start as usual, with the difference that instead of either `DQMC_TDM1_Meas` or `DFPT_Meas_Ref_G`, another subroutine names `DFPT_Meas_Dual_Sigma` is called:

```

267      ! Fetch a random slice for (equal time)-measurement
268      call ran0(i, randn, Hub%seed)
269      slice = ceiling(randn(1)*Hub%L)
270      ! Output of Master
271      if (mpi_rank .eq. master) then
272          write(*, '(A,3I6)') ' Measurement Sweep, bin, iter, slice : ', ii, jj, slice
273      end if
274
275      if (comp_tdm > 0) then
276          !
277          ! Compute A-Matrix, which contains full GF for specific (l,l').
278          !
279          ! Note: - Contains all (l,l') if nOrth = 1!
280          !
281          call DQMC_Gtau_LoadA(tau, TAU_UP, slice, Hub%G_up%sgn)
282          call DQMC_Gtau_LoadA(tau, TAU_DN, slice, Hub%G_dn%sgn)
283          ! Measure equal-time properties
284          call DQMC_Hub_FullMeas(Hub, tau%nnb, tau%A_up, tau%A_dn, tau%sgnup, tau%sgndn)
285          !
286          ! =====
287          ! Newest version
288          ! =====
289          !
290          ! From loaded A-Matrix: Measure full G(l,j,t,t') from current HS-Config; subtract
291          ! G_ref to obtain G_tilde, perform 6D-FFT and evaluate the dual Self-Energy contribution
292          !
293          call DFPT_Meas_Dual_Sigma(tn, tau, mk, ref_GF_full, dual_G0_full, GF_up_full, GF_dn_full, Sdual)
294          !
295      else if (comp_tdm == 0) then
296          write(*,*) 'TDM parameter is zero! Stopping program...'
297          stop
298      endif
299
300      !Write fields
301      !if (nhist > 0) call DQMC_Hub_Output_HSF(Hub, .false., slice, HSF_output_file_unit)
302  end do

```

Figure 7.2.7: Inside the Monte Carlo loop in `dfpt_mpi.f90`.

As the name suggests, `DFPT_Meas_Dual_Sigma` obtains the dual self-energy  $\tilde{\Sigma}(\mathbf{k}, i\omega_n)$  for each measurement step in the loop. For now, the subroutine works only for the input parameter `nOrth = 1`, which means that in each measurement step, the full  $g_{ij}(l, l')$  is obtained from scratch.  $\tilde{g}_{ij}(l, l')$  is then obtained by subtracting the reference  $g$ . The double loop over time indices then looks like:

```

422      !
423      ! Loop over both time-indices
424      !
425      do i0 = 1, L
426          do idt = 0, L-1
427
428              it = mod(i0+idt-1,L) + 1
429              tau0 = (i0 - 1) * dtau
430              tau1 = (it - 1) * dtau
431              zf = exp( Xi * (tau0+tau1) * ONEPI / Beta ) * dtau * dtau
432
433              ! Get the Green's functions for (it,i0) from full A-matrix
434              call DQMC_Gtau_DumpA(tau, TAU_UP, it, i0)
435              ! (if necessary, for Spin-Dn as well)
436              if (tau%comp_dn .or. .not.tau%neg_u) &
437                  call DQMC_Gtau_DumpA(tau, TAU_DN, it, i0)
438              !
439              ! Check whether tau or tau' is bigger, and put sign accordingly
440              !
441              ! Note: Important! The measured GF's (e.g. upt0) are defined in QMC
442              ! notation (with a "+"-sign), while the reference GF already has
443              ! the correct sign. Hence, the addition in the brackets and the
444              ! "-"-sign before
445              !
446
447              ! Loops over lattice sites
448              do i1 = 1, N
449                  iks = i1 + (it - 1) * N
450                  do i2 = 1, N
451                      jks = i2 + (i0 - 1) * N
452                      ! Measure current HS-QMC-g and subtract reference g
453                      GF_up_full(iks,jks) = - zf * ( upt0(i1,i2) + ref_GF_full(iks,jks) )
454                      GF_dn_full(iks,jks) = - zf * ( dnt0(i1,i2) + ref_GF_full(iks,jks) )
455                  end do
456              end do
457              !
458          end do
459      end do
460  end do
461
462      ! Now: Call the subroutine to get 6D-FFT of G-Tilde!
463      call FFT6D(T1, tau, V, GF_up_full, GF_dn_full)

```

Figure 7.2.8: Snippet 1 from the subroutine **DFPT\_Meas\_Dual\_Sigma** in **dfpt\_tools.f90**: Measurement of  $\tilde{g}_{ij}(l, l')$  and Fourier transform.

## 7 OVERCOMING THE FERMIONIC QMC SIGN PROBLEM THROUGH DUAL FERMION PERTURBATION THEORY

We already add the prefactor  $\mathbf{z}\mathbf{f} = \exp[i(\tau_0 + \tau_1)\pi/\beta](\Delta\tau)^2$  here to ensure correct normalization. **FFT6D** performs the Fourier transform from  $\tilde{g}_{ij}(l, l')$  to  $\tilde{g}_{\mathbf{k}\mathbf{k}'}(i\omega_n, i\omega'_n)$  which, for a two-dimensional lattice, is a six-dimensional transformation. The FFTW library offers a general, multidimensional complex Fourier transform, which we access in the following way:

```

501  subroutine FFT6D(T1, tau, V, GF_up_full, GF_dn_full)
502  !
503  ! Purpose
504  ! =====
505  !
506  ! 6D complex FFT from FFTW-3 version
507  !
508  use, intrinsic :: iso_c_binding
509  implicit none
510
511  include 'fftw3.f03'
512
513  type(C_PTR) :: plan
514  !
515  type(TDM1), intent(in)  :: T1
516  type(Gtau), intent(in)  :: tau
517  !
518  integer :: N, L, V, Nx
519  integer :: NN(6), Ndim
520  complex(wp) :: GF_up_full(V,V), GF_dn_full(V,V)
521
522
523  L = tau%L
524  N = T1%properties(1)%n
525  Nx = NINT( sqrt(real(N)) )
526
527
528  Ndim = 6
529  NN(1) = Nx
530  NN(2) = Nx
531  NN(3) = L
532  NN(4) = Nx
533  NN(5) = Nx
534  NN(6) = L
535
536  ! FFTW interface old-style Fortran:
537  call dfftw_plan_dft(plan, ndim, nn, GF_up_full, GF_up_full, 'FFTW_FORWARD', 'FFTW_ESTIMATE')
538  call dfftw_execute_dft(plan, GF_up_full, GF_up_full)
539  call dfftw_execute_dft(plan, GF_dn_full, GF_dn_full)
540  call dfftw_destroy_plan(plan)
541
542
543  end subroutine FFT6D
544

```

Figure 7.2.9: Subroutine **FFT6D** in `dfpt.tools.f90`: Interface to the FFTW-library.

Once  $\tilde{g}_{\mathbf{k}\mathbf{k}'}(i\omega_n, i\omega'_n)$  is available, we can evaluate the first-order dual self-energy according to Eq.(4.2.23) (again, with the combined index  $k = (\mathbf{k}, i\omega_n)$ ):

$$\tilde{\Sigma}_k^{\uparrow(1)} = \frac{(-1)}{N_{\text{MC}}(\beta N)^2} \sum_{\{s\}} \sum_{k'} \left[ \tilde{g}_{kk}^{\uparrow} \tilde{g}_{k'k'}^{\uparrow} + \tilde{g}_{kk}^{\uparrow} \tilde{g}_{k'k'}^{\downarrow} - \tilde{g}_{kk'}^{\uparrow} \tilde{g}_{k'k}^{\uparrow} \right] \tilde{G}_k^0$$

For the paramagnetic case, the evaluation can be simplified by evaluating the Hartree- and Fock-part separately. We define  $H$  (= const.) and  $F_k$  ( $k$ -dependent) as:

$$H = \sum_{k'} \left( \tilde{g}_{k'k'}^{\uparrow} + \tilde{g}_{k'k'}^{\downarrow} \right) \tilde{G}_{k'}^0 \quad (7.2.2)$$

$$F_k = \sum_{k'} \left( \tilde{g}_{kk'}^{\uparrow} \tilde{g}_{k'k}^{\uparrow} + \tilde{g}_{kk'}^{\downarrow} \tilde{g}_{k'k}^{\downarrow} \right) \tilde{G}_{k'}^0 \quad (7.2.3)$$

Then, the spin-averaged self-energy reads as:

$$\tilde{\Sigma}_k^{(1)} = -\frac{1}{2N_{\text{MC}}(\beta N)^2} \sum_{\{s\}} \left[ (\tilde{g}_{kk}^\uparrow + \tilde{g}_{kk}^\downarrow) \cdot H - F_k \right] \quad (7.2.4)$$

In the code, this corresponds to:

```

465 ! Get dual self-energy, for now: up to first order
466 Hc = dcmplx(0.d0,0.d0)
467
468 do k1 = 1, V
469   km1 = mk(k1)
470   Sk = dcmplx(0.d0,0.d0)
471   Hc = Hc + ( GF_up_full(k1,km1) + GF_dn_full(k1,km1) ) * dual_g0_full(k1)
472   !
473   do k2 = 1, V
474     km2 = mk(k2)
475     Sk = Sk + ( GF_up_full(k1,km2) * GF_up_full(k2,km1) &
476               & + GF_dn_full(k1,km2) * GF_dn_full(k2,km1) ) * dual_g0_full(k2)
477   end do
478   Eq(k1) = Sk
479 end do
480
481 ! Final evaluation of first-order correction
482 do k1 = 1, V
483   km1 = mk(k1)
484   Sd = ( GF_up_full(k1,km1) + GF_dn_full(k1,km1) ) * Hc - Eq(k1)
485   ! Normalization: Factor 2 due to Spin-Average
486   Sdual(k1) = Sdual(k1) - Sd * sgnup*sgndn / 2.0_wp / (beta * N)**2
487 end do
488

```

Figure 7.2.10: Snippet 2 from the subroutine **DFPT\_Meas\_Dual\_Sigma** in **dfpt\_tools.f90**: Evaluation of  $\tilde{\Sigma}_k^{(1)}$

After finishing the Monte Carlo loop, the result is normalized by the number of measurement sweeps and MPI processes used. The first MPI rank then calls **DFPT\_Get\_Lattice\_G** to obtain the actual lattice Green's function from the dual self-energy, and saves it for all **k**-points via the subroutine **DFPT\_Write\_Lattice\_G**:

```

339 if (mpi_rank .eq. master) then
340   ! Normalize by Number of Measurements and MPI-Ranks
341   Sdual(:) = SdualMPI(:) / nMeas / mpi_size
342   ! Get Lattice Green's function
343   allocate(lattG(N*L))
344   lattG = ZERO
345   call DFPT_Get_Lattice_G(tp,mu,N,L,k_vecs,ref_GF_kkp_tau,Sdual,Nom,tm%dtau,lattG)
346   ! Write to File
347   call DFPT_Write_Lattice_G(N,L,lattG)
348 end if

```

Figure 7.2.11: After the Monte Carlo loop in **dfpt\_mpi.f90**: Obtain the lattice Green's function and save the results.

Inside **DFPT\_Get\_Lattice\_G**, we can see how Eq.(4.2.24) translates into the code:

## 7 OVERCOMING THE FERMIONIC QMC SIGN PROBLEM THROUGH DUAL FERMION PERTURBATION THEORY

---

```

1054  !
1055  ! Put Gref(kk,iw) into the same shape as Sdual, i.e. G(N*L), and get
1056  ! the lattice GF
1057  !
1058  do kk = 1, N
1059    ! Perturbation
1060    tdk(kk) = - mu - 4.0_wp * tp * cos(k_vecs(kk,1)) * cos(k_vecs(kk,2))
1061    ! Positive Frequencies
1062    do ll = 0, L/2 - 1
1063      idx = kk + ll * N
1064      greftmp(idx) = gkw0(kk,ll)
1065      !
1066      lattG(idx) = ( ( greftmp(idx) + Sdual(idx) )**(-1.0_wp) - tdk(kk) )**(-1.0_wp)
1067    end do
1068
1069    ! Negative Frequencies
1070    do ll = L/2, L-1
1071      idx = kk + ll * N
1072      greftmp(idx) = conjg(gkw0(kk, L-1-ll ))
1073      lattG(idx) = ( ( greftmp(idx) + Sdual(idx) )**(-1.0_wp) - tdk(kk) )**(-1.0_wp)
1074    end do
1075  end do
1076

```

Figure 7.2.12: Snippet from `DFPT_Get_Lattice_G` in `dfpt_tools.f90`: Evaluation of  $G_k$  from the reference Green's function and  $\tilde{\Sigma}_k^{(1)}$ .

### 7.2.4. Parallelization

The `dfpt_mpi`-program is compiled by the MPI-compiler defined in the top Makefile, and can thus be run through the `mpirun`-command. Since we are only interested in taking as many independent measurements as possible, the parallelization becomes trivial, and the independent MPI ranks do not need complicated communication.

After the variable declarations in `dfpt_mpi.f90`, the MPI initialization block follows:

```

68
69 ! =====
70 !
71 ! Get in contact with MPI
72 !
73 call MPI_INIT(ierr)
74 if (ierr .ne. MPI_SUCCESS) then
75     write(*,*) 'MPI_INIT returned an error. Terminating.'
76     call MPI_ABORT(MPI_COMM_WORLD, rc, ierr)
77 end if
78 !
79 call MPI_COMM_RANK(MPI_COMM_WORLD, mpi_rank, ierr)
80 call MPI_COMM_SIZE(MPI_COMM_WORLD, mpi_size, ierr)
81 master = 0
82
83 ! =====
84

```

Figure 7.2.13: MPI Initialization block in `dfpt_mpi.f90`.

After the basic initializations, we give a new seed for random number generation to each process:

```

222 ! =====
223 !
224 ! New Seed for each MPI process!
225 ! (In the most trivial way for now, change later)
226 !
227 call MPI_BARRIER(MPI_COMM_WORLD, ierr)
228 Hub%seed = Hub%seed + mpi_rank
229 Hub%idum = Hub%idum + mpi_rank
230 write(*,*) "Seed for ran1: ", Hub%seed, ", From Rank: ", mpi_rank
231 write(*,*) "Seed for ran2: ", Hub%idum, ", From Rank: ", mpi_rank
232 !
233 ! =====
234

```

Figure 7.2.14: New seeds for each MPI rank, in `dfpt_mpi.f90`.

Once all MPI ranks independently finished their Monte Carlo loop, the measured dual self-energies are collected into one rank:



## 7 OVERCOMING THE FERMIONIC QMC SIGN PROBLEM THROUGH DUAL FERMION PERTURBATION THEORY

---

```
321 ! =====
322 !
323 ! MPI: Collect and reduce everything to master process
324 !
325 write(*,*) "Sweeps over! From Rank: ", mpi_rank
326 call MPI_BARRIER(MPI_COMM_WORLD,ierr)
327
328 call MPI_REDUCE(Sdual, SdualMPI, N*L ,MPI_DOUBLE_COMPLEX, &
329               & MPI_SUM, master, MPI_COMM_WORLD, ierr)
330
331 if (ierr .ne. MPI_SUCCESS) then
332   write(*,*) 'MPI_REDUCE returned an error.'
333 end if
334
335 call MPI_BARRIER(MPI_COMM_WORLD,ierr)
336
337 ! =====
338
```

Figure 7.2.15: Collecting  $\tilde{\Sigma}_k^{(1)}$  in one rank, in `dfpt_mpi.f90`.

The master rank obtains and saves the lattice Green's function, and a simple call to `MPI_FINALIZE` ends the program.

### 7.2.5. Examples

Here, some first results obtained from our code are shown. On a periodic 4x4-lattice, there are only six distinct  $\mathbf{k}$ -points for which we show how the first-order approximation behaves. For all line-plots, the reference system (**build\_ref**-program) was built with 10000 warm-up and 100000 measurement sweeps, while the second run with **dfpt\_mpi** was done with 10000 warm-up and 250 measurement sweeps with 4 MPI ranks, i.e. 1000 measurement sweeps after warm-up.

For Figs.(7.2.16,7.2.17),  $U/t = 5.56$  was chosen in order to be able to compare to [74]. In Fig.(7.2.16), where the perturbation is only in  $\mu$ , the average sign of a direct simulation is still on the scale of  $\approx 0.5$ , so exact data can still be obtained easily for a 4x4 lattice. The comparison shows that, despite only doing a first-order approximation of the dual self-energy, the change in the Green's function is captured very well. Fig.(7.2.17) shows a small  $t'$ -perturbation. What both have in common is that the imaginary parts of the Green's function are pushed down at the  $\Gamma$ -point  $\mathbf{k} = (0,0)$  and the point  $\mathbf{k} = (\pi/2,0)$  which is closest to it, while the functions at the  $M$ -point  $\mathbf{k} = (\pi,\pi)$  and  $\mathbf{k} = (\pi,\pi/2)$  increase through the perturbation. For  $\mathbf{k} = (\pi/2,\pi/2)$  and  $\mathbf{k} = (\pi,0)$ , the imaginary part is, aside from the low-frequency region, barely affected. For the real part, the opposite is true: At the  $X$ -point  $\mathbf{k} = (\pi,0)$  and  $\mathbf{k} = (\pi/2,\pi/2)$ , the change is the largest, as they obtain a  $i\omega_n$ -dependence only through the perturbation.

With Figs.(7.2.18,7.2.19), we provide two more, similar plots for  $U = 5.6$ , two temperatures  $\beta t = 5, 10$  and a perturbation both in  $(\mu, t')$  [98]. The effects of the perturbation are very similar to the previously discussed plots, although the  $\beta t = 10$ -case which has twice the number of time-slices gives a better resolution. Additionally, our results show that there is a strong temperature-dependence for the two  $\mathbf{k}$ -points close to the Fermi-surface, i.e.  $\mathbf{k} = (\pi,0)$  and  $(\pi/2,\pi/2)$ .

Fig.(7.2.20) shows, for a 16x16 periodic square lattice, a result for the spectral function at the first Matsubara frequency. One can see the formation of a pseudo-gap at  $\mathbf{k} = (\pi,0)$  and the so-called Fermi-arcs at  $\mathbf{k} = (\pi/2,\pi/2)$  which are a generic feature of the electronic structure in doped cuprates [99]. Direct QMC approaches are not possible with these parameters due to the severity of the sign problem. After improving our implementation further, the aim is to study even larger doped systems.

## 7 OVERCOMING THE FERMIONIC QMC SIGN PROBLEM THROUGH DUAL FERMION PERTURBATION THEORY

---

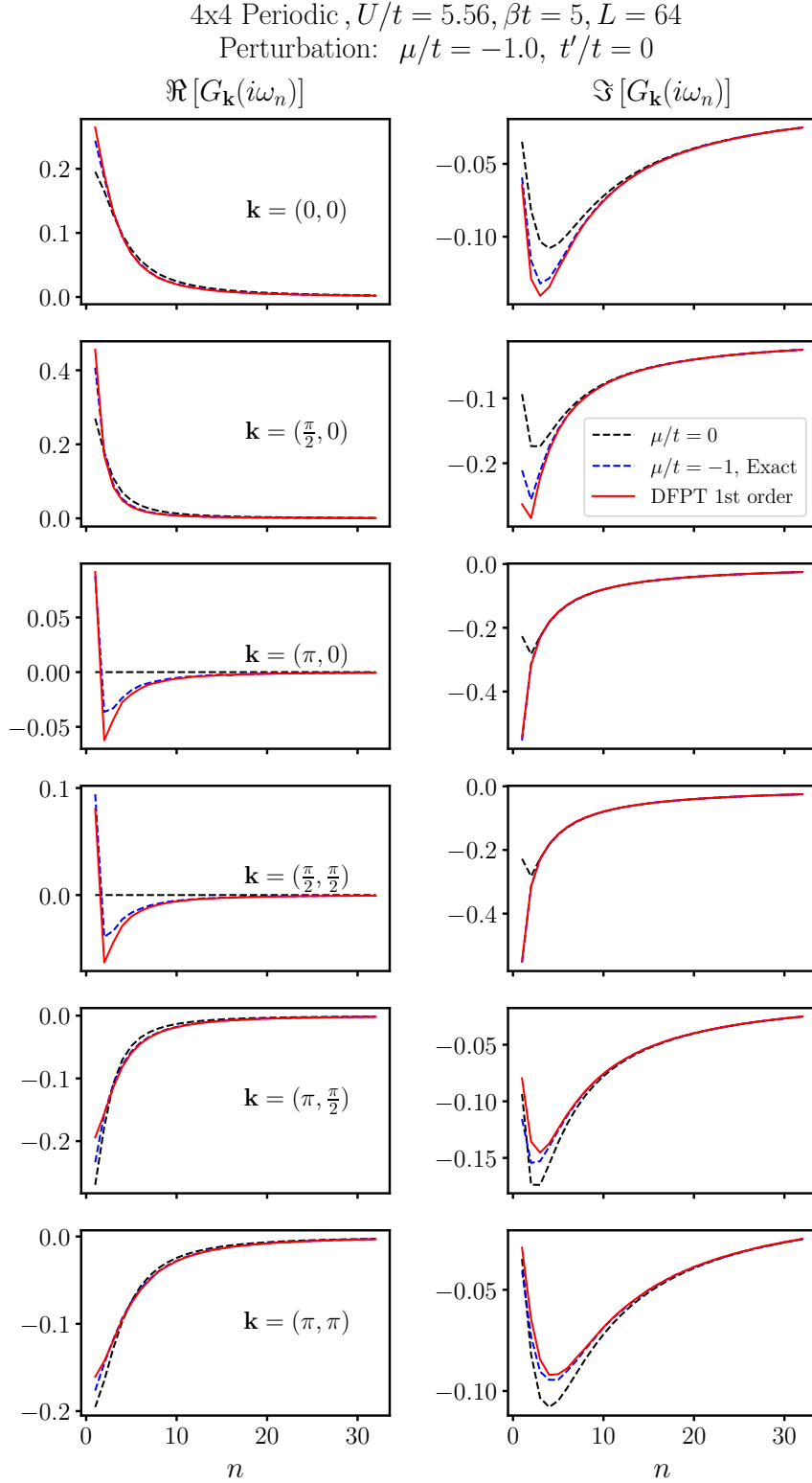


Figure 7.2.16: Green's functions  $G_{\mathbf{k}}(i\omega_n)$  for a periodic 4x4 lattice. The perturbation is  $\mu/t = -1$ , which corresponds to  $\approx 5$  percent hole doping.

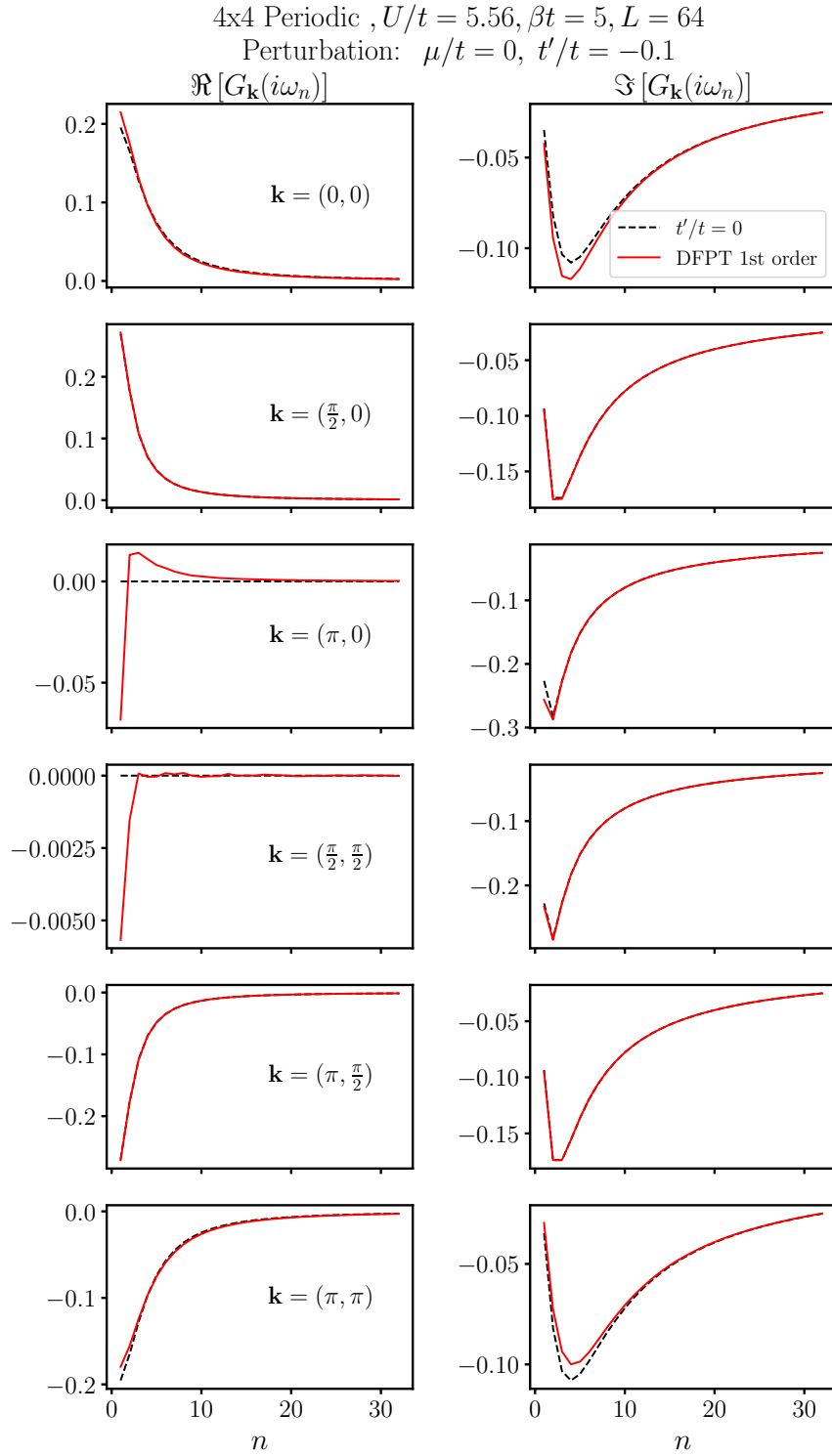


Figure 7.2.17: Green's functions  $G_{\mathbf{k}}(i\omega_n)$  for a periodic 4x4 lattice. The perturbation is  $t'/t = -0.1$ .

7 OVERCOMING THE FERMIONIC QMC SIGN PROBLEM THROUGH  
DUAL FERMION PERTURBATION THEORY

---

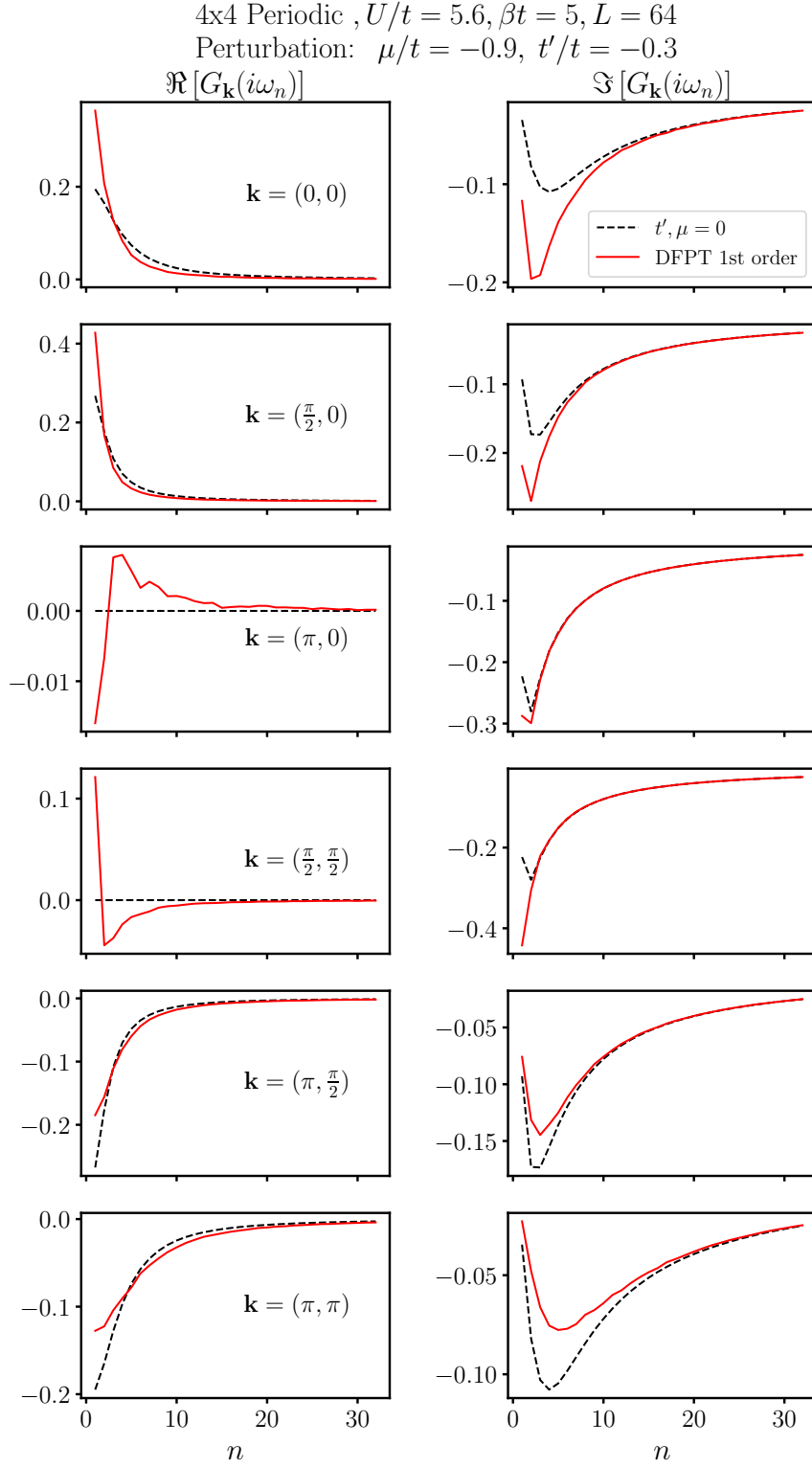


Figure 7.2.18: Green's functions  $G_{\mathbf{k}}(i\omega_n)$  for a periodic 4x4 lattice, at  $\beta t = 5$ . The perturbation is  $(\mu/t = -0.9, t'/t = -0.3)$ .

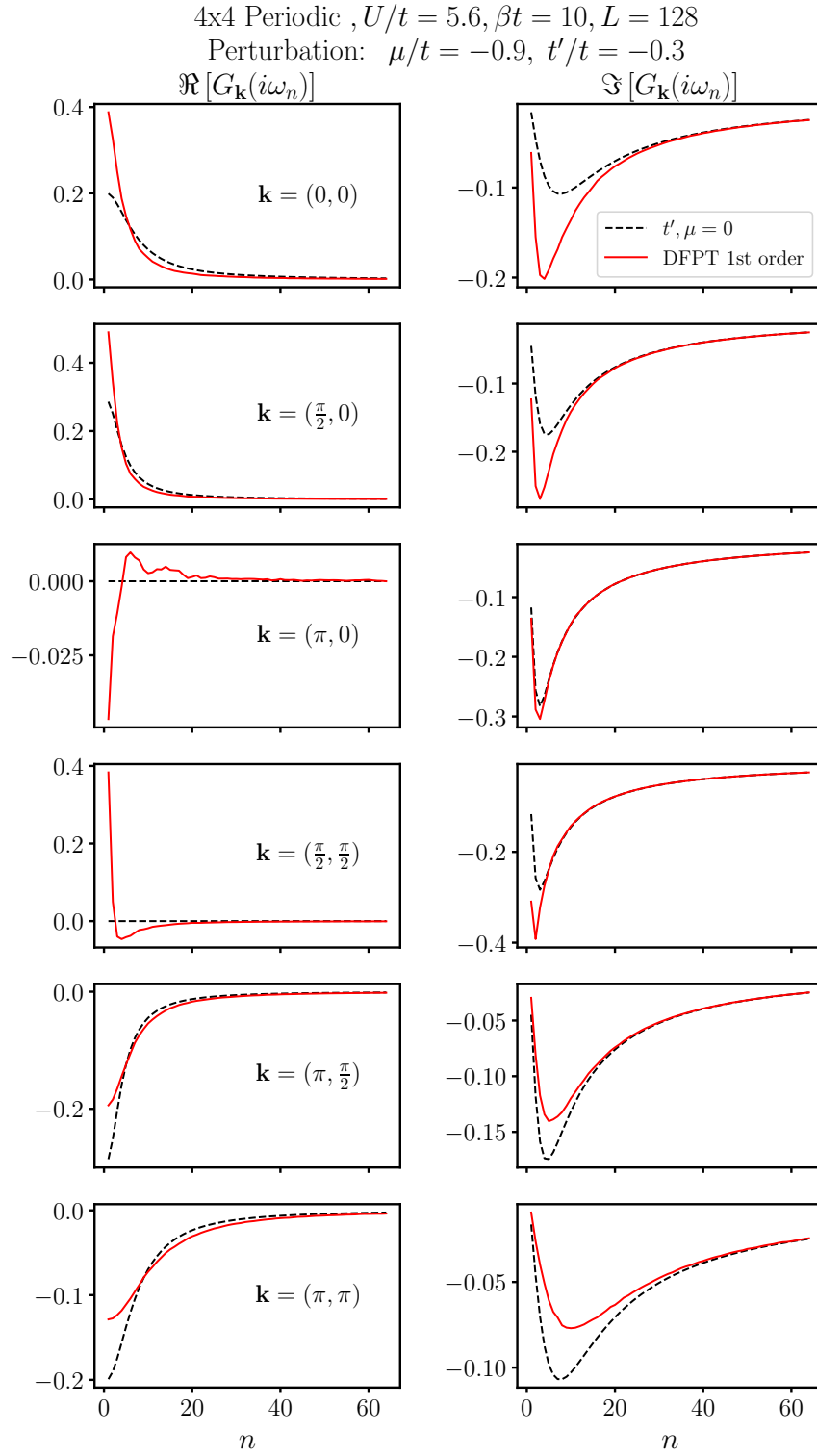


Figure 7.2.19: Green's functions  $G_{\mathbf{k}}(i\omega_n)$  for a periodic 4x4 lattice, at  $\beta t = 10$ . The perturbation is  $(\mu/t = -0.9, t'/t = -0.3)$ .

16x16 Periodic,  $U/t = 5.6$ ,  $\beta t = 5$ ,  $L = 64$

$$\mu/t = -1.45, \quad t'/t = -0.3$$

$$A_{\mathbf{k}}(i\omega_0) = -\frac{1}{\pi} \Im [G_{\mathbf{k}}(i\omega_0)]$$

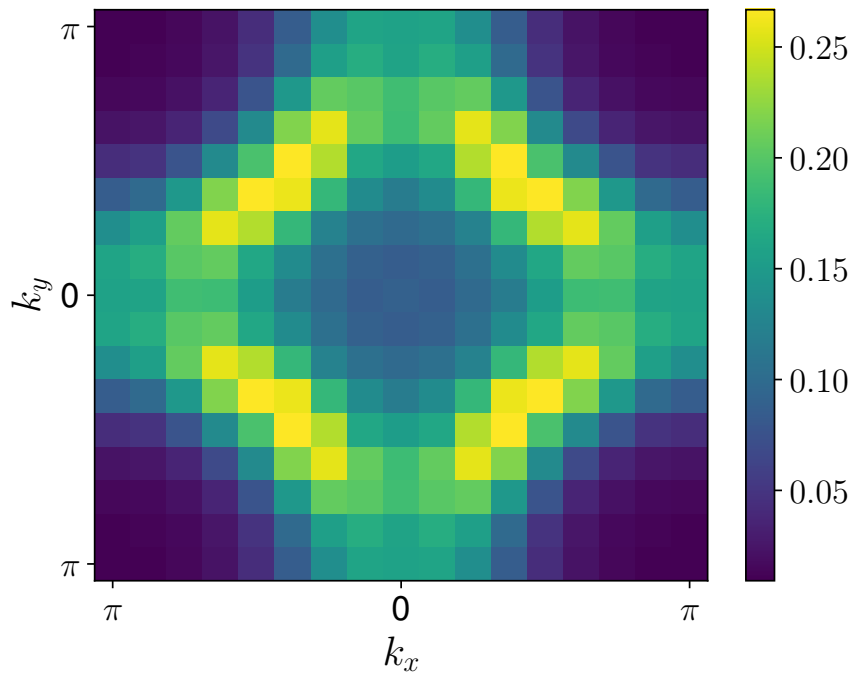


Figure 7.2.20: Imaginary part of the Green's function on the first Matsubara frequency in a doped 16x16 Hubbard model at  $\approx 15\%$  hole doping.

### 7.3. Open Problems

While the program in its current stage is already sufficient to obtain data on a square lattice, there is a large room for improvement and further implementations.

For example, as shown in the explanations of the code, the dispersion of the square lattice has been put manually at the points where the perturbation matrix  $\tilde{t}$  has been built. In order to deal with general lattices,  $\tilde{t}$  should be built in a general fashion through QUEST-internal parameters. The subroutine **DQMC\_Gtau\_GetG0** in the **DQMC\_Gtau**-module could be used to obtain the non-interacting Green's functions with and without the perturbation, and  $\tilde{t}$  could be obtained through the definition  $\tilde{t} = \mathcal{G}_0^{-1} - G_1^{-1}$ .

Furthermore, **dfpt\_mpi** currently only works with the input parameter **nOrth** = 1, which means that after each Monte Carlo sweep, the full Green's function  $g_{ij}(l, l')$  for all pairs of time slices  $(l, l')$  is calculated from scratch. While this provides good accuracy and a working example, one could probably achieve a significant increase in speed by allowing **nOrth**  $\neq$  1. As explained earlier, this leads to the Green's function being built from scratch only for a few, specific  $(l, l')$ . In the unaltered QUEST program, one of the time slice indices is shifted through all possibilities through the subroutine **DQMC\_change\_gtau\_time** with the arguments **TPLUS** and **TMINUS**. Since the subroutine also accepts **ZPLUS** and **ZMINUS** as arguments, which shift the other time-index, one could come up with an efficient scheme to obtain the full matrix  $g_{ij}(l, l')$  only from a few, exact Green's functions.



## 8. Conclusions and Future Outlook

In this thesis, three projects have been presented. They all share the aim of improving Hubbard-type modelling of strongly correlated electron systems, which becomes increasingly more complex with the emergence of novel, two-dimensional quantum materials that require an accurate description.

In the first project, through the Peierls-Feynman-Bogoliubov variational principle, an approach has been developed which allows the description of an extended Hubbard model including nonlocal exchange interactions. The basis is a Hubbard model with an effective local interaction and a broken spin-symmetry. Merit and demerit are discussed, and it was shown that the method captures important transitions in magnetic correlation functions more accurately than standard mean-field methods. Specifically, on a square lattice, a continuous transition of the sign of nearest-neighbor spin-spin correlators is predicted, while a standard Hartree-Fock approach wrongly predicts a first-order phase transition.

The second work discusses spatial charge correlations and screening in the doped Hubbard model on a square lattice. The measurement of complicated four-particle correlators has been implemented into a Monte Carlo scheme, and it was shown how doubly-occupied and empty sites are distributed spatially. Surprisingly, the findings show that in the doped case, empty and doubly-occupied sites tend to stick together. Data from Exact Diagonalization implies that this finding holds for the strong-coupling case, although a binding of holes is the common expectation. Together with additional Dynamical Cluster calculations, the available data was also used to obtain information about the doped extended Hubbard model with nonlocal repulsion. Through the variational scheme, we find an effective, purely local Hubbard interaction, and thus discuss how the nonlocal terms effectively lead to screening of the local one. Hole-doping the system away from half-filling leads to an increase of the screening, which reduces the interaction strength. This doping-dependence should be taken into account when attempting to downfold a complex structure onto a Hubbard-type model.

The last project is a contribution towards the solution of the long-standing sign problem which prohibits Monte Carlo simulation of Hubbard-like and other models in many interesting parameter spaces, especially the areas where superconductivity is suspected. To that end, a dual-fermion method which allows for arbitrary choices of reference systems from where a perturbation is developed has been implemented through a Determinantal Quantum Monte Carlo code (QUEST). A few Green's functions which would be difficult to obtain through direct approaches are shown. While the current version of the code is restricted to periodic square lattice and a  $(t', \mu)$ -perturbation, possible ways of generalizing and optimizations are discussed.

With the new approaches presented in this thesis, the aim for the future is that, by including nonlocal interactions and circumventing the Monte Carlo sign problem, calculations which are currently not feasible become possible both for multi-band models and a wide range of geometries. This could lead to accurate descriptions of many highly complex materials.

---

## A. Acknowledgements/Danksagung

Als Erstes möchte Ich Tim Wehling und Alexander Lichtenstein danken, die mir nach einer Auszeit die Gelegenheit gaben, meine Promotion zum Abschluss zu bringen. Auch erwähnen möchte Ich Gerd Czycholl, der während meiner Zeit in Bremen stets ein offenes Ohr für mich hatte. Generell bedanke Ich mich bei der gesamten Arbeitsgruppe für die stets angenehme Atmosphäre und Unterstützung, sowohl in der aktuellen Zusammensetzung an der Universität Hamburg als auch insbesondere bei denen, mit denen Ich bereits in Bremen viel gemeinsame Zeit verbrachte.

Bezüglich meines gesamten Werdegangs bis zu diesem Punkt geht großer Dank an meine ganze Familie, insbesondere meine Eltern, Hanefija und Edita, sowie meiner Schwester Majda. Ohne eure fortwährende Unterstützung wäre Vieles nicht möglich gewesen.

Außerdem bedanke Ich mich bei allen Freunden von mir, die mich während der gesamten Zeit unterstützt haben. Besonders erwähnen möchte Ich Tristan Oltmanns und Sebastian Miksch, mit denen Ich bereits seit Studienzeiten viele Feierabende verbrachte.

Als Letztes und Wichtigstes geht mein größter Dank an Zeynep Işık, mit der Ich sowohl die alltäglichen Herausforderungen des Lebens als auch alle schönen Dinge teile. Deine durchgehende Unterstützung war ein großer Beitrag zum Abschluss dieser Arbeit.

## B. Declaration

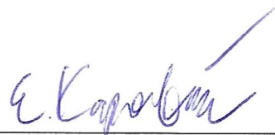
### Eidesstattliche Versicherung

Hiermit versichere ich an Eides statt, die vorliegende Dissertationsschrift selbst verfasst und keine anderen als die angegebenen Hilfsmittel und Quellen benutzt zu haben.

Sofern im Zuge der Erstellung der vorliegenden Dissertationsschrift generative Künstliche Intelligenz (gKI) basierte elektronische Hilfsmittel verwendet wurden, versichere ich, dass meine eigene Leistung im Vordergrund stand und dass eine vollständige Dokumentation aller verwendeten Hilfsmittel gemäß der Guten wissenschaftlichen Praxis vorliegt. Ich trage die Verantwortung für eventuell durch die gKI generierte fehlerhafte oder verzerrte Inhalte, fehlerhafte Referenzen, Verstöße gegen das Datenschutz- und Urheberrecht oder Plagiate.

16-09-2024

Datum



Unterschrift der Doktorandin / des Doktoranden

---

## C. Publications

### During the time as a doctorate student:

- **Nonlocal exchange interactions in strongly correlated electron systems**  
Edin Kapetanović, Malte Schüler, Gerd Czycholl, Tim O. Wehling  
*Physical Review B*, **101**, 235165, 26 June 2020
- **Charge correlation, doublon-holon binding and screening in the doped Hubbard model**  
Edin Kapetanović, Guglielmo Nicola Gigante, Malte Schüler, Tim O. Wehling, Erik van Loon  
*Preprint*: arXiv:2409.05640, URL: <https://arxiv.org/abs/2409.05640v1>, 9 Sep 2024

### Before:

- **Dephasing-controlled particle transport devices**  
Edin Kapetanović, César A. Rodríguez-Rosario, Thomas Frauenheim  
*Europhysics Letters*, **116**, 60015, 16 February 2017

## D. Conference Contributions

- **Talk:** *P3: Many-body approaches to realistic quantum impurity models and Coulomb engineering*; Christina Steinke, **Edin Kapetanović**, Niklas Witt, Bin Shao, Gerd Czycholl, Tim Wehling  
Midterm Workshop RTG QM3, Etelsen, 26th September 2018
- **Poster:** *Extended Hubbard model with nonlocal exchange - Magnetism in correlated systems*; **Edin Kapetanović**, Malte Schüler, Tim Wehling, Gerd Czycholl  
CECAM Workshop, Bremen, 4th-8th February 2019
- **Talk:** *Nonlocal Exchange Interactions in Strongly Correlated Systems*; **Edin Kapetanović**, Malte Schüler, Tim Wehling, Gerd Czycholl  
DPG-Frühjahrstagung, Regensburg, 31th March - 05th April 2019
- **Poster:** *Extended Hubbard model with nonlocal exchange - Magnetism in correlated systems*; **Edin Kapetanović**, Malte Schüler, Tim Wehling, Gerd Czycholl  
CORPES19, Oxford, 15th-19th July 2019
- **Poster:** *Extended Hubbard model with nonlocal exchange - Magnetism in correlated systems*; **Edin Kapetanović**, Malte Schüler, Tim Wehling, Gerd Czycholl  
XXVI International Summer School 'Nicolás Cabrera', Madrid, 8th-13th September 2019
- **Talk:** *P3: Many-body approaches to realistic quantum impurity models and Coulomb engineering*; **Edin Kapetanović**, Christina Steinke, Gerd Czycholl, Tim Wehling  
Midterm Workshop RTG QM3, Etelsen, 28th October 2019
- **Talk:** *P3: Many-body approaches to realistic quantum impurity models*; **Edin Kapetanović**, Niklas Witt, Erik van Loon, Tim Wehling, Gerd Czycholl  
Virtual Retreat - RTG QM3, 30th October 2020
- **Talk:** *Doping-dependent effective Hubbard interactions for cuprate superconductors*; **Edin Kapetanović**, Erik van Loon, Malte Schüler, Xinyang Dong, Emanuel Gull, Tim Wehling  
APS March Meeting (Virtual), 15th-19th March 2021
- **Poster:** *Doping-dependent effective Hubbard interactions*; **Edin Kapetanović**, Erik van Loon, Malte Schüler, Tim O. Wehling  
CUI Annual Meeting, Hohwacht (Ostsee), 11th-13th October 2023

---

## E. Bibliography

It should be noted that this bibliography applies to the text of this thesis **excluding** the attached papers in Ch.(5) and Ch.(6), which have their own respective reference lists at the end.

## References

- [1] J. Hubbard. Electron correlations in Narrow Energy Bands. *Proc. Roy. Soc. Lond. A*, 276:238–257, November 1963.
- [2] J. Hubbard. Electron Correlations in Narrow Energy Bands ii. The Degenerate Band Case. *Proc. Roy. Soc. Lond. A*, 277:237–259, January 1964.
- [3] J. Hubbard. Electron Correlations in Narrow Energy Bands iii. An Improved Solution. *Proc. Roy. Soc. Lond. A*, 281:401–419, September 1964.
- [4] Martin C. Gutzwiller. Effect of correlation on the ferromagnetism of transition metals. *Phys. Rev. Lett.*, 10:159–162, Mar 1963.
- [5] Junjiro Kanamori. Electron Correlation and Ferromagnetism of Transition Metals. *Progress of Theoretical Physics*, 30(3):275–289, 09 1963.
- [6] Masatoshi Imada, Atsushi Fujimori, and Yoshinori Tokura. Metal-insulator transitions. *Rev. Mod. Phys.*, 70:1039–1263, Oct 1998.
- [7] Elliott H. Lieb and F. Y. Wu. Absence of mott transition in an exact solution of the short-range, one-band model in one dimension. *Phys. Rev. Lett.*, 20:1445–1448, Jun 1968.
- [8] Charles L. Cleveland and Rodrigo Medina A. Obtaining a heisenberg hamiltonian from the hubbard model. *American Journal of Physics*, 44, January 1976.
- [9] Yosuke Nagaoka. Ferromagnetism in a narrow, almost half-filled  $s$  band. *Phys. Rev.*, 147:392–405, Jul 1966.
- [10] Hal Tasaki. Extension of nagaoka’s theorem on the large- $u$  hubbard model. *Phys. Rev. B*, 40:9192–9193, Nov 1989.
- [11] H.J. Schulz. Domain walls in a doped antiferromagnet. *J. Phys. France*, 50(18):2833 – 2849, Sep 1989.
- [12] Tianyi Liu, Daniel Jost, Brian Moritz, Edwin W. Huang, Rudi Hackl, and Thomas P. Devereaux. Tendencies of enhanced electronic nematicity in the hubbard model and a comparison with raman scattering on high-temperature superconductors. *Phys. Rev. B*, 103:134502, Apr 2021.

- [13] Edwin W. Huang, Christian B. Mendl, Shenxiu Liu, Steve Johnston, Hong-Chen Jiang, Brian Moritz, and Thomas P. Devereaux. Numerical evidence of fluctuating stripes in the normal state of high- $T_c$  cuprate superconductors. *Science*, 358(6367):1161–1164, 2017.
- [14] Edwin W. Huang, Ryan Sheppard, Brian Moritz, and Thomas P. Devereaux. Strange metallicity in the doped hubbard model. *Science*, 366(6468):987–990, 2019.
- [15] Jan R. Engelbrecht, Mohit Randeria, and Lizeng Zhang. Landau f function for the dilute fermi gas in two dimensions. *Phys. Rev. B*, 45:10135–10138, May 1992.
- [16] P. W. Anderson. The Resonating Valence Bond state in  $\text{La}_2\text{CuO}_4$  and superconductivity. *Science*, 235(4793):1196–1198, 1987.
- [17] V. J. Emery. Theory of high- $T_c$  superconductivity in oxides. *Phys. Rev. Lett.*, 58:2794–2797, Jun 1987.
- [18] Andrea Damascelli, Zahid Hussain, and Zhi-Xun Shen. Angle-resolved photoemission studies of the cuprate superconductors. *Rev. Mod. Phys.*, 75:473–541, Apr 2003.
- [19] Motoaki Hirayama, Takahiro Misawa, Takahiro Ohgoe, Youhei Yamaji, and Masatoshi Imada. Effective hamiltonian for cuprate superconductors derived from multiscale ab initio scheme with level renormalization. *Phys. Rev. B*, 99:245155, Jun 2019.
- [20] Mark S. Hybertsen, Michael Schlüter, and Niels E. Christensen. Calculation of coulomb-interaction parameters for  $\text{La}_2\text{CuO}_4$  using a constrained-density-functional approach. *Phys. Rev. B*, 39:9028–9041, May 1989.
- [21] F. C. Zhang and T. M. Rice. Effective hamiltonian for the superconducting cu oxides. *Phys. Rev. B*, 37:3759–3761, Mar 1988.
- [22] D. J. Scalapino and S. A. Trugman. Local antiferromagnetic correlations and dx<sup>2</sup>-y<sup>2</sup> pairing. *Philosophical Magazine B*, 74(5):607–610, 1996.
- [23] J. E. Hirsch. Discrete hubbard-stratonovich transformation for fermion lattice models. *Phys. Rev. B*, 28:4059–4061, Oct 1983.
- [24] R. Mondaini, S. Tarat, and R. T. Scalettar. Quantum critical points and the sign problem. *Science*, 375(6579):418–424, 2022.
- [25] Matthias Troyer and Uwe-Jens Wiese. Computational complexity and fundamental limitations to fermionic quantum monte carlo simulations. *Phys. Rev. Lett.*, 94:170201, May 2005.

- 
- [26] T. O. Wehling, E. Şaşıoğlu, C. Friedrich, A. I. Lichtenstein, M. I. Katsnelson, and S. Blügel. Strength of effective coulomb interactions in graphene and graphite. *Phys. Rev. Lett.*, 106:236805, Jun 2011.
- [27] Y. Zhang and J. Callaway. Extended hubbard model in two dimensions. *Phys. Rev. B*, 39:9397–9404, May 1989.
- [28] Hanna Terletska, Tianran Chen, and Emanuel Gull. Charge ordering and correlation effects in the extended hubbard model. *Phys. Rev. B*, 95:115149, Mar 2017.
- [29] Robert A. Bari. Effects of short-range interactions on electron-charge ordering and lattice distortions in the localized state. *Phys. Rev. B*, 3:2662–2670, Apr 1971.
- [30] Sebastião dos Anjos Sousa-Júnior, Natanael C. Costa, and Raimundo R. dos Santos. Half-filled extended hubbard model on a square lattice: Phase boundaries from determinant quantum monte carlo simulations. *Phys. Rev. B*, 109:165102, Apr 2024.
- [31] A. L. Kuzemsky. Variational principle of Bogoliubov and generalized mean fields in many-particle interacting systems. *Int. J. Mod. Phys. B*, 29(1530010), Jul 2015.
- [32] Raimundo R. dos Santos. Introduction to Quantum Monte Carlo Simulations for Fermionic Systems. *Braz. J. Phys.*, 33(1), Mar 2003.
- [33] A. N. Rubtsov, M. I. Katsnelson, and A. I. Lichtenstein. Dual fermion approach to nonlocal correlations in the hubbard model. *Phys. Rev. B*, 77:033101, Jan 2008.
- [34] S. Isakov, M.I. Katsnelson, and A.I. Lichtenstein. Perturbative solution of fermionic sign problem in quantum monte carlo computations. *npj Computational Materials*, 10(36), Feb 2024.
- [35] M. H. Hettler, A. N. Tahvildar-Zadeh, M. Jarrell, T. Pruschke, and H. R. Krishnamurthy. Nonlocal dynamical correlations of strongly interacting electron systems. *Phys. Rev. B*, 58:R7475–R7479, Sep 1998.
- [36] Edin Kapetanović, Malte Schüler, Gerd Czycholl, and Tim O. Wehling. Nonlocal exchange interactions in strongly correlated electron systems. *Phys. Rev. B*, 101:235165, Jun 2020.
- [37] Anders B. Eriksson, Torbjörn Einarsson, and Stellan Östlund. Symmetries and mean-field phases of the extended hubbard model. *Phys. Rev. B*, 52:3662–3675, Aug 1995.
- [38] Edin Kapetanović, Guglielmo Nicola Gigante, Malte Schüler, Tim O. Wehling, and Erik van Loon. Charge correlation, doublon-holon binding and screening in the doped hubbard model, 2024. <https://arxiv.org/abs/2409.05640>.



- [39] M. Schüler, M. Rösner, T. O. Wehling, A. I. Lichtenstein, and M. I. Katsnelson. Optimal hubbard models for materials with nonlocal coulomb interactions: Graphene, silicene, and benzene. *Phys. Rev. Lett.*, 111:036601, Jul 2013.
- [40] Malte Schüler, Erik G. C. P. van Loon, Mikhail I. Katsnelson, and Tim O. Wehling. Thermodynamics of the metal-insulator transition in the extended Hubbard model. *SciPost Phys.*, 6:067, 2019.
- [41] QUEST code. <https://code.google.com/archive/p/quest-qmc/>.
- [42] W. Nolting. *Grundkurs Theoretische Physik 5/1: Quantenmechanik - Grundlagen*. Springer Spektrum Berlin, Heidelberg, 8 edition, May 2013.
- [43] W. Nolting. *Grundkurs Theoretische Physik 7: Viel-Teilchen-Theorie*. Springer Spektrum Berlin, Heidelberg, 8 edition, Apr 2016.
- [44] V. Fock. Konfigurationsraum und zweite Quantelung. *Zeitschrift für Physik*, 75(9-10):622–647, Sep 1932.
- [45] W. Pauli. The Connection Between Spin and Statistics. *Phys. Rev.*, 58(716), Oct 1940.
- [46] Josiah Willard Gibbs. *Elementary Principles in Statistical Mechanics: Developed with Especial Reference to the Rational Foundation of Thermodynamics*. Cambridge Library Collection - Mathematics. Cambridge University Press, 2010.
- [47] T. Fließbach. *Statistische Physik*. Spektrum Akademischer Verlag, Heidelberg, 2010.
- [48] W. Nolting. *Grundkurs Theoretische Physik 6: Statistische Physik*. Springer Spektrum Berlin, Heidelberg, 7 edition, Oct 2013.
- [49] G. C. Wick. The evaluation of the collision matrix. *Phys. Rev.*, 80:268–272, Oct 1950.
- [50] G. Czycholl. *Theoretische Festkörperphysik*. Springer-Verlag Berlin Heidelberg, 2008.
- [51] Henrik Bruus and Karsten Flensberg. *Many-Body Quantum Theory in Condensed Matter Physics*. Oxford Graduate Texts. Oxford University Press, Sep 2004.
- [52] Gerald D. Mahan. *Many-Particle Physics*. Physics of Solids and Liquids. Springer New York, 3 edition, Oct 2000.
- [53] Takeo Matsubara. A New Approach to Quantum-Statistical Mechanics. *Progress of Theoretical Physics*, 14(4):351–378, Oct 1955.
- [54] Jozef Spalek. t-J model then and now: A personal perspective from the pioneering times. *Acta Physica Polonica A*, 111(409-24), 2007.

- 
- [55] T. Schäfer, F. Geles, D. Rost, G. Rohringer, E. Arrigoni, K. Held, N. Blümer, M. Aichhorn, and A. Toschi. Fate of the false mott-hubbard transition in two dimensions. *Phys. Rev. B*, 91:125109, Mar 2015.
- [56] The hubbard model at half a century. *Nature Physics*, 9(523), September 2013.
- [57] Daniel P. Arovas, Erez Berg, Steven A. Kivelson, and Srinivas Raghu. The Hubbard Model. *Annual Review of Condensed Matter Physics*, 13:239–274, 2022.
- [58] Mingpu Qin, Thomas Schäfer, Sabine Andergassen, Philippe Corboz, and Emanuel Gull. The Hubbard Model: A Computational Perspective. *Annual Review of Condensed Matter Physics*, 13:275–302, 2022.
- [59] Motoaki Hirayama, Youhei Yamaji, Takahiro Misawa, and Masatoshi Imada. Ab initio effective hamiltonians for cuprate superconductors. *Phys. Rev. B*, 98:134501, Oct 2018.
- [60] S. V. Tyablikov. *Methods in the Quantum Theory of Magnetism*. Plenum Press, New York, 1967.
- [61] A. Isihara. The Gibbs-Bogoliubov inequality. *J. Phys. A: Gen. Phys.*, 1(5), Sep 1968.
- [62] Mark M. Wilde. *Quantum Information Theory*. Cambridge University Press, 2013.
- [63] N. D. Mermin and H. Wagner. Absence of ferromagnetism or antiferromagnetism in one- or two-dimensional isotropic heisenberg models. *Phys. Rev. Lett.*, 17:1133–1136, Nov 1966.
- [64] J. E. Hirsch. Two-dimensional hubbard model: Numerical simulation study. *Phys. Rev. B*, 31:4403–4419, Apr 1985.
- [65] S. R. White, D. J. Scalapino, R. L. Sugar, N. E. Bickers, and R. T. Scalettar. Attractive and repulsive pairing interaction vertices for the two-dimensional hubbard model. *Phys. Rev. B*, 39:839–842, Jan 1989.
- [66] Ernst Ising. Beitrag zur theorie des ferromagnetismus. *Zeitschrift für Physik*, 31(1):253–258, Feb 1925.
- [67] Kurt Binder and Dieter W. Heermann. *Monte Carlo Simulation in Statistical Physics*. Springer Berlin, Heidelberg, 1997.
- [68] Nicholas Metropolis, Arianna W. Rosenbluth, Marshall N. Rosenbluth, Augusta H. Teller, and Edward Teller. Equation of State Calculations by Fast Computing Machines. *The Journal of Chemical Physics*, 21(6):1087–1092, Jun 1953.

- [69] B. Efron and C. Stein. The Jackknife Estimate of Variance. *The Annals of Statistics*, 9(3):586 – 596, 1981.
- [70] Masuo Suzuki. *Quantum Monte Carlo Methods in Equilibrium and Nonequilibrium Systems*. Springer Berlin, Heidelberg, 1986.
- [71] W. Kohn and L. J. Sham. Self-consistent equations including exchange and correlation effects. *Phys. Rev.*, 140:A1133–A1138, Nov 1965.
- [72] Antoine Georges, Gabriel Kotliar, Werner Krauth, and Marcelo J. Rozenberg. Dynamical mean-field theory of strongly correlated fermion systems and the limit of infinite dimensions. *Rev. Mod. Phys.*, 68:13–125, Jan 1996.
- [73] Walter Metzner and Dieter Vollhardt. Correlated lattice fermions in  $d = \infty$  dimensions. *Phys. Rev. Lett.*, 62:324–327, Jan 1989.
- [74] Eva Pavarini and Erik Koch, editors. *Orbital Physics in Correlated Matter*, volume 13 of *Schriften des Forschungszentrums Jülich. Reihe Modeling and Simulation*. Forschungszentrum Jülich GmbH Zentralbibliothek, Velag, Jülich, Sep 2023.
- [75] Richard P. Feynman and Albert R. Hibbs. *Quantum Mechanics and Path Integrals*. Dover Books on Physics. Dover Publications, Jun 2010.
- [76] Alexander Altland and Ben D. Simons. *Condensed Matter Field Theory*. Cambridge University Press, 2 edition, Aug 2010.
- [77] R. Mondaini, S. Tarat, and R. T. Scalettar. Quantum critical points and the sign problem. *Science*, 375(6579):418–424, 2022.
- [78] Hong-Chen Jiang and Thomas P. Devereaux. Superconductivity in the doped hubbard model and its interplay with next-nearest hopping  $t_2$ . *Science*, 365(6460):1424–1428, 2019.
- [79] Yi-Fan Jiang, Jan Zaanen, Thomas P. Devereaux, and Hong-Chen Jiang. Ground state phase diagram of the doped hubbard model on the four-leg cylinder. *Phys. Rev. Res.*, 2:033073, Jul 2020.
- [80] Malte Harland, Mikhail I. Katsnelson, and Alexander I. Lichtenstein. Plaquette valence bond theory of high-temperature superconductivity. *Phys. Rev. B*, 94:125133, Sep 2016.
- [81] S. Pairault, D. Sénéchal, and A.M. Tremblay. Strong-coupling perturbation theory of the hubbard model. *Eur. Phys. J. B*, 16:85–105, Jul 2000.
- [82] S. Brener, H. Hafermann, A. N. Rubtsov, M. I. Katsnelson, and A. I. Lichtenstein. Dual fermion approach to susceptibility of correlated lattice fermions. *Phys. Rev. B*, 77:195105, May 2008.

- 
- [83] Eva Pavarini, Erik Koch, Alexander Lichtenstein, and Dieter Vollhardt, editors. *DMFT: From Infinite Dimensions to Real Materials*, volume 8 of *Schriften des Forschungszentrums Jülich. Reihe Modeling and Simulation*. Forschungszentrum Jülich GmbH Zentralbibliothek, Velag, Jülich, Sep 2018.
- [84] D. Vollhardt. Dynamical mean-field theory for correlated electrons. *Annalen der Physik*, 524(1):1–19, 2012.
- [85] Elliott H. Lieb and F. Y. Wu. Absence of mott transition in an exact solution of the short-range, one-band model in one dimension. *Phys. Rev. Lett.*, 20:1445–1448, Jun 1968.
- [86] U. Brandt and C. Mielsch. Thermodynamics and correlation functions of the falicov-kimball model in large dimensions. *Z. Physik B - Condensed Matter*, 75:365–370, Sep 1989.
- [87] P. W. Anderson. Localized magnetic states in metals. *Phys. Rev.*, 124:41–53, Oct 1961.
- [88] M. H. Hettler, M. Mukherjee, M. Jarrell, and H. R. Krishnamurthy. Dynamical cluster approximation: Nonlocal dynamics of correlated electron systems. *Phys. Rev. B*, 61:12739–12756, May 2000.
- [89] Eva Pavarini, Erik Koch, and Piers Coleman, editors. *Many-Body Physics: From Kondo to Hubbard*, volume 5 of *Schriften des Forschungszentrums Jülich. Reihe Modeling and Simulation*. Forschungszentrum Jülich GmbH Zentralbibliothek, Verlag, Jülich, Sep 2015.
- [90] Peter Staar, Thomas Maier, and Thomas C. Schulthess. Dynamical cluster approximation with continuous lattice self-energy. *Phys. Rev. B*, 88:115101, Sep 2013.
- [91] M. Jarrell, Th. Maier, C. Huscroft, and S. Moukouri. Quantum monte carlo algorithm for nonlocal corrections to the dynamical mean-field approximation. *Phys. Rev. B*, 64:195130, Oct 2001.
- [92] Emanuel Gull, Andrew J. Millis, Alexander I. Lichtenstein, Alexey N. Rubtsov, Matthias Troyer, and Philipp Werner. Continuous-time monte carlo methods for quantum impurity models. *Rev. Mod. Phys.*, 83:349–404, May 2011.
- [93] E. Gull, P. Werner, O. Parcollet, and M. Troyer. Continuous-time auxiliary-field monte carlo for quantum impurity models. *Europhysics Letters*, 82(5):57003, may 2008.
- [94] S. M. A. Rombouts, K. Heyde, and N. Jachowicz. Quantum monte carlo method for fermions, free of discretization errors. *Phys. Rev. Lett.*, 82:4155–4159, May 1999.

- [95] Our dual fermion perturbation theory code. <https://github.com/EKapet93/DFPT-Thesis>.
- [96] OpenBLAS library. <https://www.openblas.net/>.
- [97] FFTW library. <https://www.fftw.org/>.
- [98] Wei Wu, Michel Ferrero, Antoine Georges, and Evgeny Kozik. Controlling feynman diagrammatic expansions: Physical nature of the pseudogap in the two-dimensional hubbard model. *Phys. Rev. B*, 96:041105, Jul 2017.
- [99] Jonathan A. Sobota, Yu He, and Zhi-Xun Shen. Angle-resolved photoemission studies of quantum materials. *Rev. Mod. Phys.*, 93:025006, May 2021.

---

## F. List of changes/Liste der Änderungen

Abseits der nicht explizit aufgelisteten Korrekturen von kleineren Rechtschreib- und Grammatikfehlern wurden folgende, redaktionelle Änderungen/Korrekturen im Vergleich zur bewerteten Version dieser Arbeit vorgenommen:

- Hinzufügen dieser Seite
- Aktualisierung des Frontblattes: Disputationsdatum und Prüfungskommission
- Seite 103, Fig.(7.2.20): Korrektur des Labels von "4x4 Periodic" zu "16x16 Periodic"
- Ergänzung des fehlenden arXiv-Links in Referenz [38]